



# VCU

Virginia Commonwealth University  
VCU Scholars Compass

---

Theses and Dissertations

Graduate School

---

2014

## Mammary Epithelial Cells Cultured onto Non-Woven Nanofiber Electrospun Silk-Based Biomaterials to Engineer Breast Tissue Models

Yas Maghdouri-White  
*Virginia Commonwealth University*

Follow this and additional works at: <https://scholarscompass.vcu.edu/etd>



Part of the [Biomedical Engineering and Bioengineering Commons](#)

© The Author

---

Downloaded from

<https://scholarscompass.vcu.edu/etd/3358>

This Dissertation is brought to you for free and open access by the Graduate School at VCU Scholars Compass. It has been accepted for inclusion in Theses and Dissertations by an authorized administrator of VCU Scholars Compass. For more information, please contact [libcompass@vcu.edu](mailto:libcompass@vcu.edu).

© Yas Maghdouri-White, 2014  
All Rights Reserved

# **Mammary Epithelial Cells Cultured onto Non-Woven Nanofiber Electrospun Silk- Based Biomaterials to Engineer Breast Tissue Models**

A dissertation submitted in partial fulfillment of the requirements for the degree of Doctor of  
Philosophy in Biomedical Engineering at Virginia Commonwealth University.

by

Yas Maghdouri-White

Bachelor of Science, University of North Carolina at Charlotte, 2001

Master of Science, University of North Carolina at Charlotte, 2004

Director: Christopher Lemmon, PhD  
Assistant Professor, Biomedical Engineering

Virginia Commonwealth University  
Richmond, Virginia  
April, 2014

## Acknowledgments

Through my Ph.D studies I have benefited from mentorship and support from many people who made this journey possible. First I would like to thank my mentors and committee members Drs. Dréau, Bowlin, Lemmon, Simpson, Elmore, Yang, and Conway for their efficient leadership and support throughout this process. I would especially like to give thanks to Dr. Didier Dréau for giving me the opportunity to continue my studies in his lab; I will always be grateful for his continuous guidance and support. I would also like to give special thanks to Dr. Gary Bowlin for his understanding of my life circumstances and his constant mentorship.

I would like to thank my past and present lab colleagues Dr. Scott Sell, Dr. Parthasarathy Madurantakam, Dr. Koyal Garg, Dr. Michael McClure, Dr. Anna Bulysheva, Dr. Michael Francis, Dr. Isaac Rodriguez, Dr. Patricia Wolfe, Jennifer McCool, and Ryan Clohessy at VCU and Dr. Stephen Rego, Dr. Danielle Van, Dr. Michelle Coleman, Rachel Helms, Amanda Lance, and Alex De Piante at UNC Charlotte for their friendly support, whether in answering my technical questions, having a friendly conversation, or hanging out at conferences. Working with and getting to know all of you has been a pleasure.

Last but not least I would like to thank my family for their unconditional love and support. I would like to thank my dad, Houshang Maghdouri, for always having my back and encouraging me to be my best in life. I would like to thank my mom, Nahid Safaei, for all the sacrifices she has made and for taking care of my son so I can pursue my dreams. I would like to thank my sister, Rose Maghdouri, and my brother, Mohammad Reza Maghdouri, for always being there when I need extra love and support. I would like to give special thanks to my husband, Justin White, for always believing in me and supporting me in this process even when it meant being

away from our son and I for weeks at a time. I would also like to thank my little angel, our 4-year old son, Liyam White, for enduring time away from mommy and especially daddy, he has been my motivation and drive throughout this process. I would also like to acknowledge our unborn child whose first few months of life have been stressful thanks to mommy's work load and schedule.

## Table of Contents

Acknowledgments.....	ii
List of Figures.....	xi
List of Tables.....	xiii
List of Abbreviations.....	xiv
Abstract.....	xvi
CHAPTER 1: INTRODUCTION.....	1
1.1. Abstract.....	1
1.2. Introduction.....	1
1.3. Biological Features of the Breast Tissue.....	5
1.3.1. Anatomy and Structure of the Breast Tissue.....	5
1.3.2. Mechanical Properties of the Breast Tissue.....	6
1.3.3. Breast Development.....	7
1.3.4. Cancer Development & Progression.....	8
1.4. Breast Tissue Modeling.....	9
1.4.1. Clinical Potential and Other Uses.....	9
1.4.2. 2D vs. 3D <i>In Vitro</i> Models.....	11
1.4.3. Biomaterial Properties and Suitability for Tissue Regeneration.....	11
1.4.4. Early 3D Breast Models.....	13
1.4.5. Epithelial Cell Interactions with ECM Proteins.....	14

1.4.6.	Silk in Biomedical Applications .....	15
1.5.	Silk Bioengineered Scaffolds .....	17
1.5.1.	Source, Type, Physical and Chemical Properties .....	17
1.5.2.	Mechanical Properties.....	19
1.5.3.	Biocompatibility .....	20
1.5.4.	Biodegradation.....	20
1.5.5.	Binding sites.....	22
1.6.	Engineered Silk-based Constructs.....	23
1.6.1.	Preparations.....	23
1.6.2.	Nanofibrous SF Scaffolds.....	25
1.7.	Conclusion and Rationale.....	26
<b>CHAPTER 2: PHYSICAL PROPERTIES AND MAMMARY EPITHELIAL</b>		
<b>BIOCOMPATIBILITY OF SILK FIBROIN ELECTROSPUN NANOFIBER SCAFFOLDS... 29</b>		
2.1.	Abstract .....	29
2.2.	Introduction .....	30
2.3.	Materials & Methods.....	32
2.3.1.	Silk Extraction .....	32
2.3.2.	Electrospinning .....	32
2.3.3.	Scaffold Characterization.....	32
2.3.4.	Specific Surface Area Evaluations.....	33

2.3.5.	Mechanical Testing.....	33
2.3.6.	Cell Cultures .....	34
2.3.7.	Cell Attachment Analyses.....	34
2.3.8.	Cell Viability Analyses .....	35
2.3.9.	Statistical Analysis.....	35
2.4.	Results .....	36
2.4.1.	Physical and Mechanical Characteristics of Electrospun SF Scaffolds.....	36
2.4.2.	Mechanical Strength of SF-derived Electrospun Scaffolds .....	38
2.4.3.	MCF10A Cell Attachment and Viability on Electrospun SF Scaffolds .....	39
2.5.	Discussion .....	40
2.6.	Conclusion.....	43
CHAPTER 3: EFFECTS OF AIR-FLOW ELECTROSPINNING ON PHYSICAL, MECHANICAL, AND BIOCOMPATIBILITY OF ELECTROSPUN SILK-BASED SCAFFOLDS .....		
		44
3.1.	Abstract .....	44
3.2.	Introduction .....	45
3.3.	Materials & Methods.....	48
3.3.1.	Silk Extraction .....	48
3.3.2.	Electrospinning .....	49
3.3.3.	Scaffold Characterization.....	50



3.3.4.	Cell Culture and Staining.....	50
3.3.5.	Cell Viability Analysis.....	51
3.3.6.	Cell Infiltration Measurements and Analyses.....	52
3.3.7.	Statistical Analysis.....	52
3.4.	Results .....	52
3.4.1.	Characteristics of Electrospun Silk Scaffolds.....	52
3.4.2.	Effects of Air-flow Rate on Fiber Diameters and Pore Sizes in 7% Silk Scaffolds	53
3.4.3.	Effect of Air-flow Rate on Fiber Diameters and Pore Sizes in 12% Silk Scaffolds	56
3.4.4.	MCF-10A Cell Growth and Viability Seeded on 7% and 12% Electrospun Silk Scaffolds .....	58
3.4.5.	MCF-10A Cell Infiltration into 7% and 12% Porous Silk Scaffolds .....	61
3.5.	Discussion .....	65
3.6.	Conclusion.....	67
CHAPTER 3S: EFFECTS OF AIR PRESSURE ON MECHANICAL PROPERTIES AND		
BIOCOMPATIBILITY OF SILK FIBROIN DERIVED ELECTROSPUN SCAFFOLDS .....		
68		
3S.1.	Abstract.....	68
3S.2.	Introduction.....	69
3S.3.	Materials & Methods .....	69
3S.3.1.	Silk Extraction.....	69
3S.3.2.	Electrospinning.....	69

3S.3.3. Specific Surface Area Evaluations .....	69
3S.3.4. Mechanical Testing .....	70
3S.3.5. Cell Culture Media .....	70
3S.3.6. Cell Adhesion Analyses .....	70
3S.3.7. Cell Viability Analysis .....	71
3S.3.8. Statistical Analysis .....	71
3S.4 Results .....	72
3S.4.1. SSA and Mechanical Strength of SF Electrospun Scaffolds.....	72
3S.4.2. MCF10A Cell Attachment and Viability on SF-derived Scaffolds .....	74
3S.5. Discussion .....	76
3S.6. Conclusion .....	78
<b>CHAPTER 4: EFFECTS OF COLLAGEN TYPE I ON SILK-BASED ELECTROSPUN</b>	
<b>SCAFFOLDS .....</b>	<b>79</b>
4.1. Abstract .....	79
4.2. Introduction .....	80
4.3. Materials & Methods.....	83
4.3.1. Silk Extraction .....	83
4.3.2. Collagen Type I.....	83
4.3.3. Electrospinning .....	84
4.3.4. Scaffold Characterization.....	85

4.3.5.	Mechanical Testing.....	85
4.3.6.	Protein Coating .....	85
4.3.7.	Cell Culture.....	86
4.3.8.	Cell Adhesion Analyses .....	86
4.3.9.	Cell Viability Analyses .....	87
4.3.10.	Cell Infiltration Measurements.....	87
4.3.11.	Statistical Analyses .....	88
4.4.	Results .....	88
4.4.1.	Physical Characteristics of Electrospun SF-C Blended Scaffolds.....	88
4.4.2.	Blending of Collagen Type I with SF Decreased the Fiber Diameters and Pore Sizes of SF-C Electrospun Scaffolds.....	89
4.4.3.	Mechanical Strength of Electrospun SF-C Blended Scaffolds.....	90
4.4.4.	MCF10A Cell Adhesion and Viability on Electrospun SF-C Blended Scaffolds ..	92
4.4.5.	SF-C Electrospun Scaffolds Limit the Infiltration of MCF10A Cells.....	93
4.5.	Discussion .....	94
4.6.	Conclusion.....	98
CHAPTER 5: LAMININ-COATING OF ELECTROSPUN SILK FIBROIN DERIVED SCAFFOLDS IN THREE-DIMENSIONAL CULTURES OF MAMMARY EPITHELIAL CELLS .....		99
5.1.	Abstract .....	99

5.2.	Introduction .....	100
5.3.	Materials and Methods .....	103
5.3.1.	Silk Extraction .....	103
5.3.2.	Electrospinning .....	103
5.3.3.	Scaffold Characterization.....	104
5.3.4.	Laminin Coating .....	105
5.3.5.	Cell Culture .....	105
5.3.6.	Cell Adhesion Analyses .....	106
5.3.7.	Cell Viability Analyses .....	106
5.3.8.	Immunofluorescence Staining and Structure Formation Analyses.....	107
5.3.9.	Statistical Analyses .....	107
5.4.	Results .....	108
5.4.1.	Physical Characteristics of Electrospun SF Scaffolds .....	108
5.4.2.	MCF10A Cell Adhesion on Laminin Coated SF Electrospun Scaffolds.....	108
5.4.3.	MCF10A Cell Viability on Laminin Coated Electrospun SF-derived Scaffolds .	110
5.4.4.	Acinar Structures on Laminin Coated Electrospun SF-derived Scaffolds.....	110
5.5.	Discussion .....	111
5.6.	Conclusion.....	113
CHAPTER 6: CONCLUSION AND FUTURE DIRECTIONS .....		114
Literature Cited .....		121

## List of Figures

	Page
Figure 1.1: Mammary tissue microenvironment.....	6
Figure 2.1: Diameter and pore size in SF derived electrospun scaffolds.....	37
Figure 2.2: Specific surface area (SSA in $\mu\text{m}^{-1}$ ) of electrospun SF-derived scaffolds.....	38
Figure 2.3: Modulus of elasticity of 7, 12, and 17% SF-derived electrospun scaffolds.....	38
Figure 2.4: MCF10A cell attachment onto 7, 12, and 17% SF-derived electrospun scaffolds compared to attachment on control SF coated culture vessels (SCP).....	39
Figure 2.5: MCF10A cell viability after 14 days in culture.....	40
Figure 3.1: Air-flow and perforated mandrel.....	50
Figure 3.2: Randomly measured average fiber diameters for the solid mandrel and within the perforation and flat regions of air-flow electrospun 7% and 12% silk scaffolds.....	57
Figure 3.3: Randomly measured average pore size for the solid mandrel and within the flat and perforation regions of the air-flow electrospun 7% and 12% silk scaffolds.....	58
Figure 3.4: MCF-10A cell viability on 7% and 12% electrospun silk scaffolds after 14 days in culture.....	59
Figure 3.5: MCF-10A cell infiltration through 7% and 12% electrospun silk scaffolds after 7 and 14 days in culture.....	63
Figure 3.6: MCF-10A cell infiltration comparison between 7% and 12% Silk scaffolds after 7 and 14 days in culture.....	63
Figure 3S.1: Specific surface area (SSA in $\mu\text{m}^{-1}$ ) of electrospun SF-derived scaffolds.....	72
Figure 3S.2: Modulus of elasticity SF-derived electrospun scaffolds. ....	74
Figure 3S.3: MCF10A cell attachment onto SF-derived scaffolds.....	75
Figure 3S.4: MCF10A cell viability following a 14-day incubation in culture conditions.....	76
Figure 4.1: Average fiber diameters and pore sizes of pure SF and SF-C blended electrospun scaffolds.....	91
Figure 4.2: Moduli of elasticity of SF-C blended electrospun scaffolds.....	91
Figure 4.3: Percentage of MCF10A cell adherence to SF-C blended electrospun scaffolds.....	93
Figure 4.4: MCF10A cell viability onto SF-C blended and SF-C coated electrospun scaffolds.....	93
Figure 4.5: MCF10A cell infiltration through SF-C electrospun scaffolds after 14 days in	

culture.....	94
Figure 5.1: MCF10A cell adhesion on laminin-coated vessels and electrospun SF-derived Scaffolds.....	109
Figure 5.2: MCF10A cell viability on laminin-coated and non-coated vessels and scaffolds...	110
Figure 5.3: MCF10A cell morphology in 3D laminin coated SF-derived scaffolds.....	111
Figure 6.1: Silk fibroin microenvironment developed through electrospinning.....	116
Figure 6.2: Gradient electrospinning setup.....	120

## List of Tables

	Page
Table 1.1: Synthetic or natural polymers 3D culture scaffolds for the regeneration of biological tissues.....	4
Table 1.2: Current applications of silk fibroin as biomaterial.....	17
Table 1.3: Mechanical properties of silks and other materials.....	19
Table 1.4: Preparation methods and properties of 3D SF biomaterials in various forms.....	24
Table 1.5: Nanofibrous electrospun scaffolds and their tissue engineering applications.....	26
Table 2.1: Scanning Electron Micrographs of scaffolds derived from 7%, 12%, and 17% SF electrospun using a solid mandrel.....	36
Table 3.1: Micrographs of 7% and 12% electrospun silk scaffolds spun using a solid mandrel and from perforation regions subjected to AP of 0 to 400 kPa.....	54
Table 3.2: MCF-10A cell growth on 7% and 12% electrospun silk scaffolds after 1, 7, and 14 days in culture.....	60
Table 3.3: Nucleic acid staining of MCF-10A cell infiltration through 7% and 12% silk scaffolds spun using a solid mandrel and a perforated mandrel subjected to air pressure of 0 to 400 kPa.....	64
Table 3S.1: Elastic moduli of SF derived scaffolds electrospun using a solid mandrel or using various air pressures on a perforated mandrel.....	73
Table 4.1: Scanning Electron Micrographs of silk and SF-C blended electrospun scaffolds spun using a perforated mandrel subjected to an air pressure of 100 kPa.....	90
Table 4.2: Amount of collagen present in each scaffold condition.....	92
Table 5.1: Formation of acinar-like structures under different conditions .....	111

## List of Abbreviations

2D	Two-dimensional
3D	Three-dimensional
ACL	anterior cruciate ligament
AJCC	American Joint Committee on Cancer
ANOVA	One-way analysis of variance
AP	Air pressure
APs	Air pressures
BM	Basement membrane
<i>B. mori</i>	<i>Bombyx mori</i>
BMSCs	Human bone marrow stromal cells
BSA	Bovine serum albumin
CCV	Cell culture vessels
DMEM	Dulbecco's Modified Eagle Medium
ECM	Extracellular matrix
ECMs	Extracellular matrices
EDTA	Ethylenediamine tetraacetic acid
EGF	Epidermal Growth Factor
ER	Estrogen receptor- $\alpha$
HFIP	1,1,1,3,3,3 hexafluoro-2-propanol
hMSCs	human bone marrow stem cells
HNC	Hydrated with no cells
HPBS	Hydrated in PBS
HWC	Hydrated with cells
kPa	Kilo Pascal
kV	Kilo volts
LiBr	Lithium bromide
LEP	Luminal epithelial
MEP	Myoepithelial
MR	Magnetic resonance
OCT	Optimal Cutting Temperature
P(LLA-CL)	Poly(l-lactid-co- $\epsilon$ -caprolactone)
PBS	Phosphate-Buffered Saline
PCL	Poly( $\epsilon$ -caprolactone)
PDLLA	poly-DL-lactic acid
PDO	Polydioxanone
PEO	Poly(ethylene oxide)
PGA	Poly(glycolic acid)
PGA	Polyglycolic acid
PGS	Poly(glycerol sebacate)
PHB/nHA	Poly(3-hydroxybutyrate)/nano-hydroxyapatite
PHBV	poly(3-hydroxybutyric acid-co-3-hydroxyvaleric acid)
PHEMA	poly(2-hydroxyethyl methacrylate)



PLA	Poly(lactic acid)
PLAGA	poly(lactic acid-co-glycolic acid)
PLGA	Poly(D,L-lactic acid-co-glycolic acid)
PLLA	Poly(L-lactic acid)
PPE	Poly(phosphoester)
PU	polyurethanes
RGD	arginine-glycine-aspartic acid
SCP	Silk coated plates
SEM	Scanning Electron Microscopy
SF	Silk fibroin
SF-C	Silk fibroin-collagen
SFS	Silk fibroin scaffolds
SM	Solid mandrel
SSA	Specific surface area
TDLU	Terminal duct lobular unit

## **Abstract**

### **MAMMARY EPITHELIAL CELLS CULTURED ONTO NON-WOVEN NANOFIBER ELECTROSPUN SILK-BASED BIOMATERIALS TO ENGINEER BREAST TISSUE MODELS**

By Yas Maghdouri-White, M.S.

A dissertation submitted in partial fulfillment of the requirements for the degree of Doctor of Philosophy in Biomedical Engineering at Virginia Commonwealth University.

Virginia Commonwealth University, 2014

Major Director: Christopher Lemmon, PhD  
Assistant Professor, Biomedical Engineering

Breast cancer is one of the most common types of cancer affecting women in the world today. To better understand breast cancer initiation and progression modeling biological tissue under physiological conditions is essential. Indeed, breast cancer involves complex interactions between mammary epithelial cells and the stroma, both extracellular matrix (ECM) and cells including adipocytes (fat tissue) and fibroblasts (connective tissue). Therefore, the engineering of *in vitro* three-dimensional (3D) systems of breast tissues allows a deeper understanding of the

complex cell-cell and cell-ECM interactions involved during breast tissue development and cancer initiation and progression. Furthermore, such 3D systems may provide a viable alternative to investigate new drug or drug regimen and to model and monitor concurrent cellular processes during tumor growth and invasion. The development of suitable 3D *in vitro* models relies on the ability to mimic the microenvironment, the structure, and the functions of the breast tissue.

Different approaches to develop a novel 3D breast model have been investigated. Most models use gel scaffolds, including Matrigel<sup>®</sup> and collagen to generate breast tissue-like structures.

However, the physicochemical, mechanical, and geometrical properties of these scaffolds only partially meet the mechanical, physical, and chemical parameters of the breast tissue matrix.

In the present studies, we investigated the overall hypothesis that electrospun SF-derived scaffolds promote mammary cell growth and the formation of mammary-like structures depending on the composition and/or coating of the scaffolds with ECM proteins. Through an extensive literature search (1) the importance of 3D modeling of tissues and organs *in vivo*, (2) 3D modeling of the mammary tissue and currently available models, (3) the properties and applications of SF in tissue modeling and regeneration were reviewed (Chapter 1). Our studies provide evidence of the effects of various concentrations (Chapter 2) of SF along with different electrospinning techniques (Chapter 3) on the structure of electrospun scaffolds and whether those scaffolds provide suitable microenvironments for mammary epithelial cells as determined by MCF10A cell attachment, viability, and structure formation. Further, we investigated the effects of the key ECM proteins collagen I (Chapter 4) and laminin (Chapter 5) used to blend or coat, respectively, SF scaffolds on the attachment, viability and structure formation of mammary epithelial cells.

Our studies first highlight the mechanical and physical properties of the different SF-derived scaffolds through various SF concentrations and electrospinning techniques. Second, the biocompatibility of these SF electrospun scaffolds was defined based on MCF10A cell survival and adhesion. Third, our data indicate that scaffolds derived from blended and/or coated SF with collagen I also promoted human mammary cell survival and adhesion. Lastly, our observations suggest that on laminin-coated SF scaffolds MCF10A mammary cells, in the presence of lactogenic hormones, differentiated forming acinus-like structures.

Overall, these studies provide evidence that SF electrospun scaffolds closely mimic the structure of the ECM fibers and allow many advantages such as; physical and chemical modification of the microenvironment by varying electrospinning parameters and addition of various proteins, hormones, and growth factors, respectively. Further, coating these SF scaffolds with essential ECM proteins, in particular laminin, promote cell-ECM interactions necessary for cell differentiation and formation of growth-arrested structures, through providing cell integrin binding sites and appropriate chemical cues.

# CHAPTER 1: INTRODUCTION

## Bioengineered Silk Scaffolds in 3D Modeling of Mammary Tissues

### 1.1. Abstract

*In vitro* generation of three-dimensional (3D) biological tissues as organ-like structures is a promising strategy to study and closely model complex aspects of the molecular, cellular and physiological interactions of tissue in both healthy and disease states. In particular, *in vitro* 3D tissue modeling holds promises to further our understanding of breast development, and breast cancer initiation and progression. Indeed, the generation of biologically relevant 3D structures that combine mammary cells and engineered matrices have improved our knowledge of mammary tissue growth, organization, and differentiation. Several polymeric biomaterials have been used as scaffolds to engineer 3D mammary tissues. Among those, silk fibroin-based biomaterials have many biologically relevant properties and have been successfully used in multiple medical applications. Here, we review the recent advances in engineered scaffolds with an emphasis on breast-like tissue generation and the benefits of modified silk-based scaffolds.

### 1.2. Introduction

Many diseases including cancer involve complex processes and interactions between cells and their surrounding microenvironment. Understanding and unraveling these processes are crucial in disease prevention and treatment [1]. Over the years, biological research has contributed tremendously to the understanding of processes involved in human diseases.

However, these studies have been dependent on the use of animal models, humans, and two-dimensional (2D) monolayer cell culture systems, all of which have limitations and can pose ethical concerns [2,3]. Indeed, human experimentations are limited by ethics; and when possible may cause discomfort or have side effects and risks for the subjects [2]. The use of animal models is often limited by their availability and feasibility of the test procedures. Furthermore, for human-specific diseases animal models are not always adequate [4] and their responses to therapeutics may be drastically different, limiting the usefulness of such animal modeling in the investigations of therapeutics for human diseases [2,5]. Conventional 2D cell culture models have contributed significantly to our biological understanding, however, they lack the 3D microenvironment of tissues that has been shown to play a critical role in tissue morphogenesis and function [2,3,6,7].

Tissue engineering is an interdisciplinary field that combines principles of biological, chemical, and engineering sciences towards the goal of tissue regeneration [8]. Tissue engineering aims to generate tissues and organs mimicking the physiological properties of original targeted tissues [8,9]. *In vitro* 3D models, which strive to more closely mimic the biological microenvironment and physiological cell-extracellular matrix (ECM) interactions than 2D cultures, are created by combining cells with 3D structures (scaffolds) to generate functional 3D tissues that allow normal cell growth, organization, and differentiation [8,9]. *In vitro* engineered 3D tissues provide excellent models to investigate human tissue physiology and pathophysiology, therefore, bridging the gap between the conventional 2D models and animal model systems [2,3,5-7,9,10]. The key promises of *in vitro* engineered 3D organ and tissue models are (1) the improvement of the development, testing, and delivery of new drugs, (2) the substitution for animal and/or human studies that may raise ethical concerns [2,3,5], (3) the

furthering of our understanding of the complex interactions between cells and the stromal components during complex biological processes including cancer [3,5,10-12], and (4) the reduction of the need for organ replacement by engineering potential tissue and organ substitutes.

3D cell culture models generated using different forms of biodegradable and biocompatible natural or synthetic polymeric scaffolds have been used in a broad range of studies, including organ development [13], analyses of disease including cancer [3,14,15], drug testing [2], and functional tissue repair and implantation [13,16]. Specific ECM proteins including collagen, elastin, elastin-like-peptides, albumin and fibrin have been used as tissue scaffolds, hemostatic agents, and drug delivery vehicles [17]. 3D culture systems have been used towards the regeneration of many tissues and organs such as skin, bone, cardiac tissue, cartilage, tendon, ligament, lung, nerve, mammary gland, and vascular grafts (Table 1.1).

Recently, *ex vivo* regenerated tissues have shown clinical promise. For example, in 2006 *ex vivo* engineered bladders, using urothelial and muscle cells grown on collagen or the combination collagen and polyglycolic acid (PGA), were implanted into patients by Atala *et al.* [13]. The patients were monitored for up to five years. Post-operation, renal function was preserved and the engineered bladder biopsies showed an adequate structural architecture and phenotype [13]. Also, in 2008, Macchiarini *et al.* replaced the left main bronchus of a patient with a decellularized donor trachea [16]. Within 96 hours of bioreactor culture, the donor trachea was colonized by the recipient's epithelial cells and mesenchymal stem-cell-derived chondrocytes. The graft provided the recipient with a functional airway immediately after implantation. Lung-function tests performed at 2 months were within the normal range for the age and sex of the recipient, and after 4 months the graft showed normal appearance and mechanical properties [16].

**Table 1.1.** Synthetic or natural polymers 3D culture scaffolds for the regeneration of biological tissues.

Target Tissue	ECM Materials	References
Bone	Chitosan and its composites Poly(3-hydroxybutyrate)/nano-hydroxyapatite (PHB/nHA) Poly( $\epsilon$ -caprolactone) (PCL) and its composites Poly(L-lactic acid) (PLLA) and its composites Poly(D,L-lactic acid-co-glycolic acid) (PLGA) and its composites Regenerated silk fibroin and its composites Collagen and its composites	[18-25]
Heart	Collagen and its composites Poly(lactic acid) (PLA)/PCL Alginate	[26-29]
Cartilage	Collagen and its composites Regenerated Silk Fibroin Alginate, Polyglycolic acid (PGA) PLLA PGA and PLLA copolymers PCL poly(3-hydroxybutyric acid-co-3-hydroxyvaleric acid) (PHBV)	[30-40]
Ligament	Regenerated silk fibroin Collagen Alginate Chitosan PLGA	[41-45]
Lung	Collagen and its composites decellularized lung ECM poly-DL-lactic acid (PDLLA)	[46-49]
Breast	Matrigel Collagen and its composites Regenerated silk fibroin PLGA/Poly(lactic acid) (PLA)	[14,50-58]
Nerve	Poly(glycerol sebacate) (PGS) Poly(phosphoester) (PPE) PLLA	[59-62]
Skin	Collagen and its composites Chitosan PCL and its composites Poly(lactic acid-co-glycolic acid)	[63-67]
Tendon	Alginate Chitosan PLGA Collagen and its composites PGA	[44,45,68-71]
Vessels	PLLA Collagen and its composites PCL Chitosan Poly(ethylene glycol) (PEG) Poly(lactic acid) PLA/PCL Regenerated silk fibroin	[72-78]



### **1.3. Biological Features of the Breast Tissue**

#### **1.3.1. Anatomy and Structure of the Breast Tissue**

Breast tissue is composed of glandular, ductal, and stromal tissue containing epithelial cells, adipocytes and various stromal cell types (e.g., mesenchymal stem cells/pre-adipocytes, endothelial cells, fibroblasts, myofibroblasts, and leukocytes) [12,79,80]. In the mammary tubulo-alveolar gland, secretory acini and ducts are lined by an outer myoepithelial (MEP) cell layer and an inner luminal epithelial (LEP) cell layer [54,80]. These structures are well organized and have an apical-basal polarity, which is required in the directional secretion of milk [10]. Within the human breast there are 15-20 lobes of glands, which are embedded in fibrous and adipose tissue [1,12]. The primary ducts reach the nipple and give rise to a complex branching pattern of secondary ducts. Further branching into smaller ducts leads to terminal ducts that give rise to blind-ended ductules called acini. A collection of acini arising from one terminal duct embedded in a layer of contractile epithelial cells and intralobular stroma is referred to as a terminal duct lobular unit (TDLU), which is considered the functional unit of the breast [1,12,81]. The breast is primarily composed of adipose tissue dispersed between glandular and fibrous components of the breast. The adipose tissue determines the bulk and contour of the breast mound [12,79]. Growth of the adipose stroma occurs normally in the absence of the ductal network, also known as parenchyma, and can fully support subsequent mammary parenchyma development [82]. The ECM of the mammary gland is mainly composed of type I collagen [54,83]; however, fibronectin and several glycosaminoglycans are also present. The basement membrane (BM) of the breast acinus and ductal epithelium contains various proteins including laminin and type IV collagen [54]. Complex interactions between the multiple cell types within the breast tissue are required for the proper development and functioning of the organ [80]. Cell-

cell and cell-microenvironment interactions modify the proliferation, survival, polarity, differentiation, and invasive capacity of mammary epithelial cells suggesting the active role of breast stroma in mammary gland development and function. Further knowledge of stromal-epithelial interactions will enhance the understanding of mammary gland function [80,82,84,85]. The cellular components of the mammary tissue microenvironment are depicted in Figure 1.1.

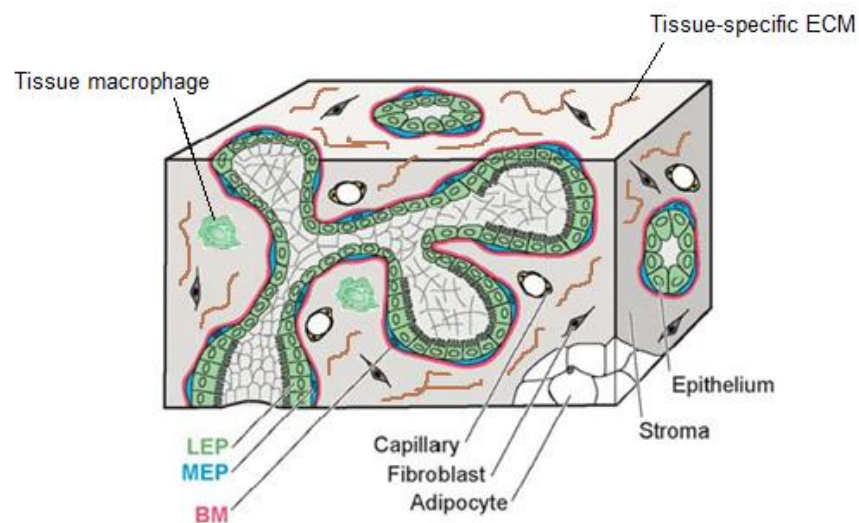


**Figure 1.1. Mammary tissue microenvironment. Adapted and modified from [86,87]**

### 1.3.2. Mechanical Properties of the Breast Tissue

Mechanical properties of the breast tissue have been investigated using various methods such as; indentation or compressive force [88,89], sonography, sonoelastography [90], and magnetic resonance (MR) elastography [91]. Using these techniques the elastic modulus of normal breast tissue was measured and ranged from 3 to 20 kPa within the fat regions and from 3 to 44 kPa within the fibroglandular regions, respectively. Many factors such as age, hormonal status, and menstrual cycle effect breast tissue's elastic modulus [90]. It has also been demonstrated that the proper organization of breast tissue is disrupted in cancer and is associated with increased breast density and stiffness [88-91].

### 1.3.3. Breast Development

Breasts arise as the result of reciprocal epithelial and mesenchymal interactions [81]. The breast development is divided into four phases: fetal, postnatal, post-pubertal, and adult [82]. The mammary epithelium is specified in the embryo and most of the branching morphogenesis required to develop the ductal tree occurs post-partum during puberty [10]. The mammary bud develops as a down-growth of a group of cells from the overlying ectoderm followed by the development of the primary ducts as a result of cell death in the lumen. Generally lined by two layers of epithelial cells, the primary duct, branches to form secondary ducts lined by a single layer of epithelial cells. This ductal network is connected to the nipple [82]. At birth, the parenchyma attains only a few orders of branching. The number of primary ducts per nipple is species dependent, with humans having approximately 20. In humans, the growth of the mammary parenchyma from birth until puberty involves ductal elongation and branching at a slow rate [82]. During puberty, as the levels of ovarian steroid increase, changes occur in both the epithelium and the stroma [82]. In the stroma, the amount of fibrous and fatty tissue increases [82]. The glandular epithelium increases in size while the mammary ducts elongate and branch through terminal end bud mitotic activity. Mitotic activity remains high until the mammary fat pad is filled with a system of ducts and side branches. Subsequently, mitotic activity regresses resulting in single layered luminal epithelial cell lobular structures with low mitotic activity and formation of terminal ductal lobular units [81,82,92]. The fourth phase of growth, further branching of the ductal network and full functional differentiation of the gland, is initiated by the hormones of pregnancy and involves a rapid and intense proliferative activity followed by alveolar differentiation [82]. This creates a system of ducts that collect the milk produced by the alveoli [10]. After pregnancy and lactation, significant reduction of milk in the breast results in

post-lactation involution, during which the mammary gland transitions to a resting non-lactating state [93]. During involution, the mammary epithelium cells are lost through apoptosis and are replaced by adipose tissue and mesenchyme that support the lobules in the non-pregnant adult. This regression of the breast leads to a resting (non-lactating) state until the next pregnancy. [10,82,93]. The structure and morphology of the post-pregnancy gland differs from that of the pre-pregnancy state [93]. Declining circulatory concentrations of sex-steroid hormones (estrogen, progesterone) triggered by decreased ovarian function result in post-menopausal involution [93].

#### **1.3.4. Cancer Development & Progression**

Breast cancer is a complex disease that requires interconnection of several signaling pathways [94]. Our current understanding of breast cancer highlights each breast cancer as unique. Thus, for each patient the development of personalized medicine could play a crucial role in the treatment of the disease [94]. The development of breast cancer is characterized by the loss of epithelial polarity and tissue organization, and almost all breast malignancies arise from TDLU [1,95]. The progression from normal mammary gland to invasive carcinoma is accompanied by enhanced vascularization, the loss of myoepithelial cells, and increases in myofibroblasts and immune cells in the stroma [1]. Early breast cancer tumors or benign *in situ* carcinomas, are defined by confinement of tumor cells within the basement membrane of the mammary ductal-lobular system. Once tumor cells invade the adjacent stroma, breast cancers are defined as malignant [1]. In addition to tumor size, malignant breast cancers are also defined based on the presence of specific molecular markers by the American Joint Committee on Cancer (AJCC) staging. Indeed, breast cancers are divided into major groups based on whether or not the tumor cells express the estrogen receptor- $\alpha$  (ER) [1], and are further divided into

subtypes. The ER-negative carcinomas are divided into three cell and molecular subtypes: basal-like, HER2+, and normal breast-like. The ER-positive breast carcinomas are divided into either luminal A or luminal B subtypes [1,96] both associated with the expression of genes expressed by lumen cells lining the mammary ducts [94]. Breast cancers of the luminal A subtype are the most common subtype (50% - 60%) and are Her2+ [94,96]. Breast cancers of luminal B subtype are Her2- and account for 10% - 20% of all breast cancers. The luminal B breast cancers have a more aggressive phenotype, higher histological grade, increased proliferative index, and worse prognosis than luminal A breast cancers [94,96]. The invasive breast cancer tumor mass is composed of cancer cells, stromal cells such as fibroblast and immune cells, and a different ECM composition and density [1]. The interactions between and amounts of these components varies amongst tumors and within each breast tumor mass. Therefore, modeling the specific characteristics of the breast cancer stroma will likely provide useful data in cancer prognosis and prediction [1].

## **1.4. Breast Tissue Modeling**

### **1.4.1. Clinical Potential and Other Uses**

As most (~90%) of human mammary carcinoma arises from ductal epithelium [10,97,98], 3D engineered mammary tissues may serve as models to deepen our understanding of cancer progression and to screen drug candidates for cancer treatments [10]. Additionally, 3D engineered mammary tissues may potentially be used to reconstruct breast tissues following various traumas including surgical removal of mammary tissue due to cancer. Based on cohort studies of women with breast cancer, as many as 34 to 40% of women with this disease undergo full mastectomy [99-101]. Different surgical approaches such as the use of autologous, implant-based materials, or a combination of these two are available to reconstruct breast tissues

[12,79,102]. Most patients opt for either autologous or silicone implants based reconstruction [12,79]. In the former, the autologous tissue used is the patient's own fat tissue from abdomen or buttocks. In the latter, silicone implants are implanted in place of the surgically removed mammary tissue. Silicone implants have been shown to result in local complications including bleeding [12], fluid collection [12] and most commonly capsular contracture due to scarring and fibrosis [12,79]. Furthermore, the implants themselves are subject to rupture [79], leakage [79], displacement [79], deflation [79] and/or deformation [79]. Autologous breast reconstruction has also been associated with poor results. In particular, a 50-70% graft volume reduction due to fat cell/tissue resorption has been observed [103,104]. Moreover, this fat resorption leads to calcium deposits that hinder mammographic examination and tumor detection [105]. The fat cells used in autologous reconstruction are mostly composed of mature adipocytes that are resistant to current *ex vivo* expansion attempts [79]. The inability to graft adipocytes capable of dividing and differentiating in large part explains the tissue defect associated with autologous reconstruction [79]. The limitations associated with either the silicon implants or autologous reconstructions highlight the need for better approaches. Thus, significant research efforts have been directed toward the generation of biocompatible, bioresorbable 3D scaffolds/tissues that would permit, following implantation, the regeneration of the patient breast tissue [14,50-58]. As a key step toward those 3D scaffolds/tissues, *in vitro* 3D scaffolds mimicking the structure and function of the mammary gland have been developed and studied. Those 3D scaffolds have been used as experimental model systems to investigate steps of breast development and cancer progression [14,50-58].

### **1.4.2. 2D vs. 3D *In Vitro* Models**

Modeling the structure and function of normal tissue allows for a better understanding of the normal tissue and of disruptions occurring in diseased tissue [10]. Mammary cells cultured in 2D monolayers have been used to investigate cellular events in mammary morphogenesis and carcinogenesis; however, these models only poorly reflect the function and structure of breast tissue [10,106,107]. Indeed, culture of mammary epithelial cells in 2D monolayer *in vitro* failed to generate acini and produce milk proteins even after stimulation with lactogenic hormones [10]. In contrast, 3D models of mammary tissues led to the formation of acinus- and duct-like structures similar to those observed *in vivo* with the ability to produce basement membrane and secrete milk proteins [10,51,52,55,108]. Moreover, distinction of normal and cancer-derived cells in 2D cultures is difficult. In 3D, however, normal mammary epithelial cells form polarized acini with central lumina as they growth-arrest. These observations contrast sharply with mammary epithelial cancer cells that do not organize and form disordered highly proliferative colonies [10]. Furthermore, in mammary tissue 3D models pathways deregulated or upregulated during the tumorigenic progression can be mimicked [10]. Overall, the use of 3D mammary tissue constructs can increase understanding of the complex processes that dictate organization and structure of mammary epithelial cells, and how disruption of those signals in cancer can alter the development, function, and physiology of mammary tissue [10,51,55,109,110].

### **1.4.3. Biomaterial Properties and Suitability for Tissue Regeneration**

Early on, artificial scaffolds were engineered to provide cells with an environment that promoted their survival [111]. However, it is now understood that mimicking the native microenvironment and the host tissue's physiochemical and mechanical properties are essential

to the maintenance and regulation of cell behavior and tissue function [111]. In tissue regeneration applications, an ideal biomaterial scaffold should:

- Be biocompatible and not evoke a sustained inflammatory or toxic response *in vivo* [17,111]
- Have physiochemical and mechanical properties similar to the native host tissue [17,111].
- Enable the fabrication of 3D constructs that can incorporate cells [111].
- Be able to incorporate growth factors and cell adhesion functional groups [111].
- Be bio-degradable and the degradation products should be non-toxic, metabolized and cleared from the body [17,111].

Synthetic and natural polymers have been utilized in the engineering of biological tissues extensively (Table 1.1). Each of these polymer types possesses several advantages and disadvantages [17]. Synthetic polymers are easy to process and modify, have more predictable properties, batch-to-batch uniformity [17], good mechanical properties and thermal stability; however, they often have associated disadvantages such as; cell toxicity, immunogenicity, and poor biocompatibility [111-114]. For example, Poly( $\epsilon$ -caprolactone) (PCL) and polyurethanes (PU) are two of the typical synthetic polymers used in tissue engineering [115]. The biologically relevant properties of PCL are its high elasticity at room or body temperature and its degradability. However, the slow degradation rate of PCL makes it less attractive for some tissue engineering applications [115]. A major limitation of PU for biomedical applications is the presence of traces of toxic precursors (such as toluene diisocyanates) used in the synthesis of PU [115].

Natural polymers such as structural proteins offer improved biocompatibility and possess diverse features, which mimic natural ECM [112-114,116]. They have the ability to present



receptor-binding ligands to cells, and they are susceptible to cell-triggered proteolytic degradation and natural remodeling [17]. However, they may trigger strong immunogenic response, their purification process is often complex, and they may be a vector of disease transmission [17]. Further, their rapid degradation, and poor mechanical strength and thermal properties limit their use [112-114,116]. Nair *et al.* [17] have recently reviewed most of the promising synthetic and natural biomaterials.

To overcome the limitations of currently available polymers, approaches that blend synthetic and natural polymers or natural and natural polymers have been developed [113]. Blending natural polymers such as collagen, gelatin, or elastin with a variety of other polymers improves their biocompatibility [25,63,117-119]. Recently, Sionkowska *et al.* [113] reviewed the blends of natural and synthetic polymers.

#### **1.4.4. Early 3D Breast Models**

Following the pioneering work of the Bissell group [6,10,84,86,106,107,120-124], 3D mammary models have been developed and refined mostly using gel-based scaffolds, such as Matrigel<sup>®</sup>, collagen, Matrigel<sup>®</sup>/collagen mix, or laminin [50,51,54,56,83,122,125-127]. In these models mammary epithelial cells exhibit low proliferation rate, form polarized growth-arrested structures, and secrete basement membrane [51]. The key roles of cell-ECM interactions in the growth and differentiation of the mammary gland in this model have been highlighted by Bissell *et al.*, Roskelley *et al.*, and Wicha *et al.* [84,106,124,128]. It has been demonstrated that the mechanical density and stiffness of the ECM plays an important role in the organization of the polarized growth-arrested structures and that the polarized organization of these acinar and ductal structures is disrupted by increased ECM stiffness [129,130]. The role of stromal cell types, especially fibroblasts, in epithelial-stromal interactions and the generation of acini were

also demonstrated in 3D gel cultures [50]. Formation of acinar and ductal structures have been observed in co-cultures of human mammary fibroblasts and epithelial cells on either 3D collagen type I or mixed Matrigel<sup>®</sup>-collagen matrices [54,110]. More recently, Wang *et al.* [55] demonstrated that mammary epithelial cells co-cultured with stromal cells, within mixed Matrigel<sup>®</sup>-collagen matrices and maintained on 3D silk sponges led to the formation of ductal and acinar structures. These Matrigel<sup>®</sup>-based gel scaffolds, however, only partially meet the physicochemical and mechanical properties of the breast tissue ECM [131] and their spontaneous gel contraction, limited mass transport, and rapid degradation after transplantation limit their applications in the field of mammary tissue engineering [55]. Furthermore, Matrigel<sup>®</sup> contains unknown concentrations of growth factors that vary substantially between batches making the reproduction of the experimental findings and understanding the role of each specific factor challenging. Also, Matrigel<sup>®</sup> is a mouse sarcoma secretion and not clinically appropriate for *in vivo* studies and human use [132-134]. Due to these challenges there is a renewed interest for other sources of natural polymers such as silk protein for use in tissue engineering/biomedical applications [112-114,116].

#### **1.4.5. Epithelial Cell Interactions with ECM Proteins**

The ECM plays an important role in the differentiation and organization of the epithelium. Epithelial cells attach to the ECM in order to establish cell polarity [135]. This cell-ECM attachment is mediated by cell integrins which are transmembrane receptors and bind to a variety of ECM components including collagen, laminin, and fibronectin [135,136]. Mammary epithelial cells attach to laminin and collagen through  $\alpha2\beta1$  integrin subunits [136].  $\beta1$ -integrin-cell interactions have been shown to be crucial in differentiation of mammary epithelial cells and secretion of milk protein,  $\beta$ -casein, by these cells [106]. Inhibiting these  $\beta1$ -integrin-cell

interactions results in disruption of the polarized and differentiated structures [106]. The BM component that interacts with  $\beta$ 1-integrin has been shown to be laminin-1 [106,137]. Polarized structures resulting from interactions with laminin, but not other ECM proteins such as collagen I, are resistant to apoptosis through  $\beta$ 4 integrin interactions [138]. Interactions of  $\beta$ 4 integrin with laminin initiate signals for cell growth, viability, and functional differentiation; it also directs tissue polarity and promotes resistance to apoptosis in both nonmalignant and malignant breast epithelial structures [138].

These findings highlight the importance of laminin in 3D modeling of the breast tissue *in vitro*.

#### **1.4.6. Silk in Biomedical Applications**

Silk fibroin (SF) is the major component of a large subset of non-bioabsorbable biomedical sutures and has been used extensively in the medical field [114,139]. Due to their easy handling and tying capacities, silk sutures are used in eye and lip surgeries, intraoral surgeries, and skin wounds [140]. More recently, silk has been used as a biomaterial scaffold due to its excellent mechanical properties [141], and thermal stability over a wide range of temperatures up to about 250°C without loss of functional integrity [142]. In addition, the biocompatibility, controlled slow degradation rate [139,143,144], hemostatic properties, low antigenicity, non-inflammatory characteristics [142,145], high oxygen permeability, high drug permeability, resistance against enzymatic cleavage [146] of silk-derived products has made it a viable option in biological environments. Different forms of SF-derived biomaterial have been assessed including films [143,145], membranes [143,145], gels [145,147], sponges [143,145], powders, scaffolds [145,147], fibers, nets, meshes, yarn [143], and nano-particles [147]. Specific biological applications encompass burn-wound dressing, enzyme immobilization matrices, vascular

prostheses and structural implants [145]. Furthermore, different forms of SF-derived biomaterials have been investigated for multiple biomedical applications such as tissue engineering, disease modeling, drug delivery, implant devices, and wound healing (Table 1.2).

As both processing and understanding of biologically relevant properties improved, SF-derived biomaterials have become an attractive option to develop bio-resorbable scaffolds [114,140]. Variations in the processing procedures employed during material formation generate SF with degradation rate ranging from months to years [142]. Further, the presence of easy accessible chemical groups offers the ability for functional modification [148]. The wide range of extensibility, elasticity, good strength, and strain hardening from different varieties of silk provide advantages to developing a range of silk-based biomaterials based on needed application [148]. These properties of silk fibroin are particularly useful for tissue engineering applications [140].

As mentioned previously, 3D models of the mammary gland have been investigated during the past three decades many of which have utilized mostly gel scaffolds, such as Matrigel<sup>®</sup> and collagen [50,51,54,56,83,122,125-127] to reconstruct the mammary tissue microenvironment. However, these scaffolds only partially meet the physicochemical and mechanical properties of the breast tissue ECM [131] and their spontaneous gel contraction, limited mass transport, and rapid degradation after transplantation limit their applications in the field of mammary tissue engineering [55]. Furthermore, the use of Matrigel<sup>®</sup> is associated with several disadvantages mentioned previously in section 1.4.4. Considering the advantages of SF biomaterials and their wide range of processing, they offer significant benefits in maintaining long-term 3D mammary culture models *in vitro* and as potential *in vivo* transplants [55].

**Table 1.2.** Current applications of silk fibroin as biomaterial.

Applications	Target Tissues	Sources	Silk Fibroin Forms
Tissue Engineering	Anterior cruciate ligament	– <i>B. mori</i> silk fibroin – <i>B. mori</i> silk fibroin	– Silk fiber wire-robe [42] – Knitted silk mesh [149]
	Adipose-like tissue	– <i>B. mori</i> silk fibroin	– Sponges [150]
	Bone	– <i>B. mori</i> silk fibroin – <i>B. mori</i> silk fibroin – <i>B. mori</i> silk fibroin	– Films [151] – Sponges [152-156] – Electrospun fibers [23]
	Cardiac Tissue	– Not specified – <i>Antheraea mylitta</i> and <i>B. mori</i> silk fibroin	– Microparticle patches [157] – Sponges [158]
	Cartilage	– <i>B. mori</i> silk fibroin – <i>B. mori</i> silk fibroin – <i>B. mori</i> silk fibroin	– Sponges [33-35] – Films [34,35] – Electrospun fibers [159]
	Corneal Tissue	– <i>B. mori</i> silk fibroin	– Films [160,161]
	Cervical Tissue	– <i>B. mori</i> silk fibroin	– Sponges [162]
	Liver	– <i>B. mori</i> silk fibroin – <i>Antheraea mylitta</i> silk fibroin	– Films [163,164] – Micro/nano fibrous nonwoven scaffold [165]
	Nerve Tissue	– <i>B. mori</i> silk fibroin – <i>B. mori</i> silk fibroin	– Fibers [166,167] – Film [168]
	Soft Tissue	– <i>B. mori</i> silk fibroin	– Gels [169]
	Skin	– <i>B. mori</i> silk fibroin – Not specified	– Films [170] – Electrospun fibers [171]
	Tendon	– <i>Antheraea pernyi</i> silk fibroin	– Braided fibers [172]
	Vascular Tissue	– <i>B. mori</i> silk fibroin – <i>B. mori</i> silk fibroin	– Electrospun fibers [78,173] – Tubes [174]
	Disease Models	Mammary Gland	– <i>B. mori</i> silk fibroin – <i>B. mori</i> silk fibroin
Kidney		– <i>B. mori</i> silk fibroin	– Sponges [175,176]
Tumor Model		– <i>Antheraea mylitta</i> and <i>B. mori</i> silk fibroin	– Films and Sponges [139]
Drug Delivery		– <i>B. mori</i> silk fibroin – <i>B. mori</i> silk fibroin	– Spheres [177-179] – Films [180]
Implants	Femur	– <i>B. mori</i> silk fibroin	– Sponges [181]
Wound Healing		– <i>B. mori</i> silk fibroin	– Electrospun fibers [182,183]

## 1.5. Silk Bioengineered Scaffolds

### 1.5.1. Source, Type, Physical and Chemical Properties

Naturally, silks are polymeric fibrous proteins present in the glands of silk producing arthropods such as silkworms, spiders, scorpions, mites, and bees [143,148,184]. Despite some variations in the primary organization and structural features at the nanometer scale between silk types, all silkworm silk fibers follow similar hierarchical structural arrangements [148]. Silks consist of two types of proteins: a filament core protein, SF, and a glue-like coating family of

hydrophilic proteins holding two fibroin fibers together, the sericins [143,145,185]. These two silk proteins are self-assembling proteins and both contain the same 18 amino acids such as glycine, alanine and serine in different amounts [145]. Depending on the organism, the secondary structure of silk can be helical,  $\beta$ -sheet, or cross- $\beta$ -sheet [184]. Structurally, SF is composed of hydrophobic blocks with highly preserved repetitive sequence consisting of short side-chain amino acids such as glycine and alanine, and hydrophilic blocks with more complex sequences that consist of larger side-chain amino acids as well as charged amino acids [143]. The hydrophobic blocks, also referred to as crystalline portions, contain highly repetitive amino acid sequences (-Gly-Ala-Gly-Ala-Gly-Ser-), forming an antiparallel  $\beta$ -sheet structure [143,145,186,187]. The physiochemical and mechanical properties of SF, resistance to dissolution, thermal and enzymatic degradation strongly depends on its conformational transition of  $\alpha$ -helix and random coil to highly stable  $\beta$ -sheets [143,145,148,171,186,188].

The most widely studied silks are silkworm cocoon silk from *Bombyx mori* (*B. mori*, also known as mulberry silk) and dragline silk from the spider *Nephila clavipes* [143,148]. However, compared to silkworm silk, there are no commercial supply chains available for spider silks mainly due to the more aggressive nature of spiders and the more complex and smaller quantity of silk generated [140]. The yield of silk fiber from a single silkworm cocoon is 600-1500 meters, compared to only ~12 meters from the spider web [148]. Thus, silk-based biomaterials are commonly prepared from *B. mori* SF [114,143,148]. *B. mori* SF is composed of a heavy (H) and a light (L) chain linked together by a disulfide bond, as well as, a 25 kDa glycoprotein (P25) which is non-covalently linked to these chains [148,189]. The hydrophobic domains of H chains contain Gly-X (X being Ala, Ser, Thr, Val) repeats and can form anti-parallel  $\beta$ -sheets. The L-

chain is hydrophilic in nature and relatively elastic. P25 protein is thought to play a significant role in maintaining the integrity of the complex [148].

### 1.5.2. Mechanical Properties

Mechanically, silks exhibit toughness, elasticity, high strength, and are lightweight [143]. The toughness of silk fibers is greater than Kevlar 49, which is the benchmark in high-performance synthetic fiber technology [140]. The strength-to-density of silk is ten times higher than that of steel [148]. Silk fibroin possesses an anti-thrombotic surface with good resistance to high shear stress and blood flow pressure [148]. It must be noted that despite high mechanical strength of native silk fibers, the strength of materials prepared from regenerated silk fibroin solution are weak [148]. The tensile strength of native fibers are in the 0.5-0.6 GPa range whereas the tensile strength of a regenerated silk material, such as silk films, is about 0.02 GPa in its dry state [190]. This is due the loss of secondary structure in the processed silk. Various investigations are ongoing to improve the strength of regenerated silk materials [148]. Mechanical properties of silks and other materials are listed in Table 1.3.

**Table 1.3.** Mechanical properties of silks and other materials. Adapted from [140]

Material	Stiffness, $E_{init}$ (GPa)	Strength, $G_{max}$ (GPa)	Extensibility $\epsilon_{max}$	Toughness (MJ m <sup>-3</sup> )
<i>Araneus MA silk</i>	10	1.1	0.27	160
<i>Araneus viscid silk</i>	0.003	0.5	2.7	150.65
<i>Bombyx mori cocoon silk</i>	7	0.6	0.18	70
<b>Tendon collagen</b>	1.5	0.15	0.12	7.5
<b>Bone</b>	20	0.16	0.03	4
<b>Breast tissue (fat regions)</b>	$3 - 20 \times 10^{-6}$	-	-	-
<b>Breast tissue (fibroganular region)</b>	$3 - 44 \times 10^{-6}$	-	-	-
<b>Kevlar 49 fiber</b>	130	3.6	0.027	50
<b>High-tensile steel</b>	200	1.5	0.008	6

### 1.5.3. Biocompatibility

Sericins, the gum/glue-like proteins present in silk have been shown to cause decreased biocompatibility and increased hypersensitivity to non-purified silk. However, properly degummed and sterilized silk (purified silk) has good biocompatibility comparable to other commonly used biomaterials such as collagen [191,192]. The successful use of silk as medical sutures over the years has demonstrated the biocompatibility of this material [114,148,193]. Indeed, several studies have demonstrated minimal or no inflammation during subcutaneous implantation and *in vivo* testing of SF biomaterials for up to one year [144,149,194,195]. Despite these positive findings, mild pro-inflammatory cytokine production [192] and possible amyloidogenesis due to the presence of silk fibroin and degraded products of silk fibroin, respectively, have been observed [196]. Consequently, it is of great importance to extensively investigate the safety of SF biomaterials and their degraded products for long-term use *in vivo*.

*In vitro* studies have demonstrated the ability of SF to support the adhesion, growth and function of a variety of cell types including fibroblasts, keratinocytes [143,146,197], mesenchymal stem cells, chondrocytes, hepatocytes [139,148], neurons, macrophages, endothelial cells [139,197], epithelial cells, glial cells, osteoblasts [139,197], dorsal root ganglia, and Schwann cells [166] without affecting their normal phenotype or functionality, suggesting their biocompatibility for *in vitro* tissue modeling.

### 1.5.4. Biodegradation

The United States Pharmacopeia defines an absorbable biomaterial as a material that “loses most of its tensile strength within 60 days” post implantation *in vivo* [191]. Since silk has negligible tensile strength loss *in vivo* it is thus classified as a non-degradable biomaterial. Nevertheless, silk has been shown to be biodegradable over periods of time greater than 60 days



[191]. The degradation rate of SF biomaterials is dependent upon several processing factors such as preparation of SF scaffolds using aqueous or organic solvents, concentration of SF solution, and pore size [144]. Through *in vivo* subcutaneous implantations of SF porous scaffolds in Lewis rats, Wang *et al.* [144] demonstrated that aqueous-derived SF scaffolds degraded at a faster rate than SF scaffolds prepared using the organic solvent 1,1,1,3,3,3 hexafluoro-2-propanol (HFIP). It was observed that the aqueous-derived scaffolds held their structural integrity no longer than 6 months while remains of the HFIP-derived scaffolds were still present after 12 months. The increasing concentration of SF used in preparation of the scaffolds resulted in a slower degradation rate. Reduced tissue ingrowth and, therefore, a slower degradation rate was observed in scaffolds with smaller pore size. The degradation of 3D SF porous scaffolds is significantly affected by the activities of the host immune system [144,148]. Indeed, the resorption of these scaffolds was mediated by macrophages, suggesting that silk is not only biodegradable but also bio-resorbable [144,148].

*In vitro* treatment of *B. mori* SF fibers and films with proteolytic enzymes (collagenase Type F,  $\alpha$ -chymotrypsin Type I-S, and protease Type XXI from *Streptomyces griseus*) demonstrated that degradation of these materials was dependent upon the type of enzyme, treatment time, and ratio of enzyme-to-substrate [198]. Protease treatment caused a higher weight loss in SF films and higher loss of tensile strength in SF fibers than treatment with collagenase or  $\alpha$ -chymotrypsin [198]. Treatment of aqueous-derived SF electrospun scaffolds with Protease XIV confirmed the positive effects of this enzyme on SF degradation [195]. Although, the *in vitro* studies suggest that silk degradation is mediated by enzymatic digestion, Wang *et al.* [144] demonstrated that, *in vitro*, the effect of cytokines, enzymes, and other non-immune system-related factors on the degradation of SF was moderate compared to immune system-related

cellular components including macrophages. The degradation rate of SF biomaterials can be further hindered through incorporation of proteinase inhibiting agents such as ethylenediamine tetraacetic acid (EDTA) [199]. Given the factors and parameters involved in SF degradation, it is likely that the biodegradation rate of SF biomaterials can be controlled for extended time periods (from weeks to years) to meet the requirements associated with the regeneration of a target tissue or of drug delivery systems.

### 1.5.5. Binding sites

Amino acid sequences of SF determined from cDNA sequencing of *B.mori* domestic silkworm contains a large number of basic amino acids, including arginine, in their non-repetitive region near the C-terminus. On the other hand, the sequences of *Antheraea pernyi* wild silkworm contain not only the basic amino acids but also the tripeptide sequence arginine-glycine-aspartic acid (RGD) [146], a recognition site for integrin-mediated cell adhesion [200-202]. Fibroblast cell adhesion tested on both silk types demonstrated a higher cell adhesion on films formed by SF from *A. pernyi* than those from *B. mori* [146]. This difference in adhesion was attributed to the presence of the tripeptide RGD in the SF sequence from the wild silkworms. Minoura *et al.* [146] also demonstrated that removing the C-terminus region of the *B.mori* silk, which contains arginine amino acids, resulted in even less cell adhesion than adhesion on the non-modified *B.mori* silk. Thus, cell attachment onto *B. mori* SF biomaterial is likely due to alternative low-affinity cell binding domains [41] including arginine residues present in the non-repetitive region [139,146], and/or electrostatic interactions between cells and silk [41,139]. The effect of the RGD sequence on the attachment of mammalian cells to SF has been confirmed through various studies [41,143,171,186,203,204]. The cell attachment and early stages of cell-matrix interactions to *B. mori* SF are enhanced by modifying the SF biomaterial

surface through coating or chemical coupling with the integrin recognition sequence RGD or specific growth factors [41,143,186,203,204]. Introducing the fibronectin cell-adhesive sequence, RGD, onto the SF biomaterial enhanced cell attachment to this material [204,205]. Increased attachment and growth of endothelial cells were obtained when SF nets were coated with gelatin, fibronectin, or collagen type I [204]. Human bone marrow stromal cells (BMSCs) and human ACL fibroblasts showed increased cell attachment, spreading, and proliferation on RGD-modified SF matrices and silk films [41]. Moreover, human keratinocyte cell spreading, but not attachment, stimulated by laminin coating on SF microfibers, nanofibers, and films was increased [206]. Altman *et al.* [191] demonstrated that when SF films were decorated with RGD tripeptide the induction of bone formation *in vitro* was significantly enhanced due to increased integrin interaction for cell adhesion.

## **1.6. Engineered Silk-based Constructs**

### **1.6.1. Preparations**

Prior to constructing 3D SF scaffolds *B. mori* silk fibroin is extracted from silk cocoons as described by Rockwood *et al.* [207]. Although the purification process used in extraction of SF from the *B. mori* silk cocoons disrupts the  $\beta$ -sheet crystalline domains [208], treatments with organic solvents such as methanol, ethanol, or alcohol, water vapor annealing, mechanical stretching, or ultrasonic treatments lead to conformational change and self-organization of random coils into natural  $\beta$ -sheet structures [139,142,148,171,187,193,208]. This conformational change in SF and the formation of polymer crystallites upon these treatments makes the SF insoluble in aqueous environment and therefore suitable for *in vivo* implantation and *in vitro* manipulation [41,192].

Three-dimensional silk scaffolds have been used in different forms such as; films, hydrogels, microspheres, tubes, sponges, and nanofibers. The processing methods for generation of these constructs are summarized in Table 1.4.

**Table 1.4.** Preparation methods and properties of 3D SF biomaterials in various forms.

3D Form	Properties	Preparation Method
Films	<ul style="list-style-type: none"> <li>- Biocompatible</li> <li>- Water and oxygen permeable</li> <li>- Surface modification availability</li> <li>- Controlled morphological a structural features</li> <li>- Can be made patterned or non-patterned</li> <li>- Stable</li> </ul>	<ul style="list-style-type: none"> <li>- Casting [207]</li> <li>- Layer by layer deposition [209]</li> </ul>
Hydrogels	<ul style="list-style-type: none"> <li>- Biocompatible</li> <li>- Injectable</li> <li>- High water content</li> <li>- Controlled gelation</li> </ul>	sol-gel transition of aqueous SF solution by: <ul style="list-style-type: none"> <li>- Sonication [207,210,211]</li> <li>- Vortexing [207,212]</li> <li>- Presence of acids [213,214]</li> <li>- Presence of ions [213]</li> <li>- Application of direct electrical current [207,215].</li> </ul>
Microspheres	<ul style="list-style-type: none"> <li>- Biocompatible</li> <li>- Controllable size and shape</li> <li>- Tunable drug loading</li> <li>- Tunable drug release</li> </ul>	<ul style="list-style-type: none"> <li>- Phase separation [178,207]</li> <li>- Encapsulation in fatty acid lipid [177,207]</li> </ul>
Tubes	<ul style="list-style-type: none"> <li>- Biocompatible</li> <li>- Surface modification availability</li> <li>- Diameter variability</li> <li>- Surface can be texturized</li> <li>- Can be made porous if needed</li> </ul>	<ul style="list-style-type: none"> <li>- Dip method [174,207]</li> <li>- Gel-spun method [207,216]</li> </ul>
Sponges	<ul style="list-style-type: none"> <li>- Biocompatible</li> <li>- Porous structure</li> <li>- Controlled porosity</li> <li>- High strength</li> <li>- Surface modification availability</li> <li>- Mimic the <i>in vivo</i> physiological micro environment</li> <li>- High strength</li> <li>- Rough and hydrophilic surfaces</li> </ul>	<ul style="list-style-type: none"> <li>- Salt leaching [207,217]</li> <li>- Gas foaming [217]</li> <li>- Use of organic solvents [218]</li> <li>- Freeze-drying [217]</li> </ul>
Nanofibers	<ul style="list-style-type: none"> <li>- Biocompatible</li> <li>- Nano/micro fibrous structure</li> <li>- Controlled fiber size</li> <li>- Porous structure</li> <li>- Controlled porosity</li> <li>- High strength</li> <li>- Surface modification availability</li> <li>- Mimic the <i>in vivo</i> physiological micro environment</li> <li>- High strength and structural stability</li> </ul>	<ul style="list-style-type: none"> <li>- Electrospinning [58,141,188]</li> </ul>

### 1.6.2. Nanofibrous SF Scaffolds

The nano-fibrous structures within the ECM, mainly composed of structural proteins collagens types I, II, and III have diameters varying from 50 to 500 nm. These nano-fibrous structures provide the cells with the appropriate biological environment for embryologic development, organogenesis, cell growth, and wound repair [115,219,220]. These nanofibers are one to two orders of magnitude smaller than the cells allowing cell interaction with multiple fibers simultaneously and maintaining a 3D orientation [221]. This organization of the ECM in the form of nanofibers provides steady anchorage to cells, through integrin binding, and also activates intracellular signaling pathways affecting almost all aspects of cell behavior [222].

Recent advances in nanotechnology have led to a variety of approaches for the development of engineered scaffolds to create biomimetic ECM analogues [10,220]. More recently, the electrospinning process, a unique and versatile technique, enabled the development of nanofiber-based biomaterial scaffolds. The electrospinning technique is simple, efficient, inexpensive, and can be scaled-up for large-scale production [141,142]. With this technique a diverse set of polymers can be used to produce fibers from a few micrometers down to the tens of nanometers in diameter [131,141,142,223]. The generated scaffolds are useful for tissue engineering and regenerative medicine in part due to the similarity of the nanoscale properties of fibrous components to the native ECM [8,142,171]. Electrospinning offers the ability to tailor and control several aspects of ECM-like scaffolds such as the thickness and composition of nanofibers as well as fiber diameters and porosity [8,141,224,225]. The high surface area and porosity of electrospun nanofiber scaffolds allow favorable cell interactions [8]. The similarity of their 3D structure to natural ECM provides an excellent micro/nano environment for cell growth and natural function [8,171]. Further, electrospinning allows for the incorporation of growth

factors into the electrospun matrix for improved culture conditions [23]. As a result, electrospun nanofibrous structures have been extensively investigated as scaffolds for tissue engineering applications [8]. Table 1.5 summarizes the investigations of nanofibrous electrospun scaffolds in tissue engineering applications.

**Table 1.5.** Nanofibrous electrospun scaffolds and their tissue-engineering applications.

Target Tissue	Material	References
Bone	– Regenerated SF – PCL	[23,226-228] [21,229]
Bladder	– Fibrinogen – PCL and its composites	[230] [231]
Cardiac tissue	– Chitosan – Gelatin and its composites	[232] [233]
Cartilage	– Regenerated SF – PCL	[234] [39]
Mammary gland	– Regenerated SF	[58]
Nerve	– PCL and its composites – Gelatin and its composites – Chitosan – PLLA	[235,236] [235] [237] [238,239]
Skin tissue / Wound healing	– Collagen and its composites – PCL and its composites – Gelatin and its composites – Regenerated SF – poly(lactic acid-co-glycolic acid) (PLAGA) – Polyurethane (PU)	[65,240] [65,241] [241,242] [171,243] [67] [244]
Vascular grafts	– Regenerated SF – Collagen and its composites – PCL and its composites – Elastin and its composites – Gelatin and its composites – PLGA and its composites	[78,173] [119,245-251] [119,246-248] [117,249-253] [117] [117]

## 1.7. Conclusion and Rationale

Tissue engineering provides the medical field with approaches/tools to generate improved *in vitro* 3D culture models mimicking the physiological microenvironment of various biological tissues including normal and diseased breast tissues. Additionally, those approaches are also focused towards the goal of tissue and organ regeneration as an alternative to autologous and allogeneic tissue repairs. One of the major challenges of tissue engineering i.e., mimicking the nano-structures of ECM can be approached using electrospun nanofibrous polymeric scaffolds.

Data available underline the potential of nanofiber-based scaffolds for a variety of tissue engineering applications and their mimicry of ECM properties. In particular, SF-based electrospun nanofibrous scaffolds have led to the regeneration of biocompatible tissue culture conditions. SF is an attractive polymeric biomaterial for design, engineering, and processing into scaffolds for applications in controlled drug delivery, tissue repair and functional tissue engineering as highlighted by its successful applications.

Engineered 3D models of mammary tissue have been great tools for studying breast development and cancer initiation over the past three decades. Based on these studies, the importance of physical and chemical characteristics of the ECM, cell-cell, and cell-ECM interactions in the function and organization of the breast tissue have been highlighted. Although these 3D models have contributed tremendously to our knowledge of physiological activities in the normal or diseased mammary tissue, they can be improved upon to more accurately mimic not only the chemical characteristics of the biological tissue but also the physical environment to increase their appropriateness for *in vivo* testing and as potential implants.

SF nonfibrous scaffolds hold promise in developing appropriate 3D breast models and potential implants. Although the use of SF in modeling of mammary tissues is recent, proper physical and chemical SF nanofibrous scaffold modifications along with the incorporation of stromal cells likely will favor the development of functional mammary models as well as resorbable breast implants.

Our overall rationale for developing 3D breast models using laminin coated SF electrospun scaffolds is that constructing a 3D breast model system through the use of tissue engineered biocompatible nanofibrous scaffolds may prove to be more beneficial to the understanding of cancer development and the regeneration of a functional breast tissue than the current models

due to its structural properties closely mimicking the breast tissue ECM and the potential to allow direct control of the microenvironment at multiple levels and scales. Silk, which exhibits excellent biocompatibility and slow degradability will generate a tissue-engineered scaffold with great potential for use in breast tissue engineering. The formation of electrospun SF scaffolds composed of nanofibers will exhibit a structure similar to that of the ECM. The similarities between such a structure and the microenvironment of the breast tissue likely will result in cell-matrix interactions that are similar to those observed between cells and the ECM *in vivo*. The slow degradation time and excellent mechanical properties of SF will provide a stable structure for MCF10A cell attachment and survival. Air-flow electrospinning of SF scaffolds will result in formation of large pores resulting in MCF10A cell adhesion, survival, and infiltration. In addition to this structural support, MCF10A cells require integrin-mediated interactions with ECM protein laminin to organize into polarized growth-arrested structures that are resistant to apoptosis. Therefore, the coating of the nanofibers with the ECM protein laminin will enhance initial cell attachment and will promote MCF10A cell differentiation and structure formation.



## CHAPTER 2: PHYSICAL PROPERTIES AND MAMMARY EPITHELIAL BIOCOMPATIBILITY OF SILK FIBROIN ELECTROSPUN NANOFIBER SCAFFOLDS

### 2.1. Abstract

In the present study, the effects of various silk fibroin (SF) concentrations used in the generation of electrospun fiber scaffolds were investigated. First, the physical and mechanical properties of scaffolds obtained from 7%, 12%, and 17% silk concentrations were defined. In addition, attachment and viability of MCF10A mammary epithelial cells cultured onto these scaffolds were used to assess the biological suitability of these nanostructures. Results indicate that both fiber diameters and pore sizes significantly increased as SF concentration increased. The largest fibers ( $5.4 \pm 0.22 \mu\text{m}$ ) and pores ( $12.96 \pm 0.87 \mu\text{m}$ ) were formed following the electrospinning of 17% SF. Scaffolds with the largest fiber diameters exhibited the smallest specific surface areas. The average specific surface area (SSA) for 7, 12, and 17% scaffolds was  $2.54 \pm 0.04$ ,  $0.90 \pm 0.04$ , and  $0.64 \pm 0.02 \mu\text{m}^2$ , respectively. Additionally, following a 2-hour incubation, the highest cell attachment ( $66 \pm 7\%$ ) was observed on 7% SF electrospun scaffolds. MCF10A cell attachment on 7% scaffolds was significantly higher than MCF10A cell attachment on two-dimensional (2D) SF-coated cell culture vessels. MCF10A cell viability measured after 14 days in culture was similar on all electrospun scaffolds. In contrast, significantly higher MCF10A cell numbers were recorded in 2D SF-coated cell culture vessels. Taken together, these results highlight the biocompatibility of SF-based electrospun nanofiber scaffolds supporting MCF10A cell attachment and survival.

## 2.2. Introduction

Breast cancer involves complex set of interactions between mammary epithelial cells and the stroma, both extracellular matrix (ECM) and cells including adipocytes (fat cells) and fibroblasts (an abundant stromal cell within the connective tissue) [125]. Tools allowing modeling of the biological tissue including mammary tissue under physiological and pathophysiological conditions *in vitro* are becoming essential to better understand cancer initiation and progression [10]. The engineering of *in vitro* three-dimensional (3D) systems of mammary gland potentially allows a deeper understanding of the complex cell-cell and cell-ECM interactions involved during breast tissue development and cancer initiation and progression [10,107,254]. Furthermore, such 3D systems may provide a viable alternative for the investigation and testing of new drug or drug regimen [10]. The 3D engineered models of breast tissue also allow detailed monitoring of multiple concurrent cellular processes involved in tumor growth and invasion [12].

Suitable 3D *in vitro* mammary tissue models must have features of the native tissue microenvironment and ideally mimic the function and structure of the breast tissue [254]. The recent progress in tissue engineering support a tailored control of the microenvironment properties currently not possible using ECM based 3D approaches [10]. Within tissue engineering, electrospun nanofiber scaffolds in particular hold those promises. Electrospinning is a simple, efficient, and inexpensive technique that can be scaled-up for large-scale production [141,142]. Electrospinning allows the formation of fibers with diameters from a few micrometers to the tens of nanometers [131,141,142,223]. Non-woven nanofiber scaffolds electrospun from natural or synthetic polymers have been and are considered in tissue engineering and regenerative medicine in part because they have nanoscale properties similar to those of the fibrous components of biological ECM [131,142].

The potential of SF-based biomaterials in different forms, in particular, in the form of electrospun nanofibers in various tissue regeneration and repair applications has been investigated [142]. SF-based biomaterials offer significant advantages for tissue engineering applications due to their excellent mechanical properties, controllable biodegradability, hemostatic properties, low antigenicity and non-inflammatory characteristics [142,145], high oxygen permeability, high drug permeability, and resistance against enzymatic cleavage [146]. Non-woven micro-fibrous silk nets supported the adhesion and proliferation of a variety of human cell types including epithelial cells, endothelial cells, glial cells, osteoblasts, keratinocytes and fibroblasts [143,146,197]. Altman *et al.* [191] demonstrated that fibroin films induced bone tissue growth *in vitro* when seeded with osteoblasts. Moreover, 3D highly porous silk scaffolds seeded with chondrocytes supported cartilage tissue engineering and were suitable for osteogenesis and chondrogenesis of human bone marrow stem cells (hMSCs) [34]. Human adipose-derived stem cells have been grown on aqueous and HFIP-based porous silk sponges and chitosan/silk fibroin films for bone, adipose tissue engineering, and nerve regeneration applications [150,168,255].

The negligible tensile strength loss of SF-based scaffolds *in vivo* may be appropriate for the generation of long-term *in vitro* 3D mammary cell culture models and potentially *in vivo* implants [55].

In the present study we investigate the effects of increasing SF concentrations from 7% to 17% on the properties of the nanofibers generated through electrospinning and evaluate the attachment and survival of MCF10A human mammary epithelial cells.

## 2.3. Materials & Methods

### 2.3.1. Silk Extraction

*Bombyx mori* SF was extracted from silk cocoons (*Bombyx mori* silk cocoons, B quality, The Yarn Tree, Asheville, NC) as described by Rockwood *et al.* [207]. Briefly, after discarding the silk worms, 5 grams of cocoons were cut and boiled for 30 minutes in 2 liters of 0.02M Na<sub>2</sub>CO<sub>3</sub> (Sigma, Saint Louis, MO, USA) aqueous solution then rinsed 3 times (20 minutes each) in deionized (DI) water to remove the sericins. Silk fibers were left to dry overnight then dissolved in 9.3M LiBr (Fisher Scientific, Fair Lawn, NJ, USA), 12% (w/v), overnight (in 60°C for the first 4 hours). Silk solution was then dialyzed against DI water for 48 hours using 3500 MWCO dialysis tubes (Fisher Scientific) with repeated water changes after 1, 4, 6, 12, 12, and 12 hours. The regenerated dry SF sponge was collected by freezing extracted SF solution in -80°C followed by lyophilization (SP Scientific, Gardiner, NY, USA).

### 2.3.2. Electrospinning

The electrospinning techniques described by Barnes *et al.* [220] on a 6 mm in diameter solid stainless steel mandrel (Beverlin Manufacturing Company, Grand Rapids, MI, USA) was used. Extracted SF was dissolved in 1,1,1,3,3,3 hexafluoro-2-propanol (HFIP) (TCI America, Portland, OR, USA) at concentrations of 7, 12, and 17%. The SF solutions were loaded into 3 ml Becton Dickinson syringes with an 18 gauge blunt tip needle. The needle was subjected to +25 kV with an air-gap distance of 13 cm between the needle and the mandrel. A volume of 1.8 to 2 ml of the SF solution was dispensed at a rate of 5ml/h and electrospun on the target mandrel [58].

### 2.3.3. Scaffold Characterization

Scanning Electron Microscopy (SEM) was performed using a JEOL LV-5610 SEM (JEOL Ltd., Tokyo, Japan). Average fiber diameter and pore size of the electrospun structures were

measured using 100 random locations on each SEM image using ImageTool 3.0 software (Shareware provided by UTHSCSA, San Antonio, TX, USA).

#### 2.3.4. Specific Surface Area Evaluations

Statistical fiber diameter distributions in the electrospun scaffolds were determined based on the frequency distribution. Scaffold specific surface area (SSA) was evaluated as described earlier using the following equation:

$$\text{Specific surface area} = \frac{\text{Total Surface Area}}{\text{Total Volume}} = \frac{4 \sum_{i=1}^n D_i f_i}{\sum_{i=1}^n D_i^2 f_i}$$

Where  $D$  is fiber diameter,  $f$  is frequency of fiber distribution, and  $n$  is the fiber number counted [256].

#### 2.3.5. Mechanical Testing

Uniaxial tensile testing was performed on three sets of ‘dog bone’ shape scaffold samples (2.75 mm wide at their narrowest point with a gage length of 11 mm) for each silk concentration [257]. Two sets of the scaffold samples were soaked in 99.98% ethyl alcohol (PHARMCO-AAPER) for 1 hour followed by three 10-minute washes in Phosphate-Buffered Saline (PBS) (Cellgro, Manassas, VA, USA). One set of the scaffolds per each SF concentration were seeded with  $40 \times 10^3$  immortalized human mammary epithelial cells, MCF10A (ATCC, Manassas, VA, USA) per ‘dog bone’ and maintained in culture for 15 days (noted as “Hydrated With Cells” in the results section). A second set (non-cellularized) remained in culture media for 14 days (noted as “Hydrated No Cells” in the results section). The third set was soaked in 99.98% ethyl alcohol for 1 hour followed by three 10-minute washes in PBS immediately before uniaxial tensile testing (noted as “Hydrated in PBS” in the results section).

### 2.3.6. Cell Cultures

Electrospun scaffolds were disinfected through soaking in 99.98% ethyl alcohol for 1 hour followed by three 10-minute washes in PBS. Immortalized human mammary epithelial cells, MCF10A were seeded at  $40 \times 10^3$  cells per 10-mm diameter biopsy punches of electrospun SF scaffolds and maintained for up to 14 days at  $37^\circ\text{C}$  and 5%  $\text{CO}_2$ . MCF10A cells were cultured in growth media containing DMEM/F12 supplemented with 5% horse serum (both from Invitrogen, Carlsbad, CA, USA), 1% Penicillin (10,000 units/ml) and Streptomycin (10,000  $\mu\text{g}/\text{ml}$ ) (Cellgro), 20 ng/ml Epidermal Growth Factor (EGF) (BD Biosciences, San Jose, CA), 0.5  $\mu\text{g}/\text{ml}$  Hydrocortisone, 100 ng/ml Cholera Toxin, and 10  $\mu\text{g}/\text{ml}$  Insulin (all from Sigma) [51]. Half of the media volume was changed every 2 days.

### 2.3.7. Cell Attachment Analyses

Tissue culture well-plates were coated with 7.5% poly(2-hydroxyethyl methacrylate) (PHEMA) (Sigma) to prevent cells from attaching to cell culture plastic [258,259]. Ten-millimeter SF scaffold disks were disinfected through soaking in 99.98% ethyl alcohol for 1 hour followed by three 10-minute washes in PBS. Control 2D SF-coated cell culture vessels were prepared through vessel coating with SF (40 mg/ml). To reduce the adhesion of serum proteins, both scaffolds and control 2D SF-coated cell culture vessels were coated with 1% bovine serum albumin (BSA) (Gemini Bio-Products, West Sacramento, CA) solution for 30 minutes, followed by three 5-minute washes in PBS. One 10 mm diameter disinfected and BSA-coated SF scaffold disk was used per well. MCF10A cells ( $4 \times 10^4$  cells / scaffold) were seeded on these scaffold disks and the control 2D SF-coated cell culture vessels and incubated for 40 minutes before addition of further media to allow for better cell attachment. After 1 or 2 hours in culture the plates were gently shaken, each scaffold was taken out and dipped 5 times in a media-containing

well to wash off the non-attached cells. The number of non-attached cells suspended in each well was counted. The percentage of attached cells on each scaffold disk was calculated based on the number of non-attached cells.

### 2.3.8. Cell Viability Analyses

MCF10A cells ( $1 \times 10^4$  cells / scaffold) were seeded on 6-mm diameter disinfected scaffold disks and SF coated cell culture vessels. Cell viability was assessed on day 14 using colorimetric MTS [3-(4,5-dimethylthiazol-2-yl)-5-(3-carboxymethoxyphenyl)-2-(4-sulfophenyl)-2H-tetrazolium, inner salt] assays (CellTiter 96 ® Aqueous Non-Radioactive Cell Proliferation Assay, Promega, Madison, WI, USA), as described by the manufacturer. The metabolically active cells react with a tetrazolium salt in the MTS reagent to produce a soluble formazan dye with an absorption that can be measured at 490 nm. Numbers of cells per each condition were calculated based on standard curves and normalized to the percentages of attached cells.

### 2.3.9. Statistical Analysis

All parameters are expressed as mean  $\pm$  standard error of the mean (SEM). One-way analysis of variance (ANOVA) followed by the post-hoc Dunnett's Multiple Comparison Test were used to assess differences in fiber diameter, pore size, SSA, cell attachment, and cell viability between the electrospun scaffolds at different SF concentrations. Two-way ANOVA followed by the Benferroni's Multiple Comparison Test was used to assess the differences in elastic moduli between the electrospun scaffolds at different SF concentrations. *A priori*, p values below 0.05 were defined as significant.

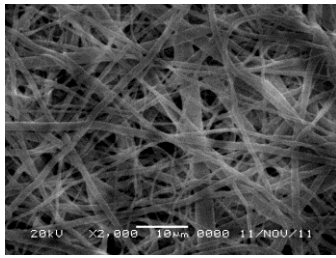
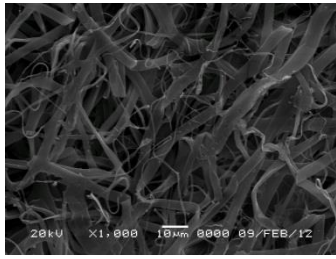
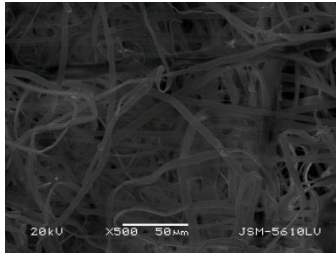
## 2.4. Results

### 2.4.1. Physical and Mechanical Characteristics of Electrospun SF Scaffolds

Electrospun scaffolds generated from three SF concentrations of 7, 12, and 17% were characterized based on SEM microphotographs (Table 2.1). Both fiber diameters and pore sizes of the electrospun SF scaffolds were measured and characterized on a sample of randomly selected fibers (Figures 2.1A and 2.1B, respectively).

Using a higher SF concentration in the generation of SF derived electrospun scaffolds lead to scaffolds with increased fiber diameters and pore sizes. The increase in fiber diameters and pore sizes was significantly correlated with an increase in SF concentrations ( $r^2 = 0.9997$ ,  $p < 0.05$  and  $r^2 = 0.9966$ ,  $p < 0.05$ , respectively, Figure 2.1A and B).

**Table 2.1.** Scanning electron micrographs of scaffolds derived from 7%, 12%, and 17% SF electrospun using a solid mandrel.

SF Concentration	Scanning Electron Microscopy Microphotographs	Average Fiber Diameter $\pm$ SEM ( $\mu\text{m}$ )	Average Pore Size $\pm$ SEM ( $\mu\text{m}$ )
7%		$1.19 \pm 0.06$	$3.2 \pm 0.13$
12%		$3.36 \pm 0.19$	$8.57 \pm 0.41$
17%		$5.40 \pm 0.22$	$12.96 \pm 0.87$



Scaffolds electrospun using 7% SF concentration resulted in the formation of significantly smaller fiber diameters and pore sizes than scaffolds electrospun using 12 and 17% SF concentrations (fiber diameter =  $1.19 \pm 0.06$  and pore size =  $3.2 \pm 0.13$   $\mu\text{m}$ ,  $p < 0.001$ ). The average scaffold fiber diameter and pore size generated following electrospinning of 12% SF were significantly smaller than the fiber diameter and pore size of scaffolds generated by electrospinning of 17% SF ( $p < 0.001$ ).

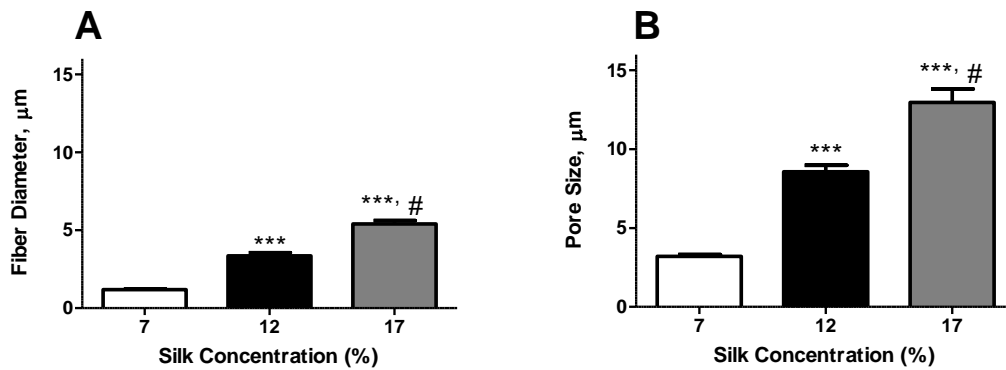


**Figure 2.1. Diameter and pore size in SF derived electrospun scaffolds. A) Fiber diameter.** \*\*\* indicates a significant difference from 7% SF ( $p < 0.001$ ). # indicates a significant difference from 12% SF ( $p < 0.001$ ). **B) Pore size.** \*\*\* indicates a significant difference from 7% SF ( $p < 0.001$ ). # indicates a significant difference from 12% SF ( $p < 0.001$ ).

To account for scaffold geometry, the SSAs of electrospun scaffolds derived from SF were calculated. Scaffolds derived from 7% SF concentration exhibited the highest SSA ( $2.54 \pm 0.04$   $\mu\text{m}^{-1}$ , Figure 2.2). This area was significantly higher than the SSA of the scaffolds derived from 12 and 17% SF ( $p < 0.001$ ). Similarly the SSA of 12% SF derived scaffolds was significantly higher than SSA of 17% SF derived scaffolds ( $p < 0.01$ ).

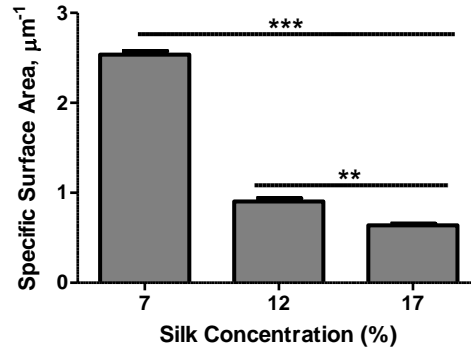


**Figure 2.2. Specific surface area (SSA in  $\mu\text{m}^{-1}$ ) of electrospun SF-derived scaffolds.** \*\*\* indicates significantly higher SSA in 7% SF derived scaffolds than 12 and 17% scaffolds ( $p < 0.001$ ). \*\* indicates significant difference between 12% and 17% SF derived scaffolds ( $p < 0.01$ ).

#### 2.4.2. Mechanical Strength of SF-derived Electrospun Scaffolds

The uniaxial tensile modulus of each scaffold hydrated with either PBS (HPBS), culture media no cells (HNC), or culture media with cells (HWC) was determined. Scaffold moduli were not different between the different hydration conditions tested (n.s., Figure 2.3). Moreover, no significant difference was observed in the elastic modulus of PBS-hydrated electrospun SF scaffolds generated using 7, 12, and 17% SF (n.s., Figure 2.3). Similarly, after an incubation in culture media alone (HNC) or with cells (HWC) for 14 days ( $37^{\circ}\text{C}$ , humidity  $>90\%$ ), the elastic moduli of scaffolds derived from 7, 12, and 17% SF were not significantly different (Figure 2.3).

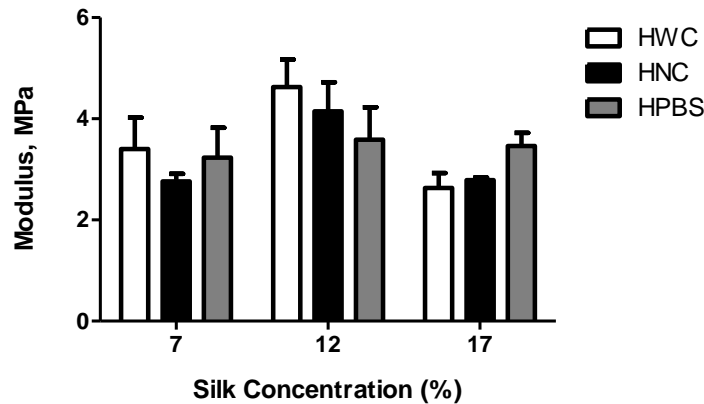


**Figure 2.3. Modulus of elasticity of 7, 12, and 17% SF-derived electrospun scaffolds.** No significant differences in the elastic moduli of the SF electrospun scaffolds.

### 2.4.3. MCF10A Cell Attachment and Viability on Electrospun SF Scaffolds

MCF10A cell attachment and viability were tested on electrospun SF scaffolds generated using 7, 12, or 17% SF and compared to cultures maintained on control 2D SF-coated culture vessels. After 1 hour in culture,  $43 \pm 7\%$ ,  $25 \pm 7\%$ , and  $32 \pm 6\%$  of the seeded MCF10A cells attached to different scaffolds derived from 7, 12, or 17% SF, respectively. After 2 hours in culture, MCF10A cell adhesion onto scaffolds generated using 7, 12, and 17% electrospun SF increased to  $66 \pm 7\%$ ,  $46 \pm 5\%$ , and  $51 \pm 5\%$ , respectively (Figure 2.4A and B). Following a 1- or 2-hour incubation, MCF10A cell attachment was not significantly different amongst the electrospun SF scaffolds tested (n.s. Figure 2.4A and B). No correlation between MCF10A cell adhesion and fiber diameter or pore size was observed ( $r^2 = 0.5371$ ,  $p > 0.05$  and  $r^2 = 0.5772$ ,  $p > 0.05$ , respectively, Figure 2.4A and B). Similarly, MCF10A cell adhesion was not significantly correlated with the SSAs of the scaffolds tested ( $r^2 = 0.9304$ ,  $p > 0.05$ , Figure 2.4A and B).

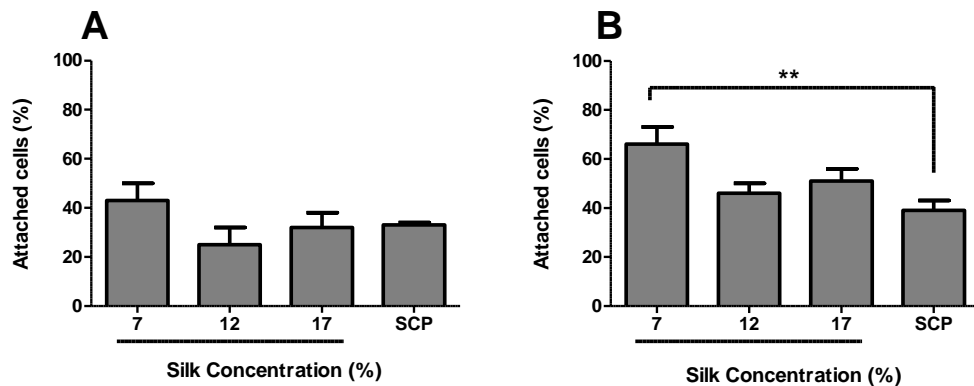


**Figure 2.4. MCF10A cell attachment onto 7, 12, and 17% SF-derived electrospun scaffolds compared to attachment on control SF coated culture vessels (SCP). A) After 1 hour.** No significant differences in cell adhesion between 3D and 2D cultures. **B) After 2 hours.** \*\* indicates significant difference from adhesion on 2D cultures ( $p < 0.01$ ).

MCF10A cell attachment on 3D electrospun SF-derived scaffolds was similar to MCF10A cell attachment to control 2D SF coated cell culture vessels after a 1-hour incubation (n.s. Figure 2.4A). Following a 2-hours incubation MCF10A cell attachment on 7% SF derived electrospun

scaffolds was significantly higher than MCF10A attachment on control SF coated culture vessels ( $p < 0.01$ , Figure 2.4B).

After 14 days in culture, numbers of viable MCF10A cells growing onto 7, 12, and 17% SF derived electrospun scaffolds were not significantly different (n.s., Figure 2.5). However, the numbers of viable MCF10A onto these SF derived scaffolds were significantly lower than the number of cells determined in the control 2D SF coated culture vessels ( $p < 0.001$ , Figure 2.5), Cell viability was not correlated with either fiber diameters, pore sizes, or SSAs of the scaffolds ( $r^2 = 0.9645$ ,  $p > 0.05$ ,  $r^2 = 0.5577$ ,  $p > 0.05$ , and  $r^2 = 0.9173$ , respectively, Figure 2.5).

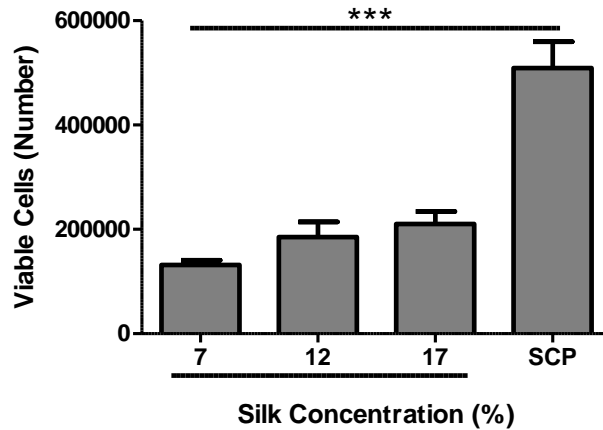


**Figure 2.5. MCF10A cell viability after 14 days in culture.** \*\*\* indicates significantly lower MCF10A cell numbers on 7, 12, and 17% SF derived scaffolds compared to SCP ( $p < 0.001$ ).

## 2.5. Discussion

Breast cancer initiation and progression involves a complex set of interactions between mammary epithelial cells and the stromal components including the ECM [125]. The engineering of appropriate *in vitro* mammary epithelial cell models will allow a deeper understanding of the complex effects of mammary stroma during breast cancer initiation, progression, and could also serve in the development and testing of new drugs [12]. Thus, here we investigated the physical and mechanical characteristics of SF electrospun scaffolds at 7, 12, and 17% SF concentrations.

The mechanical integrity of the SF scaffolds was tested by incubation in culture media with or without cells for 14 days. Biocompatibility of these scaffolds was evaluated through assessment of MCF10A cell adhesion and viability. Our results indicate that although the increasing SF concentration led to significant changes in physical properties of the electrospun scaffolds, the tensile strength of these scaffolds remained similar. Furthermore, MCF10A cell viability and adhesion on these electrospun scaffolds confirmed their biocompatibility.

As demonstrated with other polymers [220,251,260], our results indicate a linear relationship between SF solution concentrations, fiber diameters and pore sizes of SF-derived electrospun scaffolds. Specifically, fiber diameters and pore sizes significantly increased as the concentration of electrospun SF increased. Indeed, scaffolds generated using electrospun 17% SF had significantly larger pore sizes and fiber diameters than scaffolds derived from 12 and 7% SF. Furthermore, scaffolds derived from 12% SF had significantly larger pores and fibers than scaffolds generated from 7% SF. These results agree with previously demonstrated increases in fiber diameter observed when Poly(ethylene oxide) (PEO), Poly(glycolic acid) (PGA), Polydioxanone (PDO), or collagen type I were electrospun at higher polymer concentrations [220,225].

Our results also indicate that the scaffolds with smaller fiber diameters exhibited higher SSAs. Significantly higher SSAs were recorded in 7% SF derived electrospun scaffolds compared to either 12 or 17% SF derived electrospun scaffolds. Moreover, 12% SF scaffolds had significantly higher SSAs than 17% SF derived scaffolds. Our data concur with findings by Chen *et al.* [256] that electrospun poly( $\epsilon$ -caprolactone) (PCL) scaffolds with nanometer to micrometer fiber diameters demonstrated higher SSAs for scaffolds with smaller fiber diameters.

Furthermore, our data demonstrates that there is no significant difference in the elastic moduli of the 7, 12, and 17% SF derived electrospun scaffolds when hydrated in PBS. These results demonstrate that although higher elastic modulus should be seen due to larger fibers at higher concentration of SF, the presence of larger pores within these scaffolds counter balance the effects of large fibers, therefore, resulting in no change in the elastic moduli of these electrospun scaffolds. These observations and the fact that regardless of hydration condition, the electrospun SF-derived scaffolds retained their mechanical strength (after 14 days) underline the resilience of the silk mechanical properties essential to form a scaffold for tissue regeneration [42,142,186,191]. Our results also are in line with the unchanged mechanical properties of cell-seeded poly ( $\epsilon$ -caprolactone) (PCL) electrospun scaffolds compared with acellular scaffolds measured after three weeks in culture [261].

Non-woven micro-fibrous silk scaffolds have been shown to support the adhesion and proliferation of a variety of human cell types including epithelial cells, endothelial cells, glial cells, osteoblasts [197], keratinocytes and fibroblasts [143,197]. Our data indicates that SF derived scaffolds also provided support for MCF10A cell attachment. Although MCF10A cell attachments onto electrospun SF derived scaffolds all with SSAs below  $7 \mu\text{m}^{-1}$  were not significantly different, our results mimicked observations by Chen *et al.* [256] that although scaffolds with higher SSA promoted higher cell attachment, within SSA below  $7.13 \mu\text{m}^{-1}$ , cell attachment remained unchanged. As shown by Chehroudi *et al.* [262], our data comparing the adhesion of mammary epithelial cells to the fibrous scaffolds to their adhesion to the 2D SF-coated tissue culture vessels also demonstrated that epithelial cell attachment was higher onto grooved textured surfaces than flat smooth surfaces.

Although the numbers of viable cells on electrospun SF derived scaffolds were significantly lower in comparison to 2D cultures maintained on SF coated cell culture vessels, MCF10A cell viability amongst 7, 12, and 17% SF derived scaffolds were similar. This observation is comparable to observations by Xu *et al.* [263] of higher smooth muscle cell proliferation on 2D tissue culture vessels than on poly(l-lactid-co-ε-caprolactone) [P(LLA-CL)] nanofiber scaffolds.

## 2.6. Conclusion

Taken together the observations presented here suggest that electrospinning of SF leads to the formation of scaffolds with biocompatible properties. Moreover, the MCF10A cell attachment and viability on SF derived electrospun scaffolds detailed here suggest that this biomaterial will support human mammary epithelial cells and has the potential to be used in 3D modeling of the mammary tissue. The results specifically demonstrate that the ECM-like, porous nanofiber structure of electrospun SF scaffolds promoted MCF10A cell attachment. The low cell proliferation on these scaffolds is a feature that is essential in 3D modeling of breast tissue as mammary epithelial cells have low proliferation levels as they form growth-arrested differentiated structures. In further work, the generation of mammary epithelial structures will require the identification and addition of specific chemical cues to improve nanofiber electrospun SF scaffolds based mammary tissues.

## CHAPTER 3: EFFECTS OF AIR-FLOW ELECTROSPINNING ON PHYSICAL, MECHANICAL, AND BIOCOMPATIBILITY OF ELECTROSPUN SILK-BASED SCAFFOLDS

*Preface: The following manuscript has been published in the Journal of Tissue Engineering and Regenerative Medicine, 2013. The included work investigates the potential for incorporation of highly porous regions within silk fibroin electrospun scaffolds to enhance cellular infiltration and scaffold bioactivity through cellular adhesion and survival.*

### **Breast Epithelial Cell Infiltration in Enhanced Electrospun Silk Scaffolds**

Yas Maghdouri Moghaddam<sup>1,4</sup>, Lynne W. Elmore<sup>2,3</sup>, Gary L. Bowlin<sup>1</sup> and Didier Dréau<sup>4</sup>

<sup>1</sup>Department of Biomedical Engineering, Virginia Commonwealth University, Richmond, VA 23284

<sup>2</sup>Department of Pathology and <sup>3</sup>Massey Cancer Center, Virginia Commonwealth University, Richmond, VA 23298

<sup>4</sup>Department of Biology, University of North Carolina at Charlotte, Charlotte, NC 28223

### **3.1. Abstract**

In the present study, the effects of air-flow impedance electrospinning and air-flow rates on silk-based scaffolds for biological tissues were investigated. First, the properties of scaffolds obtained from 7% and 12% silk concentrations were defined. In addition, cell infiltration and viability of MCF-10A breast epithelial cells cultured onto these scaffolds were used to determine the biological suitability of these nanostructures. Air-flow impedance electrospun scaffolds resulted in an overall higher pore size than scaffolds electrospun on a solid mandrel with the



largest pores in 7% silk electrospun with an air pressure of 100 kPa and in 12% silk electrospun with an air-pressure of 400 kPa ( $13.4 \pm 0.67$  and  $26.03 \pm 1.19$   $\mu\text{m}$ , respectively). After 14 days in culture, the deepest MCF-10A cell infiltration ( $36.58 \pm 2.28$   $\mu\text{m}$ ) was observed into 7% silk air-flow impedance electrospun scaffolds subjected to an air pressure of 100 kPa. In those scaffolds MCF-10A cell viability was also highest after 14 days in culture. Taken together these results strongly support the use of 7% silk-based scaffolds electrospun with a 100 kPa air-flow as the most suitable microenvironment for MCF-10A infiltration and viability.

**Keywords:** Breast tissue engineering; Epithelial cells; Electrospinning; Porosity; Scaffold; Silk.

### 3.2. Introduction

Development of an appropriate *in vitro* breast epithelial cell model and a functional *in vitro* breast tissue depends on the ability to recreate the native tissue microenvironment. A suitable three dimensional (3D) *in vitro* microenvironment must account for the natural function and structure of the breast tissue. Indeed, the breast tissue extracellular matrix (ECM) plays an important role in the control of luminal epithelial cell gene expression and the induction and maintenance of their tissue specific function [254], and is crucial for proper patterning and function of the normal mammary gland [125]. The dominant components of the ECM are structural proteins: collagen, elastin, and reticular fibers. These proteins are synthesized as peptide monomers, which form polymers after covalent crosslinking. These polymers self-assemble to form fibrils, which then organize into fibers. These fibrous structures have diameters on the nanometer or submicrometer scales varying from 50 to 500 nm [115,219]. The structural ECM proteins are one to two orders of magnitude smaller than the cells, allowing cell interaction with multiple fibers simultaneously and maintaining a 3D orientation [221]. This organization of

the ECM in the form of nanofibers provides steady anchorage to cells, through integrin bindings, and activates intracellular signaling pathways affecting almost all aspects of cell behavior [222]. Within the past three decades multiple approaches have been used to develop *in vitro* 3D mammary gland models. Most of these 3D models use gel scaffolds, such as Matrigel<sup>®</sup> (BD Biosciences, San Jose, CA), collagen, or aqueous-derived porous silk scaffolds to mimic breast tissue microenvironment [50,51,54,56,83,122,125-127,185,186]. However, these gel scaffolds have different geometrical, mechanical, and physico-chemical properties from those of breast tissue ECM [131]. Furthermore, these scaffolds can contain residual growth factors and other unquantified substances, rendering their use challenging [264]. Nanofibers from natural or synthetic polymers electrospun into non-woven scaffolds have also been used to engineer ECM-like structures that closely resemble the microenvironments of various tissues, including breast [131]. Because they allow more control and further definition of the microenvironment parameters, nanofibers may lead to replicable *in vitro* 3D breast-like tissues that would be extremely useful tools to further our understanding of breast and other gland biology [10].

Porosity is a key parameter in the engineering of scaffolds for biomedical tissues and a highly porous scaffold is critical to control tissue formation in 3D [115]. To improve electrospun non-woven nanostructures, McClure *et al.* (2012) have introduced an air-flow impedance electrospinning technique, leading to the formation of nanofiber scaffolds that demonstrate higher porosity and greater cell infiltration without loss of mechanical property and structural integrity [221].

Natural biodegradable polymers such as collagen, gelatin, chitosan and silk fibroin (SF) have promising advantages over synthetic polymers because of their biocompatibility, biodegradability, bioresorbability [145], and high affinity for cell attachment [146]. Among these

natural polymers, silk-based biomaterials offer significant advantages for tissue engineering applications. They possess excellent mechanical properties, controllable biodegradability, hemostatic properties, low antigenicity and non-inflammatory characteristics [145], high oxygen permeability, high drug permeability, and resistance against enzymatic cleavage [146]. Naturally, silk consists of two types of proteins: a filament core protein, SF, and a glue-like coating family of hydrophilic proteins holding two fibroin fibers together, the sericins [143,145]. Sericins have been shown to decrease biocompatibility and increase hypersensitivity to silk [191]. However, when sericins are removed from silk, the biocompatibility of SF was comparable to other biomaterials [191]. Silk fibroin has been used as a biomaterial in various forms such as films [143,145], membranes [143,145], gels [145], sponges [143,145], powders, scaffolds [145], fibers, nets, meshes, and yarn [143]. Native *Bombyx mori* SF proteins do not contain arginine-glycine-aspartic acid (RGD) tripeptide binding domains associated with cell attachment [41]. Therefore, cell attachment on this biomaterial most likely results from alternative low-affinity cell binding domains [41] such as arginine residues present in the non-repetitive region near the carboxy-terminus [146], or electrostatic interactions between cells and silk [41]. Regardless of the scaffold type, *B. mori* SF supports the adhesion, growth and functions of a variety of cell types including fibroblasts, keratinocytes, mesenchymal stem cells, chondrocytes, hepatocytes, osteoblasts, neurons, macrophages, and endothelial cells [139,148]. Further non-woven micro-fibrous silk nets supported the adhesion and proliferation of a variety of human cell types including epithelial cells, endothelial cells, glial cells, osteoblasts, keratinocytes and fibroblasts [143,146,197]. Human adipose-derived stem cells have been grown on aqueous and 1,1,1,3,3,3 hexafluoro-2-propanol (HFIP)-based porous silk sponges and

chitosan/SF films for bone, adipose tissue engineering, and nerve regeneration applications [150,168,255].

Silk fibroin is the major component of a large subset of non-bioabsorbable biomedical sutures. The United States Pharmacopeia defines a biomaterial absorbable as a material that “loses most of its tensile strength within 60 days” post implantation *in vivo* [191]. Since silk has negligible tensile strength loss *in vivo* it is thus classified as a non-degradable biomaterial. Nevertheless, silk has been shown to be biodegradable over periods of time greater than 60 days [191].

The present study investigates the effects of air-flow electrospinning using increasing applied air pressure (AP) on the structure of silk scaffolds at 7% and 12% concentrations [143] and whether those scaffolds are a suitable microenvironment for breast epithelial cells as determined by MCF-10A cell infiltration and viability. This is an essential early step in the optimization of an air-flow impedance electrospun silk-based 3D nanofiber scaffold to generate functional breast-tissue 3D systems.

### **3.3. Materials & Methods**

#### **3.3.1. Silk Extraction**

*Bombyx mori* SF was extracted from silk cocoons (*B. mori* silk cocoons, B quality; The Yarn Tree, Asheville, NC, USA) as described by Rockwood *et al.* (2011) and Sofia *et al.* (2001) with minor modifications. Briefly, after discarding the silk worms, 5 grams of cocoons were cut and boiled for 30 minutes in 2 liters of 0.02M Na<sub>2</sub>CO<sub>3</sub> (Sigma, Saint Louis, MO, USA) aqueous solution then rinsed three times (20 min each) in deionized water to remove the sericins. Silk fibers were left to dry overnight then dissolved in 9.3M LiBr (Fisher Scientific, Fair Lawn, NJ), 12% (w/v), overnight (in 60°C for the first 4 hours). Silk solution was then dialyzed against

deionized water for 48 hours using 3500 MWCO dialysis tubes (Fisher Scientific) with repeated water changes after 1, 4, 6, 12, 12, and 12 hours. The regenerated dry SF sponge was collected by freezing extracted silk solution in  $-80^{\circ}\text{C}$  followed by lyophilization (SP Scientific, Gardiner, NY).

### 3.3.2. Electrospinning

The electrospinning techniques, as described by Barnes *et al.* (2007), on a solid mandrel and with air-flow impedance on a perforated mandrel, as described by McClure *et al.* (2012), were used. In the air-flow technique electrospinning the solid mandrel (Custom Design & Fabrication, Richmond, VA, USA) was replaced with a perforated mandrel connected to the air line (Figure 1). Pressurized air travelled through the lumen of this mandrel and exited through the pores impeding fiber deposition [221]. This air-flow impedance electrospinning leads to the formation of both highly porous regions (perforation regions), which allow cell infiltration, and dense fiber regions (flat regions), which provide structural stability [221].

Both mandrels were stainless steel and 6 mm in diameter. The perforated mandrel (Beverlin Manufacturing Company, Grand Rapids, MI, USA) is a hollow mandrel that contains 0.75 mm holes spaced 2.0 mm center to center, laterally. The center-to-center longitudinal distance was 1.5 mm. A lure lock (Becton Dickinson, Franklin Lakes, NJ, USA) was fitted and taped to one end of the perforated mandrel using Tartan electric tape (3M Company, St. Paul, MN, USA). A 3mm diameter solid mandrel was inserted into the opposite end of the perforated mandrel and secured in place using electric tape (3M Company) (Figure 3.1) [221]. The perforated mandrel was subjected to an applied AP of 0, 50, 100, 200, 300, and 400 kPa.

Extracted SF was dissolved in HFIP (TCI America, Portland, OR, USA) at concentrations of 7 and 12%. The silk solutions were loaded into Becton Dickinson syringes with an 18 gauge

blunt tip needle. The needle was subjected to +25 kV with an air-gap distance of 13 cm between the needle and the mandrel. A volume of 1.8 ml of the silk solution was dispensed at a rate of 5ml/h and electrospun on the target mandrel.

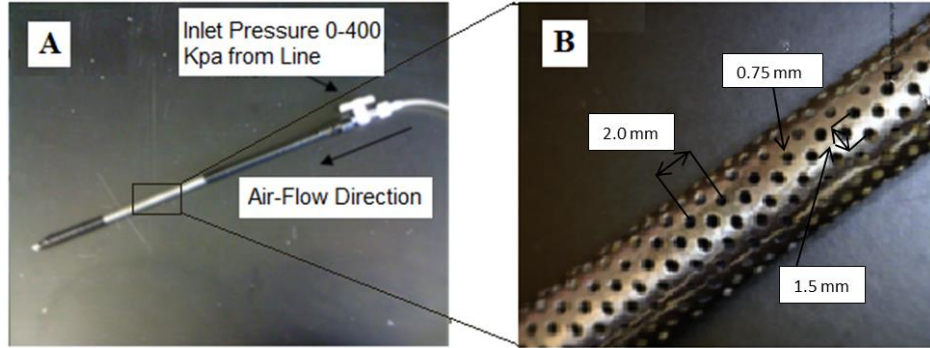


**Figure 3.1. Air-flow and perforated mandrel. A)** Air-flow connection and direction (arrows). **B)** Dimensions of the perforated mandrel used in air-flow electrospinning. Figure adapted from [221].

### 3.3.3. Scaffold Characterization

Scanning Electron Microscopy (SEM) was performed using a JEOL LV-5610 SEM (JEOL Ltd., Tokyo, Japan). Inner surface measurements were taken randomly for the solid mandrel and within the site of perforation and outside the site of perforation for the air-flow mandrel samples. Average fiber diameter and pore size of the electrospun structures were measured using 100 random locations on each SEM image using ImageTool 3.0 software (Shareware provided by UTHSCSA, San Antonio, TX, USA).

### 3.3.4. Cell Culture and Staining

Electrospun scaffolds were disinfected through soaking in 99.98% ethyl alcohol (PHARMCO-AAPER) for 1 hour followed by three 10-minute washes in Phosphate-Buffered Saline (PBS) (Cellgro, Manassas, VA, USA). Immortalized human mammary epithelial cells, MCF-10A (ATCC, Manassas, VA, USA) were seeded at  $15 \times 10^3$  cells per 10-mm diameter biopsy punch of electrospun silk scaffolds and maintained for up to 14 days at 37°C and 5% CO<sub>2</sub>.

MCF-10A cells were cultured in growth media containing DMEM/F12 (Invitrogen; Invitrogen Life Technologies, Grand Island, NY) supplemented with 5% horse serum (Invitrogen), 1% Penicillin (10,000 units/ml) and Streptomycin (10,000 µg/ml) (Cellgro), 20 ng/ml epidermal growth factor (EGF) (BD Biosciences, San Jose, CA, USA), 0.5 µg/ml hydrocortisone, 100 ng/ml cholera toxin, and 10 µg/ml Insulin (all from Sigma) [51]. Half of the media volume was changed every 2 days.

Following cell culture on electrospun silk scaffolds, scaffolds and cells were fixed in 4% formaldehyde for 20 min then rinsed in PBS at room temperature. Samples were permeabilized in 1:1000 Triton (MP Biomedicals, Solon, OH) and equilibrated briefly in 2X saline sodium citrate (SSC) (0.3 M NaCl, 0.03 M sodium citrate, pH 7.0; Kirkegard and Perry Laboratories, Gaithersburg, MD, USA) then treated with 100 µg/ml DNase-free RNase (ABgene, Surrey, U.K.) in 2X SSC for 20 minutes at 37°C. Samples were then incubated for 5 min with the fluorochrome base-intercalator propidium iodide (500nM; MP Biomedicals), which dyes the nuclei, then rinsed in 2X SSC.

### **3.3.5. Cell Viability Analysis**

MCF-10A cells ( $1 \times 10^4$  cells per scaffold) were seeded on 6-mm diameter disinfected scaffold disks and cell viability was examined on day 14. Cell viability (number of living cells) was assessed using MTS [3-(4,5-dimethylthiazol-2-yl)-5-(3-carboxymethoxyphenyl)-2-(4-sulfophenyl)-2H-tetrazolium, inner salt] assays (CellTiter 96 ® Aqueous Non-Radioactive Cell Proliferation Assay; Promega, Madison, WI, USA), as described by the manufacturer. The number of viable cells was calculated based on a standard curve defining the relationship between absorbance and cell number.

### 3.3.6. Cell Infiltration Measurements and Analyses

Fixed and stained scaffold-cell samples were soaked in 30% sucrose solution for 2 hours at 4°C. The samples were then embedded in Tissue-Tek® Optimal Cutting Temperature (OCT) compound (Ted Pella, Redding, CA, USA) and stored at -80°C. Frozen samples were cross-sectioned (20-µm thick sections) using a cryostat (MICROM GmbH, Walldorf, Germany). For each sample, 10 cross-sections were imaged using an Olympus IX71 fluorescent microscope equipped with a DP70 digital camera, using the 10X objective (Olympus, Tokyo, Japan). The distance from the surface of the scaffold to the center of 16 nuclei was measured at evenly spaced points (totaling 160 points per sample) using ImageTool 3.0 software.

### 3.3.7. Statistical Analysis

All parameters are expressed as mean  $\pm$  standard error of the mean (SEM). The characteristics of the electrospun silk samples, including their abilities to promote cell infiltration and cell viability, were analyzed using one-way analyses of variance followed by post-hoc tests to determine the differences between each treatment. *A priori*, p values below 0.05 are defined as significant.

## 3.4. Results

### 3.4.1. Characteristics of Electrospun Silk Scaffolds

Both fiber diameters and pore sizes of the inner surface of the silk scaffolds were characterized randomly for the solid mandrel and within the flat regions (dense fiber regions) and perforation regions (highly porous regions) of the perforated mandrel subjected to various AP (See Figures 3.2 and 3.3, respectively). Electrospun scaffolds generated from two silk concentrations of 7% and 12% were characterized based on SEM images (Table 3.1).

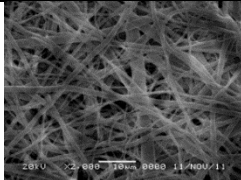
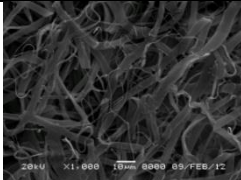
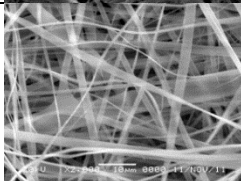
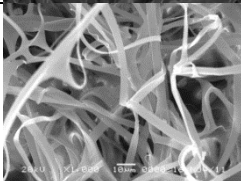
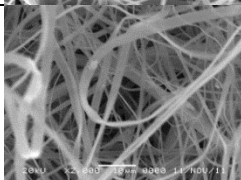
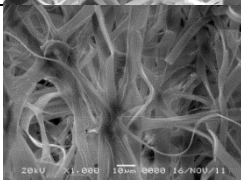
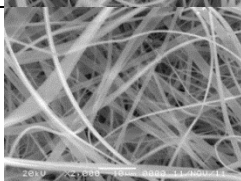
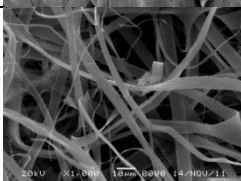
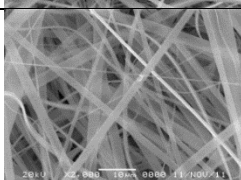
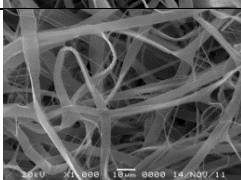
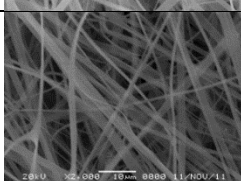
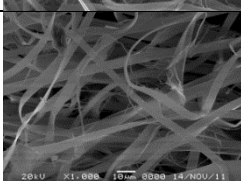
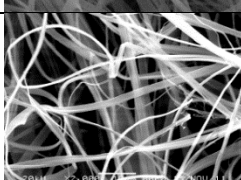
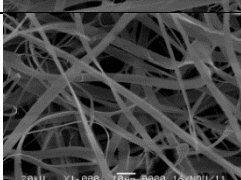


### 3.4.2. Effects of Air-flow Rate on Fiber Diameters and Pore Sizes in 7% Silk Scaffolds

As shown in Figure 3.2A, in 7% silk scaffolds the decrease in fiber diameter within the flat regions was correlated with an increase in the electrospinning AP from 0 to 400 kPa ( $r^2 = 0.97$ ,  $p < 0.001$ ). No correlation between the fiber diameter of 7% silk scaffolds and the electrospinning AP was observed within the perforation regions ( $r^2 = 0.0003$ ,  $p > 0.05$ ). However, in the flat regions, electrospinning with an AP of 0 and 50 kPa promoted significantly higher fiber diameters than the Solid Mandrel, electrospinning with AP of 300 kPa or 400 kPa ( $p < 0.05$ , 0.001, and 0.001, respectively). Electrospinning with an AP of 400 kPa promoted the smallest fiber diameter ( $0.99 \pm 0.07 \mu\text{m}$ ) in 7% silk scaffolds - a fiber diameter significantly smaller than those obtained through electrospinning at AP of either 0, 50, 100, or 200 kPa ( $p < 0.001$ , 0.001, 0.01, and 0.05, respectively).

In the perforation regions, electrospinning at AP of 50 kPa and 300 kPa promoted the smallest fiber diameter ( $0.92 \pm 0.04$  and  $1.04 \pm 0.06 \mu\text{m}$ , respectively  $p < 0.05$ ) in 7% silk scaffolds. Moreover, electrospinning at an AP of 50 kPa promoted significantly smaller fiber diameter than electrospinning on a Solid Mandrel, or at AP of 0, 100, 200, and 400 kPa ( $p < 0.05$ , 0.001, 0.01, and 0.05, respectively; Figure 3.2A). The average fiber diameter generated following electrospinning with an AP of 300 kPa was significantly smaller than the fiber diameter generated by electrospinning with an AP of 0 kPa ( $p < 0.05$ ).

**Table 3.1:** Micrographs of 7% and 12% electrospun silk scaffolds spun using a solid mandrel and from perforation regions subjected to AP of 0 to 400 kPa.

	7% Silk			12% Silk		
Mandrel Condition	SEM Image, Perforation Region 2000X	Avg. Fiber Diameter, $\mu\text{m} \pm \text{SEM}$	Avg. Pore Size, $\mu\text{m} \pm \text{SEM}$	SEM Image, Perforation Region 1000X	Avg. Fiber Diameter, $\mu\text{m} \pm \text{SEM}$	Avg. Pore Size, $\mu\text{m} \pm \text{SEM}$
<b>Solid Mandrel</b>		$1.19 \pm 0.06$	$3.20 \pm 0.13$		$3.36 \pm 0.19$	$8.57 \pm 0.41$ d.
<b>0 kPa</b>		$1.28 \pm 0.06$	$7.67 \pm 0.35$		$3.42 \pm 0.14$	$18.99 \pm 0.83$
<b>50 kPa</b>		$0.92 \pm 0.04$ a.	$7.12 \pm 0.33$		$3.60 \pm 0.21$	$13.74 \pm 0.36$ e.
<b>100 kPa</b>		$1.22 \pm 0.09$	$13.40 \pm 0.67$ b.		$3.75 \pm 0.18$	$20.36 \pm 0.7$
<b>200 kPa</b>		$1.26 \pm 0.08$	$5.52 \pm 0.33$		$2.91 \pm 0.19$ c.	$17.60 \pm 0.52$
<b>300 kPa</b>		$1.04 \pm 0.06$	$6.68 \pm 0.37$		$3.84 \pm 0.19$	$21.39 \pm 1.22$
<b>400 kPa</b>		$1.21 \pm 0.07$	$10.57 \pm 0.47$		$3.6 \pm 0.17$	$26.03 \pm 1.19$ f.

a. Significantly < SM, 0, 100, 200, 400 kPa;  $p < 0.05, 0.001, 0.01, 0.01, 0.05$   
b. Significantly > all conditions;  $p < 0.001$   
c. Significantly < 100 and 300 kPa;  $p < 0.05$  and  $0.01$   
d. Significantly < 100 and 300 kPa;  $p < 0.05$  and  $0.01$   
e. Significantly < 0, 100, 200, 300, 400 kPa;  $p < 0.001, 0.001, 0.01, 0.001, 0.001$   
f. Significantly > all conditions;  $p < 0.001$

The diameter of silk scaffold fibers in the perforation regions was not significantly different from the fiber diameters in the flat regions, except for scaffolds electrospun at an AP of 50 kPa, in which fibers had significantly smaller diameters ( $p < 0.001$ ). Overall, the average fiber diameters of 7% silk scaffolds were no different in scaffolds obtained through either air-flow electrospinning or electrospinning on a solid mandrel, except in the perforation region of scaffolds electrospun with an AP of 50 kPa ( $p < 0.05$ ; Figure 3.2A).

Air-flow electrospun scaffolds demonstrated significantly larger pore sizes compared to scaffolds spun using a solid mandrel for every condition tested ( $p < 0.001$ ; Figure 3.3A) except within the flat regions of scaffolds spun at an AP of 200 kPa. Air-flow electrospinning at AP of 0, 100, 200, 300, or 400 kPa promoted significantly larger pore sizes in scaffolds within the perforation regions compared to their counterpart flat regions ( $p < 0.001, 0.001, 0.05, 0.05, 0.001$ , respectively, Figure 3.3A). In these perforation regions, pore size increased from  $7.12 \pm 0.33$  to  $13.4 \pm 0.67 \mu\text{m}$  as electrospinning AP increased from 50 to 100 kPa ( $p < 0.001$ , Figure 3.3A). In contrast, an increase in the electrospinning AP from 100 to 200 kPa was associated with a 59% decrease in scaffold pore size (Figure 3.3A). A 48% increase in scaffold pore size was observed when the electrospinning AP was increased from 200 to 400 kPa ( $p < 0.001$ , Figure 3.3A). Pore sizes measured following an AP of 100 kPa and 400 kPa, were significantly different from each other ( $p < 0.05$ ;  $13.4 \pm 0.67$  and  $10.57 \pm 0.47 \mu\text{m}$ , respectively), and both of these conditions were significantly different from all other conditions tested ( $p < 0.001$ ).

Within the flat regions, electrospinning at AP of 50 kPa and 100 kPa promoted significantly larger pore sizes ( $6.76 \pm 0.37$  and  $6.93 \pm 0.42 \mu\text{m}$ , respectively), than those obtained in scaffolds electrospun on a solid mandrel, or with AP of 0, 200, and 300 kPa ( $p < 0.001, 0.001, 0.001, 0.01$ , respectively; Figure 3.3A). In either flat or perforation regions, no correlation was observed

between the scaffold pore size, and the electrospinning AP used to generate the 7% silk scaffolds ( $r^2 = 0.022$ ,  $p > 0.05$  and  $r^2 = 0.0025$ ,  $p > 0.05$ , respectively; Figure 3.3A).

### 3.4.3. Effect of Air-flow Rate on Fiber Diameters and Pore Sizes in 12% Silk Scaffolds

No correlation was detected between the 12% silk scaffold fiber diameters and changes in electrospinning AP within flat or perforation regions ( $r^2 = 0.53$ ,  $p > 0.05$ , and  $r^2 = 0.015$ ,  $p > 0.05$ , respectively; Figure 3.2B). In the flat regions, electrospinning with an AP of 300 kPa resulted in significantly larger fiber diameters than electrospinning on a solid mandrel, and at AP of 50, 100, and 200 kPa ( $p < 0.01$ , 0.05, 0.05, and 0.01, respectively). Electrospinning with an AP of 400 kPa promoted significantly larger fiber diameter than electrospinning on a solid mandrel ( $p < 0.05$ ).

Within the perforation regions, electrospinning at 200 kPa AP promoted significantly smaller fiber diameters than electrospinning at AP of 100 kPa and 300 kPa ( $p < 0.05$  and 0.01, respectively; Figure 3.2B). No significant difference was observed in fiber diameters between the flat and perforation regions for any of the conditions tested (Figure 3.2B). Overall, there was no improvement in the average fiber diameter of 12% silk scaffolds obtained through either air-flow electrospinning or spinning on a solid mandrel.

Pore sizes within the flat regions of 12% silk scaffolds were highly correlated with the increase in electrospinning AP from 0 to 400 kPa ( $r^2 = 0.97$ ,  $p < 0.001$ ; Figure 3.3B). However, no correlation was observed within the perforation regions of the scaffolds ( $r^2 = 0.58$ ,  $p > 0.05$ ). Within the flat regions of the 12% silk scaffolds, electrospinning at AP of 400 promoted a significantly larger pore size ( $21.36 \pm 1.11 \mu\text{m}$ ) than all other tested conditions ( $p < 0.001$ ; Figure 3.3B). Electrospinning at AP of 200 kPa and 300 kPa resulted in larger pore sizes in the

flat regions ( $13.98 \pm 0.46$  and  $16.35 \pm 0.87$ , respectively,  $p < 0.05$ ) than electrospinning with a solid mandrel or AP of 0, 50, and 100 kPa ( $p < 0.001$ , Figure 3.3B).

Pore sizes in 12% silk scaffolds were significantly larger within the perforation regions than within the flat regions for all conditions tested ( $p < 0.001$ ), demonstrating the effects of air-flow on fiber deposition. In the perforation regions, electrospinning with an AP of 400 kPa promoted significantly higher pore size ( $26.03 \pm 1.19 \mu\text{m}$ ,  $p < 0.001$ ; Figure 3.3B) than all other conditions tested. In these perforation regions, electrospinning with an AP of 50 kPa promoted significantly smaller pore sizes ( $13.74 \pm 0.36 \mu\text{m}$ ) than electrospinning with AP of 0, 100, 200, 300, and 400 kPa ( $p < 0.001, 0.001, 0.01, 0.001, 0.001$ , respectively). In addition, the pore size obtained through electrospinning with an AP of 300 kPa was significantly higher than following electrospinning with an AP of 200 kPa ( $p < 0.05$ ). Overall, scaffolds spun using air-flow electrospinning demonstrated significantly larger pore sizes in the perforation regions of all conditions tested than scaffolds spun on a solid mandrel ( $p < 0.001$ ; Figure 3.3B).

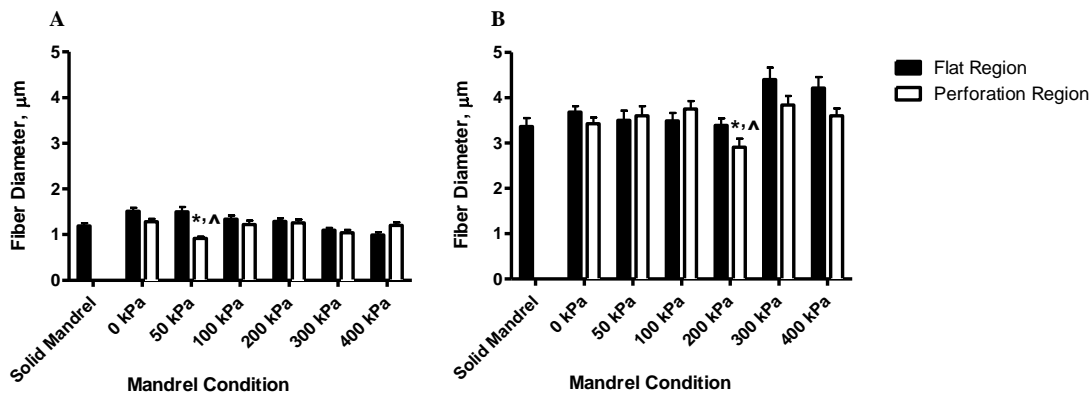


**Figure 3.2. Randomly measured average fiber diameters for the solid mandrel and within the perforation and flat regions of air-flow electrospun 7% and 12% silk scaffolds. A) 7% silk scaffolds.** \* indicates a significant difference from the flat region at AP of 50 kPa ( $p < 0.001$ ). ^ indicates a significant difference from perforation region of SM, AP of 0, 100, 200, 400 kPa ( $p < 0.05, 0.001, 0.01, 0.01, 0.05$ , respectively). **B) 12% silk scaffolds.** \* indicates a significant difference from the perforation region at AP of 100 kPa ( $p < 0.05$ ). ^ indicates a significant difference from the perforation region at AP of 300 kPa ( $p < 0.01$ ).

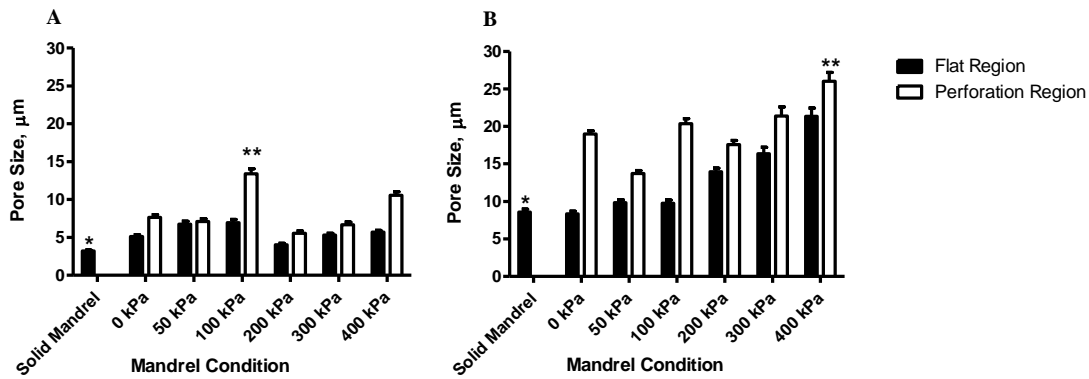
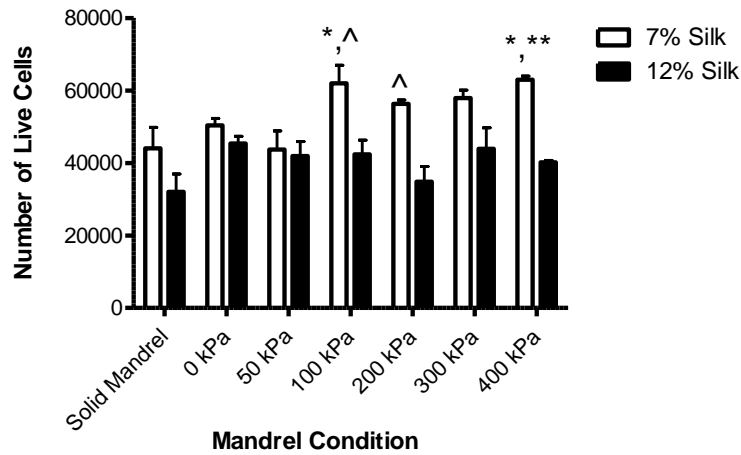


**Figure 3.3. Randomly measured average pore size for the solid mandrel and within the flat and perforation regions of the air-flow electrospun 7% and 12% silk scaffolds. A) 7% silk scaffolds.** \* indicates significantly smaller pore size than all conditions tested except the flat region at AP of 200 kPa ( $p < 0.001$ ). \*\* indicates a significant difference from all conditions tested ( $p < 0.001$ ). **B) 12% silk scaffolds.** \* indicates significantly smaller pore size from the flat regions at AP of 200, 300, and 400 kPa and the perforation regions of all conditions tested ( $p < 0.001$ ). \*\* indicates significantly higher pore size than all conditions tested ( $p < 0.001$ ).

#### 3.4.4. MCF-10A Cell Growth and Viability Seeded on 7% and 12% Electrospun Silk Scaffolds

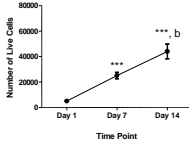
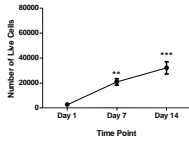
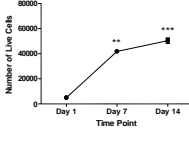
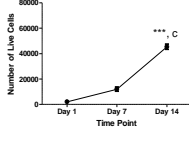
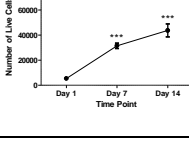
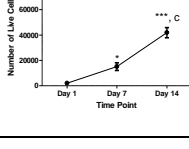
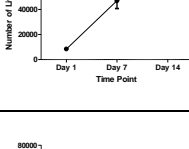
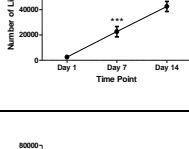
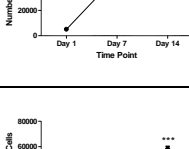
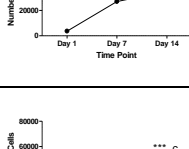
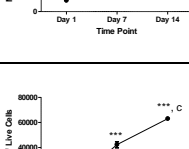
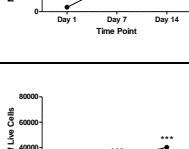
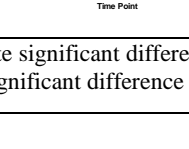
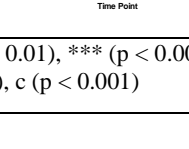
After 1 day in culture, about half of the seeded MCF-10A cells were attached to the electrospun silk scaffolds (Table 3.2). After 14 days in culture, there was a significant increase in the number of viable MCF-10A cells onto 7% and 12% silk scaffolds for all conditions tested ( $p < 0.05$ ; Table 3.2). However, this increase was modest compared to the number of viable cells in two-dimensional (2D) cultures maintained on positively coated tissue-culture treated vessels. No correlation was observed between the pore size and cell viability in either 7% or 12% silk scaffolds ( $r^2 = 0.539$ ,  $p > 0.05$  and  $r^2 = 0.293$ ,  $p > 0.05$ , respectively). Within 12% silk scaffolds, no significant difference in MCF-10A cell viability between all the conditions tested was observed (Figure 3.4). However, 7% silk scaffolds electrospun at AP of 100 and 400 kPa significantly promoted a higher MCF-10A cell viability ( $62.0 \times 10^3 \pm 5.0 \times 10^3$  cells and  $63.0 \times 10^3 \pm 1.0 \times 10^3$  cells, respectively) than 7% silk scaffolds electrospun at 50 kPa AP and

electrospun using a solid mandrel ( $43.7 \times 10^3 \pm 5.2 \times 10^3$  cells and  $44.0 \times 10^3 \pm 5.8 \times 10^3$  cells, respectively,  $p < 0.05$ ; Figure 3.4). Overall, 7% silk scaffolds obtained by electrospinning at AP of 100, 200, and 400 kPa promoted significantly higher cell viability than 12% silk scaffolds generated in the same conditions ( $p < 0.05$ , 0.05, and 0.01, respectively; Figure 3.4).



**Figure 3.4. MCF-10A cell viability on 7% and 12% electrospun silk scaffolds after 14 days in culture.** \* indicates a significant difference from Solid mandrel and 50 kPa ( $p < 0.05$ ). ^ and \*\* indicate a significant difference from their corresponding values for 12% silk (^  $p < 0.05$ , \*\*  $p < 0.01$ ).

**Table 3.2.** MCF-10A cell growth on 7% and 12% electrospun silk scaffolds after 1, 7, and 14 days in culture.

Mandrel Condition	7% Silk		12% Silk	
	Cell Growth	Number of Viable Cells at (Day 14 ± SEM) × 10 <sup>3</sup>	Cell Growth	Number of Viable Cells at (Day 14 ± SEM) × 10 <sup>3</sup>
<b>Solid Mandrel</b>		44.03 ± 5.81		32.01 ± 4.94
<b>0 kPa</b>		50.38 ± 1.92		45.37 ± 2.01
<b>50 kPa</b>		43.66 ± 5.18		41.87 ± 4.0
<b>100 kPa</b>		61.97 ± 4.96		42.33 ± 3.97
<b>200 kPa</b>		56.30 ± 1.05		34.84 ± 4.19
<b>300 kPa</b>		57.89 ± 2.19		43.91 ± 5.80
<b>400 kPa</b>		62.97 ± 0.98		40.18 ± 0.51

\*, \*\*, and \*\*\* indicate significant difference from Day 1. \* (p < 0.05), \*\* (p < 0.01), \*\*\* (p < 0.001)  
a, b, and c indicate significant difference from Day 7. a (p < 0.05), b (p < 0.01), c (p < 0.001)



### 3.4.5. MCF-10A Cell Infiltration into 7% and 12% Porous Silk Scaffolds

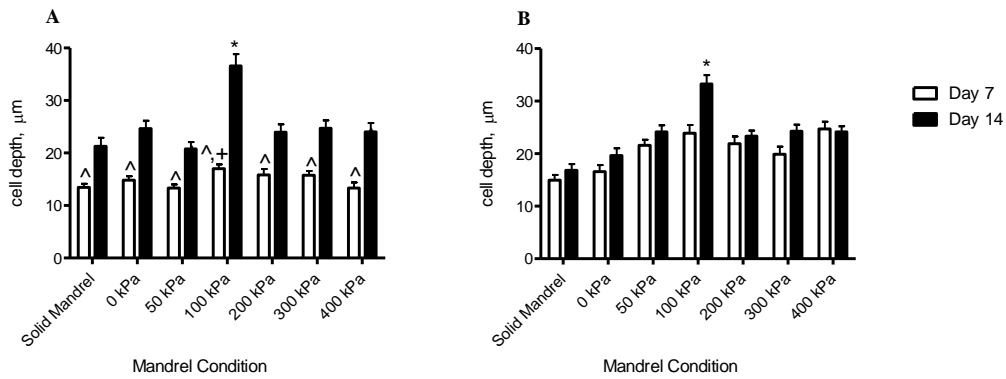
Static cultures of MCF-10A cells were maintained for up to 14 days on both 7% and 12% silk scaffolds obtained following either electrospinning using air-flow electrospinning or electrospinning on a solid mandrel. The ability of MCF-10A cells to migrate and colonize the scaffolds (i.e., the MCF-10A cell infiltration within the scaffolds) was assessed by nucleic acid staining (Figure 3.5 and Table 3.3).

In 7% silk scaffolds, no correlation was observed between the electrospinning AP used to generate the scaffolds and MCF10A cell infiltration ( $r^2 = 0.018$ ,  $p > 0.05$ ; Figure 3.5A). However, the increase in pore size within 7% silk scaffolds significantly correlated with increased cell infiltration after 14 days of culture ( $r^2 = 0.64$ ,  $p < 0.05$ ). MCF10A cell infiltration into 7% silk scaffolds increased significantly from day 7 to day 14 in all conditions tested ( $p < 0.001$ ). The greatest increase in MCF10A cell infiltration between day 7 and day 14 was observed in 7% silk scaffolds obtained through electrospinning with an AP of 100 kPa ( $17.01 \pm 0.84 \mu\text{m}$  vs.  $36.58 \pm 2.28 \mu\text{m}$ ;  $p < 0.001$ ; Figure 3.5A). MCF10A cell infiltration onto 7% silk scaffolds obtained through electrospinning with an AP of 100 kPa was significantly higher than onto 7% silk scaffolds obtained through electrospinning with an AP of 50 kPa or those electrospun on a solid mandrel ( $p < 0.05$ ) after 7 days of culture, and significantly higher than in all other scaffolds tested after 14 days in culture ( $p < 0.001$ ; Figure 3.5A). On day 14, MCF10A cell infiltrations were not different between air-flow electrospun scaffolds at AP of 0, 50, 200, 300, and 400 kPa and scaffolds spun using a solid mandrel (Figure 3.5A).

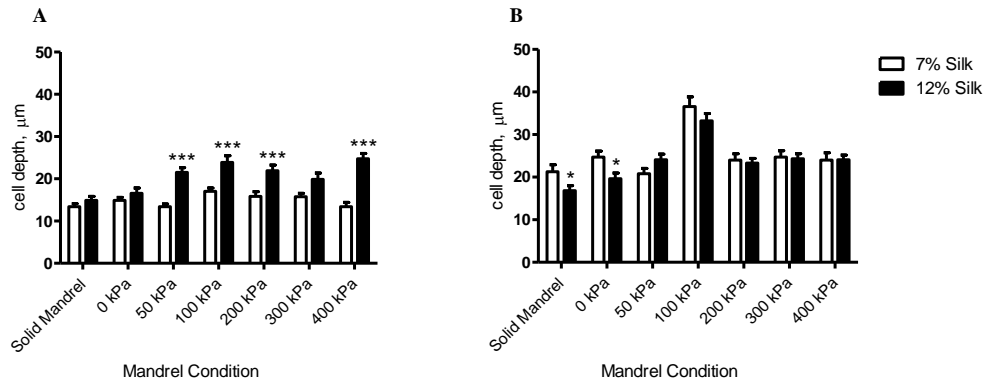
From day 7 to day 14, MCF10A cell infiltration in 12% silk scaffolds increased significantly only in scaffolds electrospun with 100 kPa AP ( $23.9 \pm 1.57$  vs.  $33.27 \pm 1.71 \mu\text{m}$ ,  $p < 0.001$ ). The AP used during the electrospinning of 7% or 12% silk to generate different scaffolds and the

resulting MCF10A cell infiltration were not correlated ( $r^2 = 0.0008$ ,  $p > 0.05$ ). In addition, in 12% silk scaffolds no correlation was observed between pore size and cell infiltration after 14 days ( $r^2 = 0.256$ ,  $p > 0.05$ ). After 7 days in culture, 7% or 12% scaffolds electrospun at AP of 50, 100, 200, and 400 kPa promoted significantly higher MCF10A cell infiltration than scaffolds electrospun on a solid mandrel ( $p < 0.01$ , 0.001, 0.01, and 0.001, respectively). On day 7, 12% silk scaffolds electrospun at AP of 100 kPa and 400 kPa promoted significantly higher MCF-10A cell infiltration than scaffolds electrospun at 0 kPa ( $p < 0.01$  and 0.001, respectively). On day 14, 7% or 12% scaffolds obtained through an AP of 100 kPa promoted significantly higher MCF10A cell infiltration ( $33.27 \pm 1.7 \mu\text{m}$ ) than all other conditions tested ( $p < 0.001$ ; Figure 3.5B). Overall, on day 14 of culture 12% silk scaffolds obtained following electrospinning at AP of 50, 100, 200, 300, and 400 kPa promoted significantly higher MCF10A cell infiltration than scaffolds electrospun on a solid mandrel ( $p < 0.01$ , 0.05, 0.01, and 0.01, respectively; Figure 3.5B).

After 7 days in culture 12% silk scaffolds generated following electrospinning at AP of 50, 100, 200, and 400 kPa promoted significantly higher MCF-10A cell infiltration than 7% silk scaffolds obtained following electrospinning at the same APs ( $p < 0.001$ , Figure 3.6). After 14 days in culture, no difference in MCF-10A cell infiltration was detected between 7% and 12% silk scaffolds except for those electrospun using a solid mandrel and those electrospun at AP of 0 kPa. Under these two conditions, using 12% silk scaffolds promoted significantly lower MCF-10A cell infiltration than 7% silk scaffolds ( $p < 0.05$ ; Figure 3.6B).

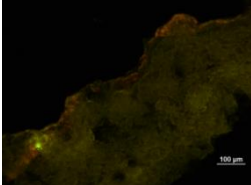
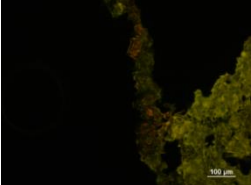
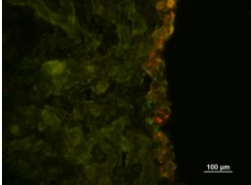
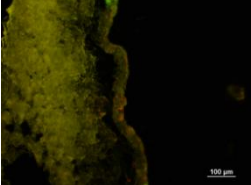
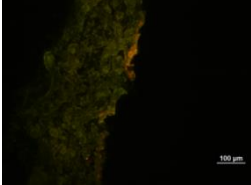
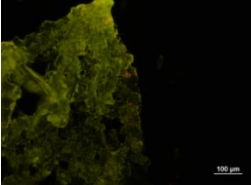
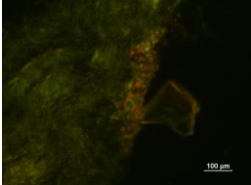
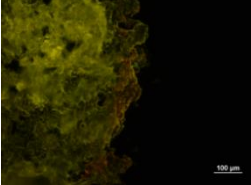
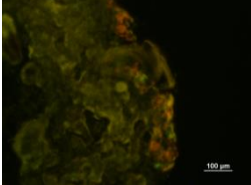
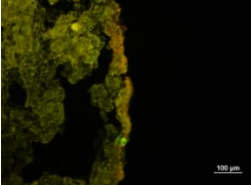
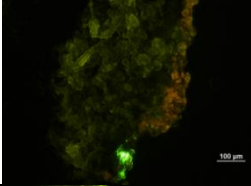
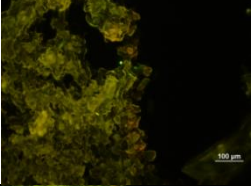
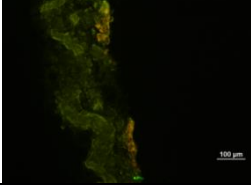
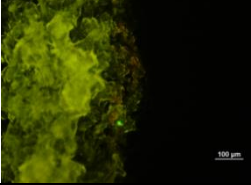


**Figure 3.5. MCF-10A cell infiltration through 7% and 12% electrospun silk scaffolds after 7 and 14 days in culture. A) 7% silk scaffold.** \* indicates a significant difference from all conditions tested at day 14 ( $p < 0.001$ ). + indicates a significant difference from Solid Mandrel and 50 kPa at day 7 ( $p < 0.05$ ). ^ indicates a significant difference between days 7 and 14 for all conditions tested ( $p < 0.05$ ). **B) 12% silk scaffolds.** \* indicates a significant difference from all conditions tested and day 7 at AP of 100 kPa ( $p < 0.001$ ).



**Figure 3.6. MCF-10A cell infiltration comparison between 7% and 12% Silk scaffolds after 7 and 14 days in culture. A) After 7 days in culture.** \*\*\* indicates a significant difference from 7% silk at AP of 50, 100, 200, and 400 kPa ( $p < 0.001$ ). **B) After 14 days in culture.** \* indicates a significant difference from 7% silk at SM and AP of 0 kPa ( $p < 0.05$ ).

**Table 3.3.** Nucleic acid staining of MCF-10A cell infiltration through 7% and 12% silk scaffolds spun using a solid mandrel and a perforated mandrel subjected to air pressure of 0 to 400 kPa.

Mandrel Condition	7% Silk			12% Silk		
	Day 14 Infiltration, 10X Objective	Avg. Thickness, $\mu\text{m} \pm \text{SEM}$ (Prior to seeding)	Avg. Cell Infiltration, $\mu\text{m} \pm \text{SEM}$	Day 14 Infiltration, 10X Objective	Avg. Thickness, $\mu\text{m} \pm \text{SEM}$ (Prior to seeding)	Avg. Cell Infiltration, $\mu\text{m} \pm \text{SEM}$
<b>Solid Mandrel</b>		300 $\pm$ 5.77	21.27 $\pm$ 1.65		693 $\pm$ 11.86	16.82 $\pm$ 1.21
<b>0 kPa</b>		167 $\pm$ 14.53	24.70 $\pm$ 1.46		807 $\pm$ 11.86	19.63 $\pm$ 1.35
<b>50 kPa</b>		463 $\pm$ 13.33	20.83 $\pm$ 1.25		937 $\pm$ 16.56	24.12 $\pm$ 1.29
<b>100 kPa</b>		177 $\pm$ 6.67	36.58 $\pm$ 2.28 a.		850 $\pm$ 18.86	33.27 $\pm$ 1.71 b.
<b>200 kPa</b>		330 $\pm$ 11.55	23.98 $\pm$ 1.48		923 $\pm$ 11.86	23.32 $\pm$ 1.11
<b>300 kPa</b>		147 $\pm$ 6.67	24.74 $\pm$ 1.49		957 $\pm$ 28.80	24.29 $\pm$ 1.22
<b>400 kPa</b>		140 $\pm$ 5.77	24.02 $\pm$ 1.73		930 $\pm$ 17	24.12 $\pm$ 1.09
a. Significantly > all conditions; $p < 0.001$ b. Significantly > all conditions; $p < 0.001$						

### 3.5. Discussion

We and others have shown the formation of acinar and ductal structures in 3D cultures of mammary epithelial cells maintained on gel matrices and aqueous-derived SF scaffolds, respectively [56,265]. Here we investigated the use of electrospun nanofiber silk-based scaffolds for similar purposes. To determine which condition provided a more suitable microenvironment for MCF-10A cell viability and infiltration, we cultured MCF-10A breast epithelial cells on 7% and 12% silk scaffolds generated by electrospinning on a solid mandrel and electrospinning on a perforated mandrel using air pressures of 0-400 kPa. The results indicate that air-flow electrospinning of 7% and 12% silk scaffolds resulted in formation of larger pore sizes than electrospinning on a solid mandrel modulating the MCF-10A cell adhesion and proliferation on these electrospun silk scaffolds.

Electrospinning is a simple process and allows the formation of porous structures with fiber diameters from a few nanometers to a few micrometers [219,220]. Tissue engineering scaffolds prepared by electrospinning process mimic the characteristics of natural ECM, such as fiber diameter, high porosity, and interconnected architecture [266]. Here, we developed scaffolds fabricated through air-flow impedance electrospinning containing highly porous regions (perforation regions), which allow cell infiltration, and dense fiber regions (flat regions), which provide structural stability. Therefore, these scaffolds offer a more porous structure without the loss of mechanical performance [221].

Our data demonstrates the effects of electrostatic forces and air-flow on fiber deposition and generation of less dense and more porous structures with larger pore sizes. More specifically, 7% silk scaffolds electrospun at 100 kPa AP and 12% silk scaffolds electrospun at 400 kPa AP demonstrated significantly larger pore sizes than all the conditions tested. Our observations

demonstrating formation of larger pore sizes within scaffolds obtained through air-flow electrospinning concur with McClure *et al.* (2012) observations in which poly ( $\epsilon$ -caprolactone) (PCL) scaffolds electrospun using a perforated mandrel at 50 kPa and 100 kPa AP exhibited significantly larger pore sizes than scaffolds spun using a solid mandrel.

The physical features of the microenvironment present in one of the conditions tested (7% silk scaffold obtained following electrospinning at 100 kPa AP) provided improved support for MCF-10A cell survival and greatest MCF-10A cell infiltration compared to all other conditions tested. The higher level of cell infiltration through 7% silk scaffolds spun at AP of 100 kPa is related to the larger pores present on this scaffold. This result mirrors the observations by McClure *et al.* [221] of an increased human dermal fibroblast cell infiltration through air-flow electrospun scaffolds subjected to 0-100 kPa AP. The higher cell viability and proliferation within 7% silk scaffolds may be related to the smaller fiber diameters. These observations support Li *et al.*'s (2006) demonstration that chondrocyte proliferation was higher in nanofiber scaffold cultures than in microfiber scaffold cultures [267]. The limited MCF-10A cell attachment to silk scaffolds observed here is remarkably similar to the attachment to *B. mori* SF films of Saos-2 osteoblast-like cells [151]. Others have shown that non-woven microfibrillar silk nets supported the adhesion and proliferation of a variety of human cell types including epithelial cells, endothelial cells, glial cells, osteoblasts [197], keratinocytes and fibroblasts [143,197].

In the conditions tested, although high MCF-10A cell infiltration through 7% silk scaffolds generated through electrospinning at an AP of 100 kPa was observed, the entire scaffold was not colonized. To further increase cell infiltration into these structures, we are currently improving both the silk scaffold and culture conditions. The observations presented here are a proof-of-concept demonstration that a perforated mandrel along with air-flow impedance electrospinning

leads to the formation of silk scaffolds with biocompatible properties. Moreover, the MCF-10A cell growth and viability on electrospun silk fibroin scaffolds detailed here suggest that this biomaterial will support human mammary epithelial cell proliferation and has the potential to be used to 3D model or regenerate the breast tissue.

### **3.6. Conclusion**

These findings further support the use of air-flow impedance technique rather than solid mandrel electrospinning to generate silk scaffolds compatible with MCF10A cell growth. The results demonstrate that nanofiber electrospun silk scaffolds spun using air-flow impedance technique generated a highly porous matrix. In particular, within the conditions tested, 7% silk electrospun scaffolds spun at an AP of 100kPa promoted higher cell infiltration and viability possibly because of the porous nanofiber structures used here had physical properties closer to the breast ECM, providing the most suitable microenvironment for the 3D *in vitro* culture of the human breast epithelial MCF-10A cells.

## CHAPTER 3S: EFFECTS OF AIR PRESSURE ON MECHANICAL PROPERTIES AND BIOCOMPATIBILITY OF SILK FIBROIN DERIVED ELECTROSPUN SCAFFOLDS

*Preface: The following chapter is supplemental data to Chapter 3. The included work investigates mechanical properties and biocompatibility of silk fibroin electrospun scaffolds derived from 7% silk fibroin following air-flow electrospinning at various air pressures.*

### 3S.1. Abstract

To supplement the data presented in the previous chapter, the effects of air-flow impedance electrospinning and air-flow rates on 7% silk fibroin (SF)-based scaffolds were investigated. First, the specific surface area (SSA) and mechanical properties of scaffolds obtained from 7% SF concentration were defined. Moreover, cell adhesion and viability of MCF10A breast epithelial cells cultured onto these scaffolds were used to determine the biological suitability of these nanostructures. There were no significant differences between the SSAs of the scaffolds derived from SF electrospun on a solid mandrel or using different air pressures (APs). All of the scaffolds retained their mechanical strengths after remaining in culture for 14 days, with or without cells. No significant difference was observed in the elastic moduli of the scaffolds hydrated in PBS. After incubation in culture media for 14 days without cells, scaffolds derived from SF electrospun with APs of 100 and 400 kPa exhibited the lowest elastic modulus. After a 14-day incubation in culture media along with cells, the elastic moduli of scaffolds derived from SF electrospun on a solid mandrel were significantly higher than the moduli of scaffolds derived



from SF electrospun at APs of 50, 300, and 400 kPa ( $p < 0.05$ ). MCF10A cell attachment was significantly higher on scaffolds derived from SF electrospun at an AP of 100 kPa than cell attachment onto scaffolds obtained following electrospinning of SF at 200 kPa AP. MCF10A viability on scaffolds derived from SF electrospun at an AP of 200 kPa was higher than cell viability on scaffolds derived from SF electrospun on a solid mandrel. These results provide additional evidence of the suitability of SF-derived scaffolds, prepared using air-flow electrospinning technique for MCF10A adhesion and viability.

### 3S.2. Introduction

Refer to section 3.2.

### 3S.3. Materials & Methods

#### 3S.3.1. Silk Extraction

Refer to section 3.3.1.

#### 3S.3.2. Electrospinning

Refer to section 3.3.2.

#### 3S.3.3. Specific Surface Area Evaluations

Statistical fiber diameter distributions in the electrospun scaffolds were determined based on the frequency distribution using fiber diameters in both flat and perforation regions. Scaffold specific surface area (SSA) was evaluated as described earlier using the following equation:

$$\text{Specific surface area} = \frac{\text{Total Surface Area}}{\text{Total Volume}} = \frac{4 \sum_{i=1}^n D_i f_i}{\sum_{i=1}^n D_i^2 f_i}$$

Where  $D$  is fiber diameter and  $f$  is frequency of fiber distribution, and  $n$  is the fiber number counted [256].

### **3S.3.4. Mechanical Testing**

Uniaxial tensile testing was performed on three sets of ‘dog bone’ shape scaffold samples for each silk concentration. Two sets of the scaffold samples were soaked in 99.98% ethyl alcohol (PHARMCO-AAPER) for 1 hour followed by three 10-minute washes in Phosphate-Buffered Saline (PBS) (Cellgro, Manassas, VA, USA). One set of the scaffolds per each SF concentration were seeded with  $40 \times 10^3$  immortalized human mammary epithelial cells, MCF10A (ATCC, Manassas, VA, USA) per ‘dog bone’ and maintained in culture for 15 days (noted as “Hydrated With Cells” in the results section). A second set (non-cellularized) remained in culture media for 15 days (noted as “Hydrated No Cells” in the results section). The third set was soaked in 99.98% ethyl alcohol for 1 hour followed by three 10-minute washes in PBS immediately before uniaxial tensile testing (noted as “Hydrated in PBS” in the results section).

### **3S.3.5. Cell Culture Media**

Refer to section 3.3.4.

### **3S.3.6. Cell Adhesion Analyses**

Tissue culture well-plates were coated with 7.5% poly(2-hydroxyethyl methacrylate) (PHEMA) (Sigma) to prevent cells from attaching to cell culture plastic [258,259]. Ten-millimeter SF scaffold disks were disinfected through soaking in 99.98% ethyl alcohol for 1 hour followed by three 10-minute washes in PBS. To reduce the adhesion of serum proteins scaffolds were coated with 1% bovine serum albumin (BSA) (Gemini Bio-Products, West Sacramento, CA) solution for 30 minutes, followed by three 5-minute washes in PBS. One 10 mm diameter disinfected and BSA-coated scaffold disk was used per well. MCF10A cells ( $4 \times 10^4$  cells / scaffold) were seeded on these scaffold disks and incubated for 40 minutes before addition of further media to allow for better cell attachment. After 1 or 2 hours in culture the plates were

gently shaken, each scaffold was taken out and dipped 5 times in a media-containing well to wash off the non-attached cells. The number of non-attached cells suspended in each well was counted. The percentage of attached cells on each scaffold disk was calculated based on the number of non-attached cells.

### **3S.3.7. Cell Viability Analysis**

MCF-10A cells ( $1 \times 10^4$  cells per scaffold) were seeded on 6-mm diameter disinfected scaffold disks and cell viability was examined on day 14. Cell viability (number of living cells) was assessed using MTS [3-(4,5-dimethylthiazol-2-yl)-5-(3-carboxymethoxyphenyl)-2-(4-sulfophenyl)-2H-tetrazolium, inner salt] assays (CellTiter 96® Aqueous Non-Radioactive Cell Proliferation Assay; Promega, Madison, WI, USA), as described by the manufacturer. The metabolically active cells react with a tetrazolium salt in the MTS reagent to produce a soluble formazan dye with an absorption that can be measured at 490 nm. Numbers of cells per each condition were calculated based on standard curves and normalized to the percentages of attached cells.

### **3S.3.8. Statistical Analysis**

All parameters are expressed as mean  $\pm$  standard error of the mean (SEM). One-way analysis of variance (ANOVA) followed by the post-hoc Dunnett's Multiple Comparison Test were used to assess differences in SSA, elastic moduli, cell attachment, and cell viability between the scaffolds derived from SF electrospun at different air pressures. *A priori*, p values below 0.05 were defined as significant.

### 3S.4 Results

#### 3S.4.1. SSA and Mechanical Strength of SF Electrospun Scaffolds

The SSAs of scaffolds derived from SF electrospun were calculated, within their flat and perforation regions, to more accurately account for scaffold geometry. Scaffolds derived from electrospinning with an AP of 50 kPa exhibited the highest SSAs within their perforation regions ( $3.63 \pm 0.07 \mu\text{m}^{-1}$ ). This SSA was significantly higher than the SSAs within the perforation region of scaffolds derived from SF electrospun at APs of 0, 100, 200 ( $p < 0.001$ ), 400 kPa and scaffolds derived from SF electrospun on solid mandrel ( $p < 0.01$ , Figure 3S.1). Within the flat regions, the SSA of scaffolds derived SF electrospun at AP of 50 kPa was significantly smaller than the SSAs of scaffolds derived from electrospun at APs of 300 ( $p < 0.001$ ) and 400 kPa ( $p < 0.01$ , Figure 3S.1)

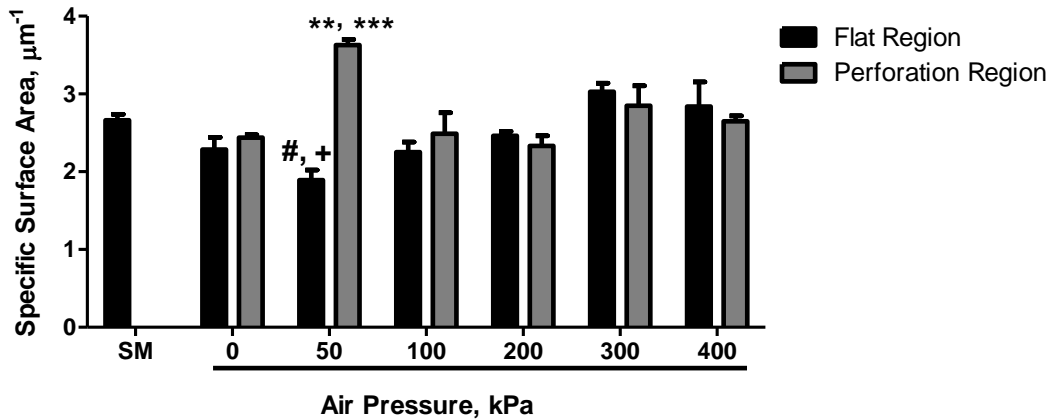


**Figure 3S.1. Specific surface area (SSA in  $\mu\text{m}^{-1}$ ) of electrospun SF-derived scaffolds.** # indicates significant difference from flat region of scaffolds derived from SF electrospun at AP of 300 kPa ( $p < 0.001$ ). + indicates significant difference from flat region of scaffolds derived from SF electrospun at AP of 400 kPa ( $p < 0.01$ ). \*\* indicates significant difference from perforation region of scaffolds derived from SF electrospun on a solid mandrel and scaffolds derived from SF electrospun at an AP of 400 kPa ( $p < 0.01$ ). \*\*\* indicates significant difference from perforation region of scaffolds derived from SF electrospun at APs of 0, 100, and 200 kPa ( $p < 0.001$ ).

The uniaxial tensile modulus of each scaffold hydrated with either PBS (HPBS), culture media no cells (HNC), or culture media with cells (HWC) was determined. Scaffold moduli, for

each scaffold electrospun at a specific air pressure, were not significantly different regardless of the hydration conditions or mandrel conditions (n.s., Table 3S.1).

**Table 3S.1.** Elastic moduli of SF derived scaffolds electrospun using a solid mandrel or using various air pressures on a perforated mandrel.

Mandrel Condition	HPBS	HNC	HWC
SM	3.23 ± 0.59	2.76 ± 0.15	3.40 ± 0.62
0	2.16 ± 0.48	2.45 ± 0.11	2.37 ± 0.13
50	2.02 ± 0.53	2.24 ± 0.26	1.85 ± 0.21
100	2.23 ± 0.46	1.42 ± 0.16	2.32 ± 0.08
200	3.17 ± 0.8	2.44 ± 0.24	2.39 ± 0.07
300	1.56 ± 0.31	1.77 ± 0.28	1.51 ± 0.07
400	2.98 ± 0.93	1.45 ± 0.18	1.73 ± 0.19

No significant difference was observed in the elastic modulus of PBS-hydrated scaffolds generated using 7% SF electrospun using a solid mandrel or at various APs using a perforated mandrel (n.s., Figure 3S.2A). However, in biologically relevant conditions, i.e., incubation in culture media alone (HNC) for 14 days (37°C, humidity >90%), the elastic moduli of scaffolds derived from SF electrospun at air pressures of 100 and 400 kPa were significantly lower than the modulus of scaffolds derived from SF electrospun at 0 and 200 kPa ( $p < 0.05$ , Figure 3S.2B) and scaffolds derived from SF electrospun on a solid mandrel ( $p < 0.01$ , Figure 3S.2B). Scaffolds (HWC) derived from electrospun SF on a solid mandrel and seeded with MCF10A cells, following a 14-day incubation (37°C, humidity >90%) in media had a significantly higher elastic moduli than the moduli of scaffolds derived from SF electrospun at air pressures of 50 and 400 kPa ( $p < 0.01$ , Figure 3S.2C) and 300 kPa ( $p < 0.001$ , Figure 3S.2C).

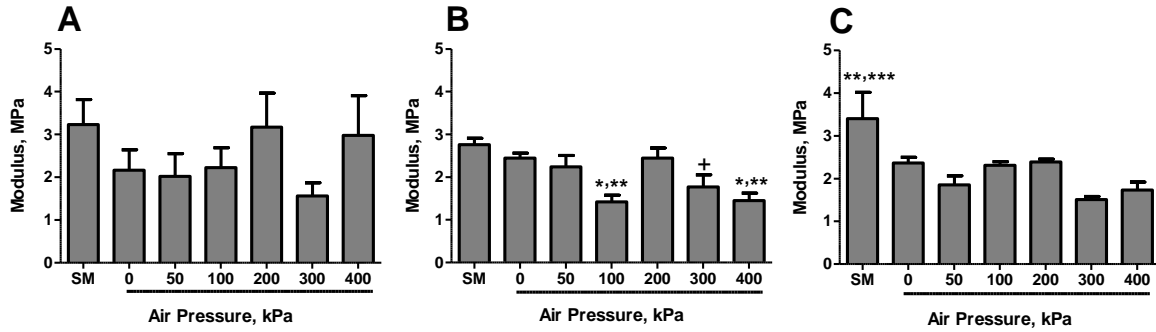


**Figure 3S.2. Modulus of Elasticity SF-Derived Electrospun Scaffolds.** **A) HPBS.** No significant difference observed. **B) HNC.** \* indicated significant differences from scaffolds derived from SF electrospun at APs of 0 and 200 kPa ( $p < 0.05$ ). \*\* indicates significant difference from SF scaffolds electrospun on a solid mandrel ( $p < 0.01$ ). + indicates a significant difference from SF scaffolds electrospun on a solid mandrel ( $p < 0.05$ ). **C) HWC.** \*\* indicates significant differences from SF-derived scaffolds electrospun at APs of 50 and 400 kPa ( $p < 0.01$ ). \*\*\* indicates significant difference from SF-derived scaffolds electrospun at an AP of 300 kPa ( $p < 0.001$ ).

### 3S.4.2. MCF10A Cell Attachment and Viability on SF-derived Scaffolds

MCF10A cell attachment was tested on SF-derived scaffolds generated on solid mandrel or at air pressures ranging from 0 to 400 kPa. Following a 1-hour incubation in culture conditions,  $35 \pm 5\%$ ,  $44 \pm 4\%$ ,  $41 \pm 3\%$ ,  $55 \pm 7\%$ ,  $36 \pm 4\%$ ,  $32 \pm 0\%$ , and  $34 \pm 0\%$  of the seeded MCF10A cells attached to scaffolds derived from SF electrospun using solid mandrel, AP of 0, 50, 100, 200, 300, and 400 kPa, respectively. After a 2-hour incubation in culture conditions, MCF10A cell adhesion onto these SF-derived scaffolds increased to  $65 \pm 5\%$ ,  $48 \pm 2\%$ ,  $50 \pm 4\%$ ,  $68 \pm 5\%$ ,  $49 \pm 4\%$ ,  $47 \pm 6\%$ , and  $65 \pm 5\%$  for scaffolds derived from SF electrospun using a solid mandrel, AP of 0, 50, 100, 200, 300, and 400 kPa, respectively (Figure 3S.3A and B). Regardless of incubation time, MCF10A cell attachment was not significantly different amongst the electrospun SF derived scaffolds tested (n.s. Figure 3S.3A and B).

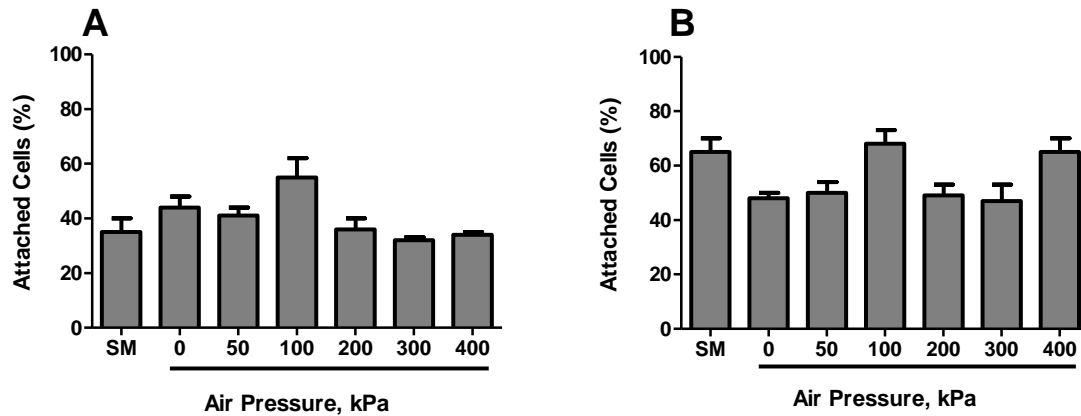


**Figure 3S.3. MCF10A cell attachment onto SF-derived scaffolds. A) After 1 hour.** No significant difference in cell adhesion between different conditions tested. **B) After 2 hours.** No significant difference in cell adhesion between different conditions tested.

Moreover, no correlation between MCF10A cell adhesion and fiber diameter, pore size, SSA of the flat region, or the SSA of the perforation region was observed ( $r^2 = 0.092$ ,  $p > 0.05$  and  $r^2 = 0.186$ ,  $p > 0.05$ ,  $r^2 = 0.012$ ,  $p > 0.05$ ,  $r^2 = 0.049$ ,  $p > 0.05$ , respectively, Figure 3S.3A and B) regardless of the electrospun SF derived scaffold and the incubation time tested.

After 14 days in culture, numbers of viable MCF10A cells present on / in SF derived scaffolds electrospun using air-flow technique were significantly higher than on / in SF-derived scaffolds electrospun using a solid mandrel. ( $p < 0.05$  for 100 and 400 kPa,  $p < 0.01$  for 50 kPa, and  $p < 0.001$  for 0, 200, and 300 kPa, Figure 3S.4). No significant difference in the number of viable cells was recorded between the SF-derived scaffolds electrospun at various APs (n.s., Figure 3S.4). MCF10A cell viability was not correlated with either fiber diameters, pore sizes, SSA of the flat region, or the SSA of the perforation regions of the scaffolds ( $r^2 = 0.017$ ,  $p > 0.05$ ,  $r^2 = 0.024$ ,  $p > 0.05$ , and  $r^2 = 0.022$ ,  $p > 0.05$ ,  $r^2 = 0.001$ ,  $p > 0.05$  respectively, Figure 3S.4).

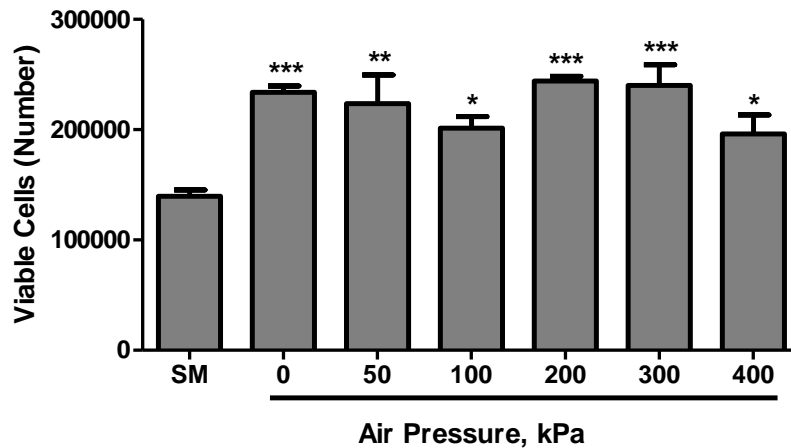


**Figure 3S.4. MCF10A cell viability following a 14-day incubation in culture conditions.** MCF10A viability was significantly higher when cultured onto SF-derived scaffolds electrospun using a perforated mandrel regardless of the AP used than SF-derived scaffolds developed using solid mandrel (SM) (\*  $p < 0.05$ ; \*\*  $p < 0.01$ ; \*\*\*  $p < 0.001$ ).

### 3S.5. Discussion

The ability of mammary epithelial cells to form acinar and ductal structures in 3D cultures maintained on gel matrices and aqueous-derived SF scaffolds have been demonstrated [56,84,122,265]. The data presented here supplement our investigation of electrospun SF-derived scaffolds tested as 3D scaffolding for MCF10A mammary epithelial cell growth. As described earlier (section 3.4), scaffolds prepared by electrospinning process mimic the physical features of the breast tissue ECM [266]. Further, the scaffolds developed here fabricated through air-flow impedance electrospinning containing highly porous regions (perforation regions) and dense fiber regions (flat regions), which allow cell infiltration and provide structural stability, respectively [221]. In complement to our previous observations [58], here we examined the effects of air-flow electrospinning on the physical and mechanical properties of SF-derived electrospun scaffolds and whether they provided a more suitable microenvironment for MCF10A cell attachment and viability. The results indicate first that SF scaffolds derived from air-flow electrospinning had similar mechanical strength as scaffolds electrospun on a solid mandrel.



Secondly, our data indicate that MCF10A cell adhesion and viability on SF-derived scaffolds generated using the air-flow electrospinning technique were improved compared to scaffolds obtained using SF electrospun on a solid mandrel.

Electrospun poly( $\epsilon$ -caprolactone) (PCL) derived scaffolds with nanometer to micrometer fiber diameters demonstrated higher SSAs for scaffolds with smaller fiber diameters [256]. Concurring with observations by Chen *et al.* [256], our data demonstrated significant difference in the SSAs of scaffolds derived from SF electrospun at an AP of 50 kPa, within both the flat and perforation regions compared to the SSA of scaffolds derived from SF electrospun at APs of 0, 100, 200, and 400 kPa. The SSA of scaffolds derived from SF electrospun at an AP of 50 kPa correspond with significantly smaller fiber diameters in their perforation regions and significantly larger fiber diameters in their flat regions (For an extended discussion of that point, please see section 3.4.2).

Our data also indicates the absence of difference in the elastic moduli of the SF derived electrospun scaffolds when hydrated in PBS. That observation and along with the fact that regardless of the hydration conditions tested, the electrospun SF-derived scaffolds retained their mechanical strength highlight the resilience of the silk mechanical properties [42,142,186,191]. The similar elastic moduli observed here regardless of the hydration condition and the presence or absence of cells within the scaffolds supports the unchanged mechanical properties of cell-seeded poly( $\epsilon$ -caprolactone) (PCL)-derived electrospun scaffolds compared with acellular scaffolds [261].

Moreover, our data demonstrated that regardless of the electrospun SF derived scaffolds tested (all with SSAs below  $7 \mu\text{m}^2$ ), MCF10A cell attachment was not significantly altered.

These results mimicked the observations by Chen *et al.* [256] that SSAs below  $7.13 \mu\text{m}^2$  were

associated no changes in cell attachment whereas scaffolds with higher SSAs promoted higher cell attachment. Furthermore, the MCF10A cell attachment observed here is comparable to the attachment of Saos-2 osteoblast-like cells to *B. mori* SF films [151].

The higher cell viability onto and within scaffolds generated from SF electrospun using air-flow electrospinning technique may be related to the development of larger pore sizes throughout these scaffolds compared to scaffolds obtained from SF electrospun on a solid mandrel. Indeed, higher MCF10A cell viability associated with larger pores noted here confirms previous observations demonstrating increased cell viability through scaffolds with larger pores [58,268]. Although, electrospun SF-derived scaffolds supported the MCF10A cell attachment and viability, they did not provide the appropriate microenvironment to promote cell differentiation and structure formation. This is possibly due to the absence of chemical cues provided by the other cell types and the stromal/ECM components present in the breast tissue.

### **3S.6. Conclusion**

These complementary observations support the use of air-flow impedance electrospinning in generation of SF-derived scaffolds compatible with MCF10A cell attachment, survival, and infiltration. Although, these SF nanofiber scaffolds electrospun using air-flow impedance technique formed highly porous matrices that resembled the ECM fibers and provided a microenvironment compatible with 3D *in vitro* culture of the human breast epithelial MCF10A cells they did not promote cell differentiation and structure formation. The absence of epithelial structures confirms the need for ECM proteins and chemical cues present in the breast tissue microenvironment. Therefore, to further improve these culture conditions, inclusion of crucial ECM proteins such as collagen and/or laminin is necessary.

## CHAPTER 4: EFFECTS OF COLLAGEN TYPE I ON SILK-BASED ELECTROSPUN SCAFFOLDS

*Preface: The following chapter has been submitted for review to the Journal of Materials Science and Engineering C. The included work investigates physical and mechanical properties and biocompatibility of silk fibroin electrospun scaffolds when blended or coated with collagen type I.*

### **Mammary Epithelial Cell Adhesion, Viability, And Infiltration On Blended Or Coated Silk Fibroin-Collagen Type I Electrospun Scaffolds**

Yas Maghdouri-White<sup>a,b</sup>, Gary L. Bowlin<sup>c</sup>, Christopher A. Lemmon<sup>b</sup>, and Didier Dréau<sup>a</sup>

<sup>a</sup> Department of Biology, University of North Carolina at Charlotte, Charlotte, NC 28223 USA

<sup>b</sup> Department of Biomedical Engineering, Virginia Commonwealth University, Richmond, VA 23284 USA

<sup>c</sup> Department of Biomedical Engineering, University of Memphis, Memphis, TN 38152 USA

#### **4.1. Abstract**

Most cellular events depend on the interactions between cells and the extracellular matrix (ECM) and play a crucial role in regulating tissue function. Silk biomaterials from *Bombyx mori* (*B. mori*) silkworm silk are widely used in tissue engineering. As this silk fibroin (SF) contains no strong adhesion sites, we assessed whether the blending or coating of SF with collagen would further improve SF biocompatibility, in part through the addition of the specific integrin recognition sequences. In the present study, electrospun scaffolds were developed by blending

7% SF and 7% type I collagen solutions at ratios of 100:0 (pure SF) , 95:5, 90:10, and 85:15 (SF:collagen , v/v) prior to electrospinning. Pure SF scaffolds were further coated with collagen type I. The physical and mechanical properties of these scaffolds and MCF10A mammary epithelial cell adhesion, viability, and infiltration into these blended or coated SF-collagen (SF-C) scaffolds were determined. The blending of SF with collagen decreased average pore sizes and fiber diameters of the electrospun scaffolds regardless of the ratio ( $p < 0.01$ ). The mechanical strength of these scaffolds, did not changed in their hydrated state (n.s.), and was decreased for 85:15 SF-C blended scaffolds in the dry state ( $p < 0.05$  and  $0.01$ ). The adhesion of MCF10A cells was significantly increased in SF-C blended or coated scaffolds compared to pure SF scaffolds ( $p < 0.01$ ). MCF10A cell viability and infiltration on SF-C coated scaffolds was significantly higher compared to all other conditions tested ( $p < 0.01$ ,  $p < 0.001$ ).

## **Keywords**

Silk Fibroin, Type I Collagen, Cell Adhesion, Cell Viability, Mechanical Properties, Electrospun Scaffolds

## **4.2. Introduction**

The activities of biological tissues are dependent on interactions between the cells present within the tissue and the cell-ECM interactions [6]. The cell-ECM interactions critically define the tissue microenvironment and thus play a crucial role in regulating homeostasis and tissue specificity [6]. Fundamental cellular events including proliferation, migration and apoptosis, are regulated by the cellular context [269]. *In vitro* three-dimensional (3D) cell cultures mimicking these physiological cell-ECM interactions provide a microenvironment closer to the native tissue than the conventional two-dimensional (2D) cell cultures [6,7]. As scaffolds for tissue engineering, natural or synthetic polymers electrospun non-woven fibrous structures led to the

engineering of tissue-like formations that closely resemble the structure of collagen fibers in the ECM [131]. Among the multiple natural biodegradable polymers available such as collagen, gelatin, chitosan and silk fibroin, silk-based biomaterials offer significant advantages for tissue engineering applications [56,145]. Indeed, silk-based biomaterials have excellent mechanical properties, controllable biodegradability, hemostatic properties, low antigenicity and non-inflammatory characteristics [145], are highly permeable to oxygen and drugs, and resist to enzymatic cleavage [146].

Silk consists of two types of proteins: SF, which is a filament core protein, and sericins, which are a glue-like coating family of hydrophilic proteins holding two fibroin fibers together [143,145]. Sericins have been shown to decrease biocompatibility and increase hypersensitivity to silk, however, when removed biocompatibility of SF was comparable to other biomaterials [191]. SF has been used as a biomaterial in various forms such as films [143,145], membranes [143,145], gels [145], sponges [143,145], powders, scaffolds [145], fibers, nets, meshes, and yarn [143]. The native *B. mori* SF protein contain no RGD sequence, a recognized binding site for integrin-mediated cell adhesion [41,200-202]. Cell adhesion to this biomaterial has been attributed to alternative low-affinity cell binding domains [41] such as arginine residues present in the non-repetitive region near the carboxy-terminus [146], or electrostatic interactions between cells and silk [41]. The cell attachment and early stages of cell-matrix interactions to *B. mori* SF can be enhanced by modifying the SF biomaterial surface through coating or chemical coupling with the RGD peptide sequence or specific growth factors [41,143,186,203,204]. Introducing the fibronectin cell-adhesive sequence, RGD, onto the SF biomaterial enhanced cell attachment to this material [204,205]. Higher attachment and growth of endothelial cells were obtained when SF nets were coated with gelatin, fibronectin, or collagen type I [204]. Human bone marrow

stromal cells (BMSCs) and human ACL fibroblasts showed higher cell attachment, spreading, and proliferation on RGD-modified SF matrices and silk films [41]. Human keratinocyte cell spreading but not attachment was stimulated by laminin coating on SF microfibers, nanofibers, and films [206]. Altman *et al.* [191] demonstrated that when SF films were decorated with the RGD peptide the induction of bone formation *in vitro* was significantly enhanced due to increased integrin interaction for cell adhesion.

In the native ECM, collagen type I serves as a structural protein, an adhesion protein that enhances cell attachment, and a signaling protein that promote proliferation through multiple binding sites including RGD integrin binding sites [270]. Thus, the addition of collagen type I to synthetic or other natural polymers likely would enhance the biocompatibility of those polymers while preserving the mechanical strength, therefore, combining the advantages of the two types of materials [119,270]. Multiple approaches have been used to introduce proteins into fibrous structures including coating, grafting and blending [113,119,245,270]. He *et al.* [119,245] determined that the spreading, viability and attachment of human coronary artery endothelial cells was enhanced on collagen-coated or blended poly (L-lactic acid)-co-poly( $\epsilon$ -caprolactone) nanofiber electrospun scaffolds. Noh *et al.* [271] demonstrated that coating chitin matrices with type I collagen significantly promoted the attachment of proliferating normal human oral keratinocytes, normal human epidermal keratinocytes, and normal human gingival fibroblasts compared to either uncoated or BSA-coated chitin matrices. Electrospinning is a simple technique that when performed using a blended mixture of proteins allows their combination both on the surface and throughout the resulting scaffold [219].

Here, we determine the effects of collagen type I on the physical and mechanical characteristics of electrospun scaffolds generated using various ratios of 7% collagen type I

blended with 7% SF solutions. We also present the human mammary epithelial, MCF10A, cell adhesion, viability, and infiltration onto these electrospun scaffolds in order to model their compatibility with SF biomaterials and their potential use in 3D modeling of the mammary gland.

### **4.3. Materials & Methods**

#### **4.3.1. Silk Extraction**

*Bombyx mori* SF was extracted from silk cocoons (*Bombyx mori* silk cocoons, B quality, The Yarn Tree, Asheville, NC, USA) as described by Rockwood *et al.* [207]. Briefly, after discarding the silk worms, 5 grams of cocoons were cut and boiled for 30 minutes in 2 liters of 0.02 Na<sub>2</sub>CO<sub>3</sub> (Sigma, Saint Louis, MO, USA) aqueous solution then rinsed 3 times (20 minutes each) in deionized water to remove the sericins. Silk fibers were left to dry overnight then dissolved in 9.3M LiBr (Fisher Scientific, Fair Lawn, NJ, USA), 12% (w/v), overnight (in 60°C for the first 4 hours). Silk solution was then dialyzed against deionized water for 48 hours using 3500 MWCO dialysis tubes (Fisher Scientific) with repeated water changes after 1, 4, 6, 12, 12, and 12 hours. The regenerated dry silk fibroin sponge was collected by freezing extracted silk solution in -80°C followed by lyophilization (SP Scientific, Gardiner, NY, USA).

#### **4.3.2. Collagen Type I**

Collagen type I, in powder form, used to prepare collagen solution for electrospinning was obtained by lyophilizing 3.0 mg/ml collagen type I solubilized in 0.01N HCL (Advanced BioMatrix, San Diego, CA, USA).

### 4.3.3. Electrospinning

The air-flow impedance electrospinning technique on a perforated mandrel described by McClure *et al.* [221] was used. In this technique the stainless steel perforated mandrel (Beverlin Manufacturing Company, Grand Rapids, MI, USA) was connected to the air line and pressurized air traveled through the lumen of this mandrel and exited through the pores impeding fiber deposition [58,221]. The air-flow impedance electrospinning method results in formation of highly porous regions (perforation regions), which allow cell infiltration, and dense fiber regions (flat regions), which provide structural stability [58,221]. The perforated mandrel is a hollow mandrel and 6 mm in diameter. It contains 0.75 mm holes spaced 2.0 mm center to center, laterally. The center-to-center longitudinal distance was 1.5 mm. A lure lock (Becton Dickinson, Franklin Lakes, NJ, USA) was fitted and taped to one end of the perforated mandrel using Tartan electric tape (3M Company, St. Paul, MN, USA). A 3mm diameter solid mandrel was inserted into the opposite end of the perforated mandrel and secured in place using electric tape (3M Company) [58,221]. The perforated mandrel was subjected to an applied air pressure of 100 kPa.

Extracted SF or collagen type I (in powder form, anhydrous) were dissolved in 1,1,1,3,3,3 hexafluoro-2-propanol (HFIP) (TCI America, Portland, OR, USA) at a concentration of 7%. The 7% SF solution was blended with 7% type I collagen solution at ratios of 95:5, 90:10, and 85:15 (SF:C type I, v/v). Pure silk and the blended solutions were loaded into Becton Dickinson syringes with an 18 gauge blunt tip needle. The needle was subjected to +25 kV with an air-gap distance of 13 cm between the needle and the mandrel. A volume of 1.5 ml of the SF-C solution was dispensed at a rate of 5ml/h and electrospun on the perforated mandrel. The average thickness of the resulting dry scaffolds was  $296 \pm 7.87 \mu\text{m}$ .



#### 4.3.4. Scaffold Characterization

Scanning Electron Microscopy (SEM) was performed using a JEOL LV-5610 SEM (JEOL Ltd., Tokyo, Japan). Inner surface measurements were taken randomly within the site of perforation. Average fiber diameter and pore size of the electrospun structures were measured using 60 random locations on each SEM image using ImageTool 3.0 software (Shareware provided by UTHSCSA, San Antonio, TX, USA).

#### 4.3.5. Mechanical Testing

Uniaxial tensile testing was performed using Tinius Olsen H10KT universal testing machine (Horsham, PA, USA). Three sets of ‘dog bone’ shape scaffold samples for each silk:collagen ratio were tested in their dry or hydrated form. The purification process used in extraction of SF from the *B. mori* silk cocoons disrupts the  $\beta$ -sheet crystalline domains of SF increasing its water solubility.[208]. In contrast, treatments with organic solvents such as methanol, ethanol, or alcohol lead to conformational change and self-organization of random coils into natural  $\beta$ -sheet structures [139,142,171,187,193,208]. Thus, the scaffold samples for mechanical testing were soaked in 99.98% ethyl alcohol (PHARMCO-AAPER) for 1 hour and then washed three times (10-minute each) in Phosphate-Buffered Saline (PBS) (Cellgro, Manassas, VA, USA). All mechanical testing was performed at room temperature.

#### 4.3.6. Protein Coating

Pure SF electrospun scaffolds were soaked in 99.98% ethyl alcohol for 1 hour followed by three 10-minute washes in PBS in order to disinfect scaffolds as well as promotion of self-organization of random coils into natural  $\beta$ -sheet structures [139,142,171,187,193,208]. The disinfected scaffolds were coated with 3.0 mg/ml collagen type I solubilized in 0.01N HCL overnight in 4°C.

#### 4.3.7. Cell Culture

Immortalized human mammary epithelial cells, MCF10A (ATCC, Manassas, VA, USA) were cultured in growth media containing DMEM/F12 supplemented with 5% horse serum (both from Invitrogen; Invitrogen Life Technologies, Grand Island, NY, USA), 1% Penicillin (10,000 units/ml) and Streptomycin (10,000 µg/ml) (Cellgro), 20 ng/ml Epidermal Growth Factor (EGF) (BD Biosciences, San Jose, CA), 0.5 µg/ml Hydrocortisone, 100 ng/ml Cholera Toxin, and 10 µg/ml Insulin (all from Sigma) [51]. Half of the media volume was changed every 2 days. Electrospun scaffolds were disinfected through soaking in 99.98% ethyl alcohol for 1 hour followed by three 10-minute washes in PBS. MCF10A cells were seeded at  $40 \times 10^3$  cells per 10-mm diameter biopsy punches of electrospun SF, SF-collagen type I blends, and collagen-coated SF scaffolds and maintained for up to 14 days at 37°C and 5% CO<sub>2</sub>.

#### 4.3.8. Cell Adhesion Analyses

Tissue culture well-plates were coated with 7.5% poly(2-hydroxyethyl methacrylate) (PHEMA) (Sigma) to prevent cells from attaching to cell culture vessels [258,259]. Ten millimeter silk scaffold disks were disinfected through soaking in 99.98% ethyl alcohol for 1 hour followed by three 10-minute washes in PBS. The SF, SF-C blends, and SF-C coated scaffolds were coated with 1% bovine serum albumin (BSA) (Gemini Bio-Products, West Sacramento, CA, USA) solution for 30 minutes, to reduce the adhesion of serum proteins to the scaffolds, followed by three 5-minute washes in PBS. One 10 mm disinfected and BSA coated scaffold disk was used per well. MCF10A cells ( $4 \times 10^4$  cells / scaffold) were seeded on these scaffold disks and incubated for 40 minutes before addition of further media to allow for better cell entrapment and attachment. After 1 or 2 hours in culture the plates were gently shaken, each scaffold was taken out and dipped in media-containing wells 5 times to remove the non-attached

cells. The number of non-attached cells suspended in each well was counted and the percentage of attached cells on each scaffold disk determined based on the total number of cells used and the number of non-adherent cells recorded.

#### **4.3.9. Cell Viability Analyses**

MCF10A cells ( $1 \times 10^4$  cells / scaffold) were seeded on 6-mm diameter disinfected SF, SF-C blended, and coated scaffold disks and cell viability was determined on day 14. Cell viability (number of living cells) was assessed using MTS [3-(4,5-dimethylthiazol-2-yl)-5-(3-carboxymethoxyphenyl)-2-(4-sulfophenyl)-2H-tetrazolium, inner salt] assays (CellTiter 96 @ Aqueous Non-Radioactive Cell Proliferation Assays, Promega, Madison, WI, USA), as described by the manufacturer. The number of viable cells was calculated based on a standard curve defining the relationship between absorbance and cell number.

#### **4.3.10. Cell Infiltration Measurements**

Following cell culture on electrospun scaffolds, scaffolds and cells were fixed in 4% formaldehyde for 20 minutes then rinsed in PBS at room temperature. Samples were permeabilized in 1:1000 Triton (MP Biomedicals) and equilibrated briefly in 2X saline sodium citrate (SSC) (0.3 M NaCl, 0.03 M sodium citrate, pH 7.0; Kirkegard and Perry Laboratories, Gaithersburg, MD, USA) then treated with 100 µg/ml DNase-free RNase (ABgene, Surrey, U.K.) in 2X SSC for 20 minutes at 37°C. Samples were then incubated for 5 minutes with the fluorochrome base-intercalator propidium iodide (500nM; MP Biomedicals), which dyes the nuclei, then rinsed in 2X SSC.

Fixed and stained scaffold-cell samples were soaked in 30% sucrose solution for 2 hours at 4°C. The samples were then embedded in Tissue-Tek® Optimal Cutting Temperature (O.C.T) compound (Ted Pella, Redding, CA, USA) and stored at -80°C. Frozen samples were cross-

sectioned (20  $\mu\text{m}$  thick sections) using a cryostat (MICROM GmbH, Walldorf, Germany). For each sample, ten cross-sections were imaged using Olympus IX71 fluorescent microscope equipped with a DP70 digital camera, using the 10X objective (Olympus, Tokyo, Japan). The distance from the surface of the scaffold to the center of sixteen nuclei was measured at evenly spaced points (totaling 160 points per sample) using ImageTool 3.0 software (Shareware provided by UTHSCSA, San Antonio, TX).

#### **4.3.11. Statistical Analyses**

All parameters are expressed as mean  $\pm$  standard error of the mean (SEM). One-way analysis of variance (ANOVA) followed by the post-hoc Newman-Keuls Multiple Comparison Test were used to assess the differences in cell infiltration, cell attachment, cell viability, fiber diameter pore size and mechanical strength between the electrospun SF-C blended scaffolds. *A priori*, p values below 0.05 were defined as significant.

### **4.4. Results**

#### **4.4.1. Physical Characteristics of Electrospun SF-C Blended Scaffolds**

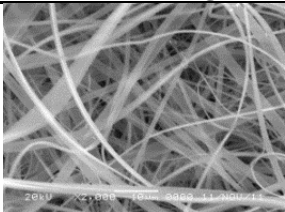
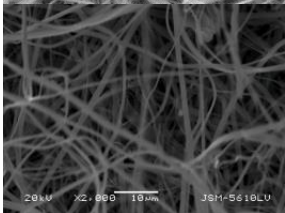
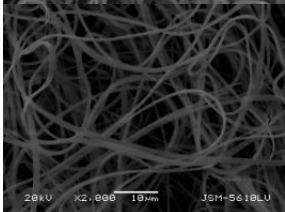
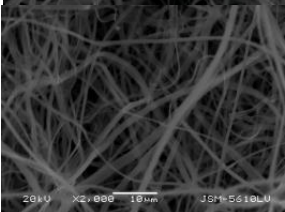
SF was blended with ratios of collagen type I (up to 15%) to improve biocompatibility without compromising mechanical strength. Both fiber diameters and pore sizes of the inner surface of the SF-C blended electrospun scaffolds were characterized at multiple randomly selected locations within the perforation regions (highly porous regions) of the perforated mandrel subjected to AP of 100 kPa (Figures 4.1 A and 4.B, respectively). Uniaxial tensile testing was performed on both dry and hydrated SF-C electrospun scaffolds (Figure 4.2). Electrospun scaffolds generated from blends of SF and collagen type I were characterized (Table 4.1).

#### 4.4.2. Blending of Collagen Type I with SF Decreased the Fiber Diameters and Pore Sizes of SF-C Electrospun Scaffolds.

As shown in Figures 4.1A and B, fiber diameter and pore size associated with addition of collagen to SF decreased ( $p < 0.001$  and  $p < 0.001$  and  $0.05$ , respectively). There was a significant correlation between the amount of collagen (up to 10%) present in the solution and fiber diameter and pore size ( $r^2 = 0.9998$ ,  $p < 0.01$ , and  $r^2 = 0.9987$ ,  $p < 0.05$ , respectively, Figure 4.1). However, this correlation was not significant as the amount of collagen was increased from 10 to 15% ( $r^2 = 0.8335$ ,  $p > 0.05$ , and  $r^2 = 0.8671$ ,  $p > 0.05$ , respectively, Figure 4.1).

Electrospun scaffolds prepared from pure SF (silk:no collagen) exhibited the largest fiber diameter and pore size ( $2.15 \pm 0.13 \mu\text{m}$ , and  $137.86 \pm 22.55 \mu\text{m}$ , respectively). The fiber diameter of pure SF scaffolds was significantly higher than of those in SF-C blended scaffolds at all ratios tested ( $p < 0.001$ , Figure 4.2A). The pore size of pure SF scaffolds was significantly higher than of those in scaffolds prepared by addition of 5, 10, or 15% collagen to SF ( $p < 0.05$ ,  $p < 0.001$ , and  $p < 0.001$ , respectively, Figure 4.1B). Increasing the collagen content from 5% to 10 or 15 % resulted in a significant decrease in fiber diameter and pore size ( $p < 0.001$  and  $p < 0.05$ , respectively). Although fiber diameters and pore sizes were not significantly different between 90:10 and 85:15 SF-C blended scaffolds (Figures 4.1A and B), fiber diameters and pore sizes were significantly lower in those blends compared to 95:5 and 100:0 ( $p < 0.05$ , Table 4.1 and Figure 4.1).

**Table 4.1.** Scanning electron micrographs of silk and SF-C blended electrospun scaffolds spun using a perforated mandrel subjected to an air pressure of 100 kPa.

SF:C Ratio (v/v)	Scanning Electron Microphotographs of the Perforation Region	Average Fiber Diameter $\pm$ SEM ( $\mu\text{m}$ )	Average Pore Size $\pm$ SEM ( $\mu\text{m}^2$ )
100:0		$2.15 \pm 0.13^a$	$137.86 \pm 22.55^c$
95:5		$1.52 \pm 0.08^b$	$90.61 \pm 15.99^d$
90:10		$0.93 \pm 0.06$	$37.11 \pm 3.44$
85:15		$1.03 \pm 0.04$	$42.06 \pm 4.39$

<sup>a</sup> Significantly > all SF-C blended scaffolds;  $p < 0.001$ .

<sup>b</sup> Significantly > 90:10 and 85:15 SF-C blended scaffolds;  $p < 0.001$ .

<sup>c</sup> Significantly > 95:5, 90:10 and 85:15 SF-C scaffolds;  $p < 0.05$ ,  $p < 0.001$ , and  $p < 0.001$ .

<sup>d</sup> Significantly > 90:10 and 85:15 SF-C blended scaffolds;  $p < 0.05$ .

#### 4.4.3. Mechanical Strength of Electrospun SF-C Blended Scaffolds.

Uniaxial tensile testing was performed on dry and hydrated SF-C blended electrospun scaffolds. Within the dry samples, there were no significant differences between the modulus of elasticity of pure SF scaffolds and the 95:5, 90:10, and 85:15 SF-C blends (ns, Figure 4.2).

However, the elastic moduli of 95:5 and 90:10 SF-C scaffolds were significantly higher than the elastic modulus of 85:15 SF-C blends ( $p < 0.01$  and  $p < 0.05$ , respectively, Figure 4.2). No

significant correlation between the collagen amount and the elastic modulus was recorded ( $p > 0.05$ ,  $r^2 = 0.9286$ ). Following hydration, the moduli of elasticity of SF-C blended electrospun scaffold samples were not significantly different (Figure 4.2).

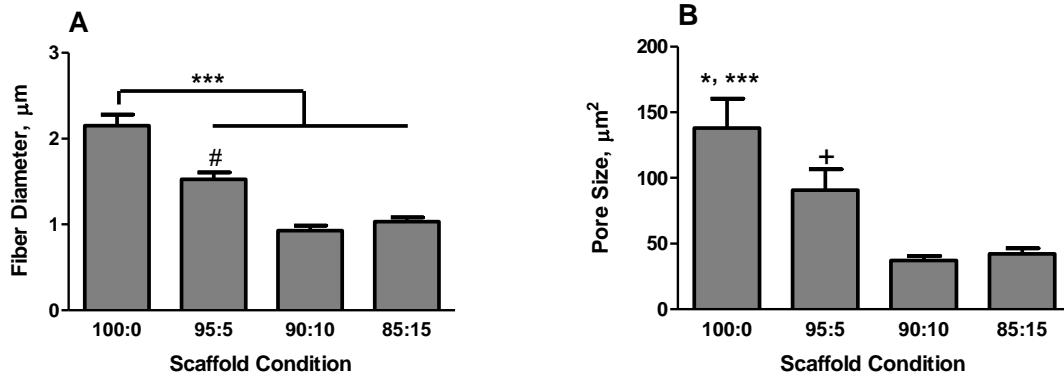


**Figure 4.1. Average fiber diameters and pore sizes of pure SF and SF-C blended electrospun scaffolds. A) Average fiber diameters.** \*\*\* indicates significant difference from all SF-C blended scaffolds ( $p < 0.001$ ). # indicates a significant difference from 90:10 and 85:15 SF-C blended scaffolds ( $p < 0.001$ ). **B) Average pore sizes.** \* indicates significant difference from 95:5 SF-C blended scaffolds ( $p < 0.05$ ). \*\*\* indicates a significant difference from 90:10 and 85:15 SF-C blended scaffolds ( $p < 0.001$ ). + indicates a significant difference from 90:10 and 85:15 SF-C blended scaffolds ( $p < 0.05$ ).

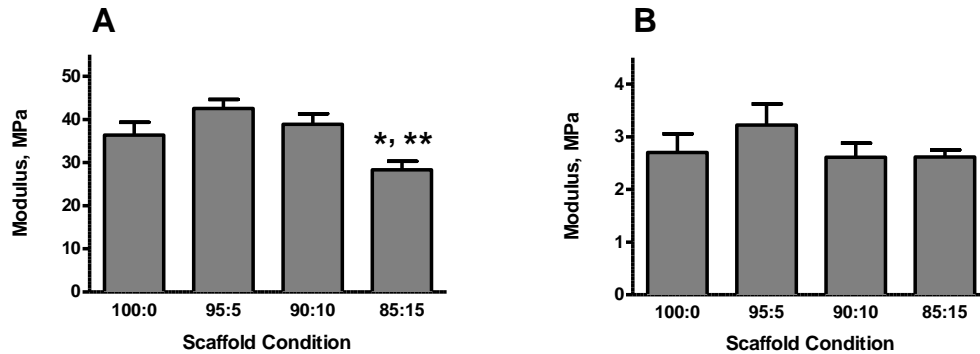


**Figure 4.2. Moduli of elasticity of SF-C blended electrospun scaffolds. A) Dry samples.** \* indicates significant difference in the elastic modulus compared to 100:0 and 90:10 SF-C blended electrospun scaffolds ( $*p < 0.05$ ). \*\* indicates significant difference in the elastic modulus compared to 95:11 SF-C blended electrospun scaffolds ( $**p < 0.01$ ). **B) Hydrated samples.** No significant differences were observed between elastic moduli regardless of the SF-C blend electrospun scaffold tested.

#### 4.4.4. MCF10A Cell Adhesion and Viability on Electrospun SF-C Blended Scaffolds

MCF10A cell adhesion on 85:15 SF-C blended scaffolds was significantly higher than of that on pure SF scaffolds after a one-hour incubation period ( $p < 0.05$ , Figure 4.3A). At that time point, cell adhesion was not significantly different amongst the SF-C blended scaffolds (ns, Figure 4.3A). Following a one-hour incubation period, MCF10A cell adhesion to SF-C coated scaffolds was not significantly different from adhesion to pure SF or the SF-C blends (ns, Figure 4.3A).

Moreover, MCF10A cell adhesion to all SF-C blended electrospun scaffolds and SF-C coated scaffolds was significantly higher than MCF10A cell adhesion to pure SF electrospun scaffolds following a two-hour incubation period ( $p < 0.01$ , Figure 4.3B). Overall, there was no significant correlation between the final collagen concentration (Table 4.2) present in the SF-C blended or coated electrospun scaffolds and cell adhesion after either 1 or 2-hour incubation ( $r^2 = 0.6021$ ,  $p > 0.05$  and  $r^2 = 0.7028$ ,  $p > 0.05$ , respectively, Figure 4.3A and B).

**Table 4.2.** Amount of collagen present in each scaffold condition<sup>a</sup>

Method	Scaffold	Collagen type I Solution Concentration, (mg/ml)	Final Collagen type I Concentration, (mg/ml)
<b>Blended</b>	100:0 (SF:C)	0	0
	95:5 (SF:C)	70	3.5
	90:10 (SF:C)	70	7
	85:15 (SF:C)	70	10.5
<b>Coated</b>	SF-C Coated	3	≤ 3

<sup>a</sup> Final Collagen type I concentrations in the blended scaffolds were calculated based on the initial concentration (70 mg/ml) and the ratio of collagen in each blended solution (i.e., in 95:5 there is 5% collagen/ml, therefore, 70 mg/ml \* 0.05= 3.5 mg/ml). The collagen type I concentration used to coat SF scaffolds was 3 mg/ml, therefore 3mg/ml or less was adsorbed onto the SF scaffolds.



There was a significant increase in MCF10A cell viability on SF-C coated scaffolds compared to pure SF scaffolds and 95:5, 90:10, and 85:15 SF-C blended scaffolds after 14 days in culture ( $p < 0.01$ ,  $p < 0.001$ ,  $p < 0.001$ , and 0.01, respectively, Figure 4.4).

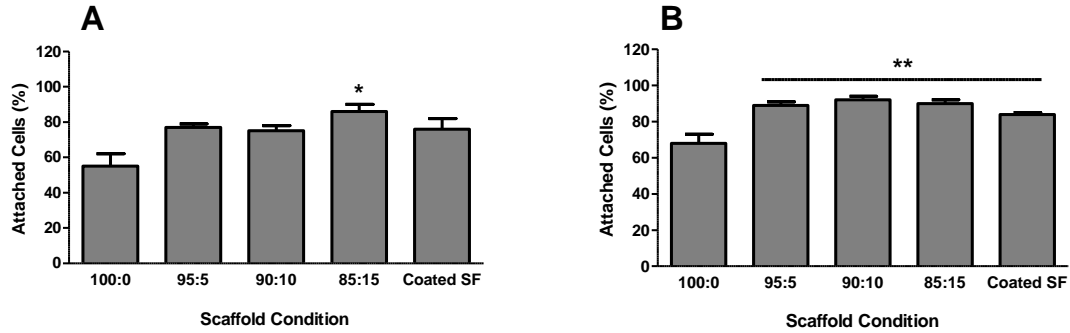


**Figure 4.3. Percentage of MCF10A cell adherence to SF-C blended electrospun scaffolds. A) After 1-Hour incubation.** \* indicates a significant difference from 100:0 ( $p < 0.05$ ). **B) After 2-Hour incubation.** \*\* indicates a significant difference from 100:0 ( $p < 0.01$ ).

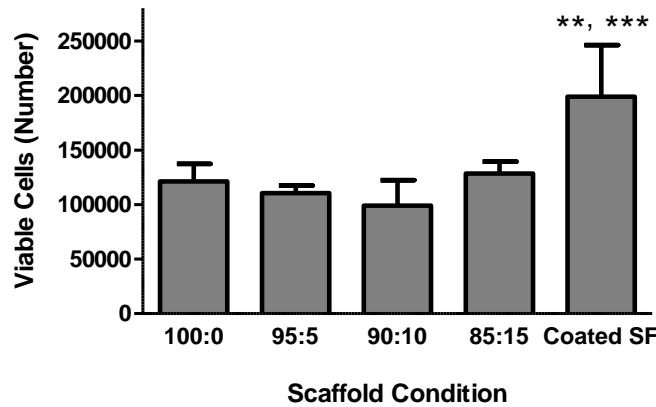


**Figure 4.4. MCF10A cell viability onto SF-C blended and SF-C coated electrospun scaffolds.** \*\* indicates significant difference from 100:0 and 85:15 SF-C blended electrospun scaffolds ( $p < 0.01$ ). \*\*\* indicates significant difference from 95:5, and 90:10 SF-C blended electrospun scaffolds ( $p < 0.001$ ).

#### 4.4.5. SF-C Electrospun Scaffolds Limit the Infiltration of MCF10A Cells

Static cultures of MCF10A cells were maintained for up to 14 days onto SF-C blended and coated electrospun scaffolds and the ability of MCF10A cells to infiltrate and colonize the scaffolds was assessed by the depth reached by MCF10 cells.

The deepest MCF10A cell infiltration was observed onto SF-C coated electrospun scaffolds. Cell infiltration through these scaffolds was significantly higher than infiltration through pure SF and SF-C blended scaffolds ( $p < 0.01$  and  $p < 0.001$ , respectively, Figure 4.5). MCF10A cell infiltration onto pure SF scaffolds was significantly higher than onto 95:5, 90:10, and 85:15 SF-C blended scaffolds ( $p < 0.01$ , Figure 4.5). There was a decrease in cell infiltration as the amount of collagen increased within the scaffolds. However, MCF10A cell infiltration onto 95:5, 90:10, and 85:15 SF-C blended scaffolds was not significantly different. The depth of MCF10A cell infiltration was significantly correlated with pore size of electrospun scaffolds ( $r^2 = 0.9388$ ,  $p < 0.05$ , Figure 4.5).

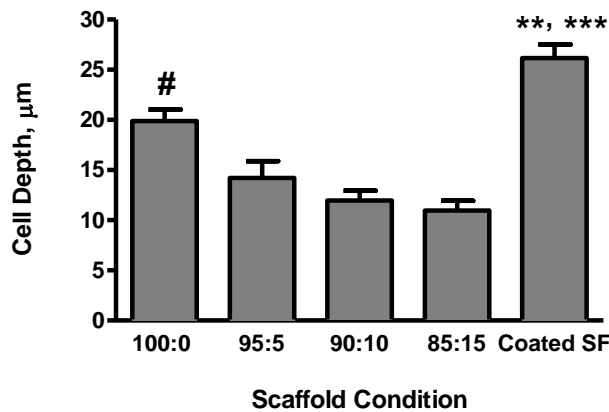


**Figure 4.5. MCF10A cell infiltration through SF-C electrospun scaffolds after 14 days in culture.** \*\* indicates significant difference from 100:0 SF-C blended scaffolds ( $p < 0.01$ ). \*\*\* indicates significant difference from 95:5, 90:10 and 85:15 SF-C blended scaffolds ( $p < 0.001$ ). # indicates significant difference from 95:5, 90:10 and 85:15 SF-C blended scaffolds ( $p < 0.01$ ).

#### 4.5. Discussion

The mechanical properties and biocompatibility of SF-based biomaterials offer significant advantages in tissue engineering applications [56,145,146]. SF-derived biomaterials from the domestic silkworm *B. mori* have been examined to develop 3D models of breast tissues [55,58]. However, in contrast with SF produced by *A. pernyi*, the wild-type silkworm, the cell attachment

to *B. mori* SF remains limited [146]. As cell adhesion to the ECM is essential for cell-ECM interactions and tissue specificity [6], cell adhesion to the SF can be enhanced by incorporating either the specific RGD peptide or ECM protein such as laminin, fibronectin, and collagen into SF through coating or blending [41,143,186,203,204]. Thus, here we investigated the characteristics of blended SF-C electrospun scaffolds. Our results indicate that although the blending of SF and collagen lead to significant changes in mechanical properties of the electrospun scaffolds, the tensile strength of the blended SF-C electrospun scaffolds remained similar. Furthermore, the biocompatibility of these blended electrospun scaffolds was improved.

Our results using blended 7% SF and 7% collagen type I solutions at ratios of 100:0, 95:5, 90:10, and 85:15 (SF:collagen type I v/v) electrospun scaffolds indicate that blending SF with collagen type I altered the physical characteristics of these fibrous structures. Specifically, the blending of SF and collagen type I led to a significant decrease in the average pore size and fiber diameters of the electrospun scaffolds. At the concentrations and ratios tested, the blended SF-C scaffolds showed no changes in their mechanical strength in their hydrated state, however, their tensile strength in their dry state decreased with high SF-C ratio (85:15).

Furthermore, our data demonstrates that increasing the collagen content in the SF-C blended electrospun scaffolds led to a significant decrease in fiber diameter and pore size. Particularly, the 90:10 and 85:15 SF-C blended scaffolds had significantly smaller fiber diameter and pore size than the 95:5 SF-C blended scaffolds. This decrease in the fiber diameter confirmed the decrease of the fiber diameter of nano-fibrous electrospun scaffolds prepared from blends of polydioxanone (PDO) and type I collagen compared to pure PDO scaffolds [220].

Interestingly, the uniaxial tensile testing results revealed no significant changes in the mechanical strength of the hydrated scaffolds when SF was blended with collagen type I in the

ratios tested (SF-C 100:0 to 85:15). Similar mechanical properties were demonstrated for hydrated PDO:collagen blended electrospun scaffolds [220]. However, in their dry state the tensile strength of SF electrospun scaffolds when blended with collagen at a ratio of 85:15 SF-C was significantly lower than that of scaffolds generated using SF-C blends with higher SF content. These observations were consistent with observations by He *et al.* [119] that demonstrated a significant decrease in tensile strength in collagen-blended poly(L-lactic acid)-*co*-poly( $\epsilon$ -caprolactone) [P(LLA-CL), 70:30] fibrous scaffolds at a ratio of 50:50 compared to the tensile strength in non-blended P(LLA-CL) scaffolds.

Furthermore, the infiltration of MCF10A epithelial cells through SF-C blended scaffolds significantly decreased as the pore size within these scaffolds decreased. In contrast, the MCF10A cell infiltration onto SF-C coated scaffolds was significantly deeper. Our results also highlight that the infiltration of MCF10A epithelial cells through SF-C blended scaffolds was significantly reduced compared to cell infiltration through pure SF scaffolds. This reduced infiltration is mainly associated with the significantly smaller pores generated within the SF-C I blended scaffolds. Furthermore, the smallest cell infiltration was associated with the highest collagen type I ratio to SF, i.e., 85:15 SF-C blended scaffolds, which exhibited the smallest pore size compared to all other conditions. These results confirm our and others previous studies [58,221,268]. In a previous study, a deeper MCF10A cell infiltration through SF electrospun scaffolds was associated with higher pore sizes generated following electrospinning SF at an air pressure of 100 kPa than all the other conditions [58]. The electrospinning conditions used here were similar excepted for the blending of SF with collagen highlighting the key importance of the biomaterial mix used in both the generation of scaffolds with various pore size and adhesion properties [119,151,268].

Although the MCF10A cell infiltration into SF-C blended scaffolds was reduced in part because of reduced pore size, our data demonstrate that cell infiltration through SF-C coated electrospun scaffolds increased in part because of the larger pore size and the presence of collagen type I cell binding sites [221,268,272]. These data confirm previous observations demonstrating increased cell infiltration through collagen-glycosaminoglycan porous scaffolds as the pore size was increased [268]. Further, McClure *et al.* [221] demonstrated increased human dermal fibroblast cell infiltration through poly( $\epsilon$ -caprolactone) (PCL) scaffolds, prepared by air-flow electrospinning, with larger pore sizes than scaffolds with smaller pores. Moreover, our data agree with Zhang *et al.*'s observations that demonstrated significantly higher infiltration of bone marrow mesenchymal stem cells in gelatin/PCL blended scaffolds compared to pure PCL scaffolds [272].

Our results also demonstrate that both collagen type I blending and coating onto fibrous SF scaffolds significantly altered the adhesion and viability of MCF10A epithelial cells. Indeed, the adhesion of epithelial cells to electrospun fibrous scaffolds was significantly increased when SF was blended or coated with collagen type I. This result is consistent with previous observations demonstrating that 3D sponge-like porous scaffolds prepared from blends of SF and collagen promoted higher chondrocyte attachment than sponge-like porous scaffolds prepared from pure SF [273,274]. Furthermore, the limited MCF10A cell attachment to pure SF scaffolds and the improved attachment to the collagen-blended scaffolds observed here are in keeping with the attachment of Saos-2 osteoblast-like cells to *B. mori* pure SF and RGD-modified SF films demonstrated by Sofia *et al.* [151].

The increase in MCF10A cell viability cultured onto SF-C coated scaffolds is associated with both the presence of cell binding site from collagen type I and the larger pores. Higher cell

viability associated with larger pores confirms previous observations demonstrating increased cell viability through scaffolds with larger pores [58,268]. In a previous study, we demonstrated significantly increased MCF10A cell viability onto 7% SF electrospun scaffolds with larger average pore size in comparison to 7% SF electrospun scaffolds with smaller pore sizes [58]. These observations also confirmed increased cell viability through collagen-glycosaminoglycan porous scaffolds as the pore size was increased [268]. Similarly, higher cell viability associated with the presence of cell binding site from collagen type I confirms previous observations demonstrating higher number of viable cells on collagen blended or collagen coated P(LLA-CL) nanofibers [119,245].

Taken together, the blended SF-C electrospun scaffolds maintained the SF tensile strength, and despite different fiber and pore size allowed an improved MCF10A cell adhesion, viability, and infiltration. The SF-C coated scaffolds also promoted enhanced MCF10A cell adhesion, viability, and infiltration. Thus, electrospun SF and collagen type I blended or coated scaffolds provide an improved *in vitro* approach to mimicking the mammary epithelial microenvironment.

#### **4.6. Conclusion**

These results provide evidence that blended or coated SF-C electrospun scaffolds support mammary epithelial cell viability and adhesion. Specifically, modifications of the SF chemical properties through the addition of the ECM protein collagen type I using coating or blending approaches promoted significant increases in the initial MCF10A cell adhesion on these biomaterials. Although, this ECM protein did not provide the cells with adequate chemical cues and integrin mediated cell-ECM interactions required for formation of epithelial structures, these results demonstrate the ability to modify the microenvironment of the SF electrospun scaffolds to modulate and enhance cell-ECM interactions.

## CHAPTER 5: LAMININ-COATING OF ELECTROSPUN SILK FIBROIN DERIVED SCAFFOLDS IN THREE-DIMENSIONAL CULTURES OF MAMMARY EPITHELIAL CELLS

### 5.1. Abstract

Cell-ECM interactions are essential to many aspects of cell behavior including adhesion, morphology, motility, and differentiation in both *in vitro* and *in vivo*. ECM proteins such as laminin, fibronectin, and collagens enhance cell adhesion and support cell-ECM interactions through ECM protein-integrin bindings. Further, laminin specifically promotes epithelial cell morphological and functional differentiation in three-dimensional (3D) culture systems. Here, we investigated the effects of laminin coating on the engineered silk fibroin (SF)-derived electrospun scaffolds on the attachment, survival, and morphological differentiation of the mammary epithelial cell MCF10A cultured onto those scaffolds under various conditions. Although MCF10A cell survival remained unchanged regardless of the conditions tested, MCF10A cell attachment significantly increased on laminin-coated electrospun SF- derived scaffolds compared to the non-laminin coated electrospun SF- derived scaffolds ( $p < 0.05$ ). Further, MCF10A cells cultured on electrospun SF-derived scaffolds coated with 15  $\mu\text{g/ml}$  of laminin in the presence of lactogenic hormones formed epithelial structures. These data highlights the potential of electrospun SF-derived scaffolds coated with the ECM protein laminin in the generation of 3D mammary structures *in vitro*.

## 5.2. Introduction

Engineered *in vitro* 3D models of the mammary tissue have contributed greatly to the study and understanding of breast development and cancer initiation [50,51,54,56,83,84,106,110,122,123,125-127,275]. Notably, the importance of cell-cell, cell-stroma, and cell-extracellular matrix (ECM) interactions, in the generation of functional breast tissue structures have been established [50,84,106,124,128]. Indeed, using 3D scaffolds to generate a microenvironment that closely mimics the structural and physiological features of breast tissue was associated with the engineering of functional mammary models and potential breast implants [10]. Previously 3D mammary models have mostly utilized gel scaffolds, such as Matrigel<sup>®</sup> and collagen to simulate the mammary tissue microenvironment [50,51,54,56,83,84,106,110,122,123,125-127,275]. Matrigel<sup>®</sup> has been especially useful in *in vitro* 3D modeling, however, the concentrations of growth factors within Matrigel<sup>®</sup> in long-term studies and *in vivo* use, may be associated with alterations of cellular activities [133,134]. Moreover, Matrigel<sup>®</sup> is derived from a mouse sarcoma, limiting its biocompatibility and use in human [133,134]. Also tested, were hydrogels including specific type I collagen gels that demonstrated rapid gel contraction and low stability [276]. More recently, Wang *et al.* [55] demonstrated that mammary epithelial cells co-cultured with stromal cells (pre-differentiated adipocytes and fibroblasts) within a collagen/Matrigel<sup>®</sup> mixture and maintained on 3D silk sponges formed ductal and acinar structures. Those 3D sponges were formed of a reticulated network with pore walls that measure several microns thick and as such were structurally differed from the more fibrillar structure of the mammary ECM [277]. Indeed, the ECM mainly composed of structural proteins collagens types I, II, and III, which have diameters varying from 50 to 500 nm forms a nano-fibrous structure [115,219,220]. These ECM fibrous proteins are one



to two orders of magnitude smaller than the cells allowing cell interactions with multiple fibers simultaneously and participating in the cell 3D polarity, migration and morphology [221].

Electrospinning is a unique and versatile technique that enables the development of nanofibers, in the nano to a few micrometer range, from a variety of polymers [131,141,142,223]. Given their similar properties with the fibrous components to the ECM, electrospun polymer-derived scaffolds have been used for tissue engineering and regenerative medicine [8,142,171]. The electrospinning process permits tailoring and control of several aspects of ECM-like scaffolds including the thickness, composition, diameters and porosity of the nano-fibers [8,141,224,225]. Furthermore, the surface area and porosity of electrospun nanofiber scaffolds also favor cell interactions [8]. The structural properties of scaffolds derived from electrospun nanofibers mimic ECM structural features and thus provides an excellent micro/nano environment for cell growth and function [8,171].

Silk fibroin (SF), the major component of a large subset of non-bio-absorbable biomedical sutures, has been used extensively in medical applications [114,139]. Silk-derived biomaterials are also investigated given their excellent mechanical properties [141], biocompatibility, slow controllable degradation rate [139,143,144], hemostatic properties, and low antigenicity [142,145], high oxygen permeability, high drug permeability, resistance against enzymatic cleavage [146], and thermal stability over a wide range of temperatures up to about 250 °C without loss of functional integrity [142]. SF-derived biomaterials have been generated in various forms such as films [143,145], membranes [143,145], gels [145,147], sponges [143,145], powders, scaffolds [145,147], fibers, nets, meshes, yarn [143], and nano-particles [147].

Earlier we provided evidence of the biocompatibility of SF nano-fibrous electrospun scaffolds with mammary epithelial cells [58]. However, in the conditions tested despite high cell

adhesion (unpublished data), viability and infiltration, no mammary acinar structure was observed. Aggeler *et al.* (1988) and Bissell *et al.* (1989), demonstrated remarkable morphological alterations and formation of many large cell aggregates with hollow lumens, as well as, increased synthesis of  $\beta$ -casein mRNA when cultures of mammary epithelial cells were maintained on 3D gels compared to two-dimensional (2D) cultures maintained on flat cell culture plastic [84,120]. Although in 2D culture conditions of epithelial cells formed a monolayer, those cells expressed elevated levels of  $\beta$ -casein mRNA when they were cultured in 2D culture conditions coated with the basement membrane protein laminin [84,120]. These observations suggests that multiple levels of regulation are involved in mammary-specific gene expression and cooperative interactions between ECM molecules and cells as well as cell-cell contact formation and the establishment of epithelial polarity positively modulate  $\beta$ -casein expression and are necessary for functional differentiation in culture [84,106]. Further, laminin gels supported the formation of multicellular structures by mouse mammary epithelial cells similar to those formed on Engelbreth-Holm-Swarm (EHS) basement membrane matrix (i.e., Matrigel<sup>®</sup>) [137]. Incubation of mouse mammary epithelial cells in the presence of lactogenic hormones onto laminin gels induced synthesis of the milk protein  $\beta$ -casein [137]. Thus, laminin along with lactogenic hormones promote the morphological and functional differentiation of mammary epithelial cells [137]. It has been demonstrated that  $\beta$ 1-integrin-cell interactions mediated by ECM protein laminin are crucial in differentiation of mammary epithelial cells and secretion of milk protein,  $\beta$ -casein, by these cells [106]. Inhibiting these  $\beta$ 1-integrin-cell interactions results in disruption of these polarized and differentiated structures [106]. Further, the polarized structures resulting from interactions with laminin, but not other ECM proteins such as collagen I, are resistant to apoptosis through  $\beta$ 4 integrin interactions [138]. Interactions

of  $\beta 4$  integrin with laminin initiate signals for cell growth, viability, and functional differentiation. These interactions direct tissue polarity and promote resistance to apoptosis in both nonmalignant and malignant breast epithelial structures as well [138].

Here, we hypothesized that the coating of the SF nanofibrous electrospun scaffolds with the ECM protein laminin would promote the polarized cellular organization and acinar formation and functional differentiation of MCF10A cells. Therefore, we determined the effects of laminin on the MCF10A cell adhesion, viability, and organization when cultured on laminin-coated electrospun SF derived scaffolds.

### **5.3. Materials and Methods**

#### **5.3.1. Silk Extraction**

*Bombyx mori* SF was extracted from silk cocoons (*Bombyx mori* silk cocoons, B quality, The Yarn Tree, Asheville, NC, USA) as described by Rockwood *et al.* [207]. Briefly, after discarding the silk worms, 5 grams of cocoons were cut and boiled for 30 minutes in 2 liters of 0.02 Na<sub>2</sub>CO<sub>3</sub> (Sigma, Saint Louis, MO, USA) aqueous solution then rinsed 3 times (20 minutes each) in deionized water to remove the sericins. Silk fibers were left to dry overnight then dissolved in 9.3M LiBr (Fisher Scientific, Fair Lawn, NJ, USA), 12% (w/v), in 60°C for 4 hours. Silk solution was then dialyzed against deionized water for 48 hours using 3500 MWCO dialysis tubes (Fisher Scientific) with repeated water changes after 1, 4, 6, 12, 12, and 12 hours. The regenerated dry silk fibroin sponge was collected by freezing extracted silk solution in -80°C followed by lyophilization (SP Scientific, Gardiner, NY, USA).

#### **5.3.2. Electrospinning**

The air-flow impedance electrospinning technique on a perforated mandrel was used [58,221]. In this technique the stainless steel perforated mandrel (Beverlin Manufacturing

Company, Grand Rapids, MI, USA) was connected to the air line and pressurized air traveled through the lumen of this mandrel and exited through the pores impeding fiber deposition [58,221]. The air-flow impedance electrospinning method results in formation of highly porous regions (perforation regions), which allow cell infiltration, and dense fiber regions (flat regions), which provide structural stability [58,221]. The perforated mandrel is a hollow mandrel and 6 mm in diameter. It contains 0.75 mm holes spaced 2.0 mm center to center, laterally. The center-to-center longitudinal distance was 1.5 mm. A lure lock (Becton Dickinson, Franklin Lakes, NJ, USA) was fitted and taped to one end of the perforated mandrel using Tartan electric tape (3M Company, St. Paul, MN, USA). A 3mm diameter solid mandrel was inserted into the opposite end of the perforated mandrel and secured in place using electric tape (3M Company) [58,221]. The perforated mandrel was subjected to an applied air pressure of 100 kPa.

Extracted SF (in dry form, anhydrous) was dissolved in 1,1,1,3,3,3 hexafluoro-2-propanol (HFIP) (TCI America, Portland, OR, USA) at a concentration of 7%. The 7% SF solution was loaded into Becton Dickinson syringes with an 18 gauge blunt tip needle. The needle was subjected to +25 kV with an air-gap distance of 13 cm between the needle and the mandrel. A volume of 1.5 ml of the SF solution was dispensed at a rate of 5ml/h and electrospun on the perforated mandrel. The average thickness of the resulting dry scaffolds was  $266.7 \pm 13.6 \mu\text{m}$ .

### **5.3.3. Scaffold Characterization**

Scanning Electron Microscopy (SEM) was performed using a JEOL LV-5610 SEM (JEOL Ltd., Tokyo, Japan). Inner surface measurements were taken randomly within the site of perforation. Average fiber diameter and pore size of the electrospun structures were measured using 60 random locations on each SEM image using ImageTool 3.0 software (Shareware provided by UTHSCSA, San Antonio, TX, USA).

#### 5.3.4. Laminin Coating

Pure SF electrospun scaffolds were soaked in 99.98% ethyl alcohol for 1 hour followed by three 10-minute washes in PBS in order to disinfect scaffolds as well as promote self-organization of random coils into natural  $\beta$ -sheet structures [139,142,171,187,193,208]. The disinfected scaffolds and cell culture vessels were coated with 0, 1, 5, 10, 15, and 20  $\mu\text{g/ml}$  of Laminin 1 from Engelbreth-Holm-Swarm murine sarcoma (basement membrane) (Sigma), solubilized in sterile deionized water, overnight in  $4^{\circ}\text{C}$ . SF scaffolds and cell culture vessels were coated with the same amount of laminin by calculating the total available surface area of the scaffolds as described by Boland *et al.* [278] and the surface area of cell culture vessels.

#### 5.3.5. Cell Culture

Immortalized human mammary epithelial cells, MCF10A (ATCC, Manassas, VA, USA) were cultured in growth media containing DMEM/F12 supplemented with 5% horse serum (both from Invitrogen, Carlsbad, CA, USA), 1% Penicillin (10,000 units/ml) and Streptomycin (10,000  $\mu\text{g/ml}$ ) (Cellgro), 20 ng/ml Epidermal Growth Factor (EGF) (BD Biosciences, San Jose, CA, USA), 0.5  $\mu\text{g/ml}$  Hydrocortisone, 100 ng/ml Cholera Toxin, and 10  $\mu\text{g/ml}$  Insulin (all from Sigma) [51]. Half of the media volume was changed every 2 days.  $1 \times 10^5$  MCF10A cells were seeded per 10-mm diameter disinfected and laminin coated and non-coated SF electrospun scaffold disks and maintained in culture for up to 14 days at  $37^{\circ}\text{C}$  and 5%  $\text{CO}_2$ . After 3 days in culture the media, some cultures were supplemented with a lactogenic cocktail (0.8 mM insulin, 0.2 mM prolactin, 1 mM Dexamethasone (Sigma) [279].

### 5.3.6. Cell Adhesion Analyses

Tissue culture well-plates were coated with 7.5% poly(2-hydroxyethyl methacrylate) (PHEMA) (Sigma) to prevent cells from attaching to cell culture vessels [258,259]. Ten millimeter disinfected and laminin coated and non-coated SF scaffold disks were further coated with 1% bovine serum albumin (BSA) (Gemini Bio-Products, West Sacramento, CA, USA) solution for 30 minutes, to reduce the adhesion of serum proteins to the scaffolds, followed by three 5-minute washes in PBS. One 10 mm disinfected laminin and BSA coated scaffold disk was used per well. MCF10A cells ( $4 \times 10^4$  cells / scaffold) were seeded on these scaffold disks and incubated for 40 minutes before addition of further media to allow for better cell entrapment and attachment. After 1 or 2 hours in culture the plates were gently shaken, each scaffold was taken out and dipped in media-containing wells 5 times to remove the non-attached cells. The number of non-attached cells suspended in each well was counted and the percentage of attached cells on each scaffold disk was determined based on the total number of cells used and the number of non-adherent cells recorded.

### 5.3.7. Cell Viability Analyses

MCF10A cells ( $1 \times 10^4$  cells / scaffold) were seeded on 10-mm diameter disinfected and laminin coated and non-coated SF scaffold disks as well as laminin coated and non-coated cell culture vessels and cell viability was determined on day 14. Cell viability (number of living cells) was assessed using MTS [3-(4,5-dimethylthiazol-2-yl)-5-(3-carboxymethoxyphenyl)-2-(4-sulfophenyl)-2H-tetrazolium, inner salt] assays (CellTiter 96 ® Aqueous Non-Radioactive Cell Proliferation Assay; Promega, Madison, WI, USA), as described by the manufacturer. The metabolically active cells react with a tetrazolium salt in the MTS reagent to produce a soluble formazan dye with an absorption that can be measured at 490 nm. For each condition, the

numbers of cells were calculated based on standard curves and normalized to the percentages of attached cells.

### **5.3.8. Immunofluorescence Staining and Structure Formation Analyses**

Following cell culture on laminin coated and non-coated electrospun silk scaffolds after 14 days, cell containing scaffolds were fixed in 4% formaldehyde for 20 minutes then rinsed in PBS at room temperature. The fixed samples were then blocked in Odyssey Blocking Buffer (LI-COR, Lincoln, NE) including 0.2% Tween 20 (Sigma). After 60 minutes at room temperature the blocking buffer was aspirated and Alexa Fluor<sup>®</sup> 555 Anti-GM130 antibody (BD Biosciences, San Jose, CA, USA) was added at 1:10 concentration and samples were incubated for 60 minutes at room temperature. Samples were then rinsed three times in PBS for 5 minutes each and treated with sterile Vybrant<sup>®</sup> DiD cell labeling solution phospholipid dye (Invitrogen) for 30 minutes at room temperature. After three 5-minute PBS rinses samples were treated with 0.1 µg/ml DAPI nucleic acid stain (Invitrogen). Formation of acinar structures was visualized using a confocal microscope (Olympus FV1000).

### **5.3.9. Statistical Analyses**

All parameters are expressed as mean  $\pm$  standard error of the mean (SEM). Two-way analysis of variance (ANOVA) followed by the post-hoc Bonferroni Multiple Comparison Test were used to assess the differences in cell attachment and cell viability between the electrospun laminin coated SF scaffolds and laminin coated cell culture vessels. *A priori*, p values below 0.05 were defined as significant.

## 5.4. Results

### 5.4.1. Physical Characteristics of Electrospun SF Scaffolds

Both fiber diameters and pore sizes of the inner surface of the SF electrospun scaffolds were characterized at multiple randomly selected locations within the perforation regions (highly porous regions) of the perforated mandrel subjected to AP of 100 kPa. The average fiber diameter was measured at  $2.15 \pm 0.13 \mu\text{m}$ . The average pore size was measured at  $137.86 \pm 22.55 \mu\text{m}^2$ .

### 5.4.2. MCF10A Cell Adhesion on Laminin Coated SF Electrospun Scaffolds

MCF10A cell adhesion after 1 and 2 hours in culture was assessed on laminin coated and non-coated SF scaffolds (SFS) (3D cultures) and laminin coated and non-coated cell culture vessels (CCV) (2D cultures). After a one-hour incubation, MCF10A cell adhesion onto SF scaffolds coated with 5 ( $p < 0.05$ , Figure 5.1A), 15 or 20  $\mu\text{g/ml}$  ( $p < 0.01$ , Figure 5.1A) laminin was significantly higher than MCF10A cell adhesion onto non-coated (0  $\mu\text{g/ml}$ ) and 10  $\mu\text{g/ml}$  laminin coated SF scaffolds. After a one-hour incubation, MCF10A cell adhesion onto electrospun SF-derived scaffolds coated laminin solutions of increasing concentrations (1-20  $\mu\text{g/ml}$ ) remained similar (ns, Figure 5.1A). In similar incubation conditions, 2D cultured MCF10A cell adhesion onto laminin-coated vessels was significantly higher than on non-coated vessels regardless of the concentration of laminin used for coating (1 and 5  $\mu\text{g/ml}$  ( $p < 0.01$ ) and 10, 15, and 20  $\mu\text{g/ml}$  ( $p < 0.001$ , Figure 5.1A). Vessels coated with 20  $\mu\text{g/ml}$  laminin promoted higher 2D MCF10A cell attachment than vessels coated with lower laminin concentrations (1 or 5  $\mu\text{g/ml}$ ;  $p < 0.01$  and  $p < 0.05$ , respectively, Figure 5.1A). MCF10A cell adhesion on 3D and 2D cultures were similar regardless of the coating and conditions tested excepted within the non-coated SF scaffolds and non-coated cell culture vessels after one-hour incubation ( $p < 0.01$ ,



Figure 5.1A). Overall, within the first hour both laminin concentrations ( $p < 0.001$ ) and culture conditions ( $p < 0.01$ ) markedly altered MCF10A cell adhesion.

After a longer incubation period (2 hours), MCF10A cell adhesion to all the laminin coated SF scaffolds was significantly higher than MCF10A cell adhesion to non-coated SF electrospun scaffolds (1, 5, and 10  $\mu\text{g/ml}$  ( $p < 0.05$ ), 15  $\mu\text{g/ml}$  ( $p < 0.001$ ), and 20  $\mu\text{g/ml}$  ( $p < 0.01$ ), Figure 5.1B). No significant correlation between the laminin concentration and MCF10A cell adhesion regardless of the incubation time tested was observed ( $r^2 = 0.4065$ ,  $p > 0.05$  and  $r^2 = 0.6314$ ,  $p > 0.05$ , respectively, Figure 5.1A and B). Overall, after a two-hour incubation, the laminin concentration had a significant effect on MCF10A cell adhesion regardless of the culture conditions ( $p < 0.001$ , Figure 5.1B).

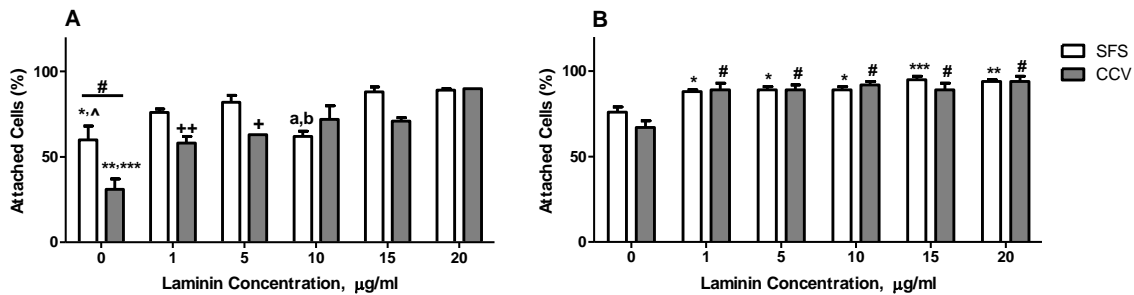


**Figure 5.1. MCF10A cell adhesion on laminin-coated vessels and electrospun SF-derived scaffolds.**  
**A) After 1-hour incubation.** # indicates a significant difference between adhesion on non-coated 3D and 2D cultures ( $p < 0.01$ ). \* indicates a significant difference from laminin coating of 5  $\mu\text{g/ml}$  ( $p < 0.05$ ). ^ indicates a significant difference from laminin coating of 15 and 20  $\mu\text{g/ml}$  ( $p < 0.01$ ). \*\* Indicates significant difference from laminin coating of 1 and 5  $\mu\text{g/ml}$  ( $p < 0.01$ ). \*\*\* indicates significant difference from 10, 15, and 20  $\mu\text{g/ml}$  ( $p < 0.001$ ). + and ++ indicate significant differences from 20  $\mu\text{g/ml}$  (+  $p < 0.01$  and ++  $p < 0.05$ ). a and b indicate significant difference from 5, 15, and 20  $\mu\text{g/ml}$  (a  $p < 0.05$  and b  $p < 0.01$ ). **B) After 2-hour incubation.** \*, \*\*, and \*\*\* indicate significant differences between laminin coated and non-coated 3D cultures (\*  $p < 0.05$ , \*\*  $p < 0.01$ , and \*\*\*  $p < 0.001$ ). # indicates significant difference between laminin coated and non-coated 2D cultures ( $p < 0.001$ ).

### 5.4.3. MCF10A Cell Viability on Laminin Coated Electrospun SF-derived Scaffolds

MCF10A cell viability was assessed on laminin-coated and non-coated electrospun SF-derived scaffolds and vessels following a 14-day incubation in cell culture conditions. Overall, more MCF10A cells were recorded in cell culture vessels (2D conditions) than 3D culture condition (electrospun SF-derived scaffolds) ( $p < 0.001$ ; 2-way ANOVA). This difference was mainly associated with significant difference in the numbers of MCF10A cells present in laminin-coated vessels (20  $\mu\text{g/ml}$ ) and scaffolds coated with the same laminin concentration ( $p < 0.05$ , Figure 5.2).

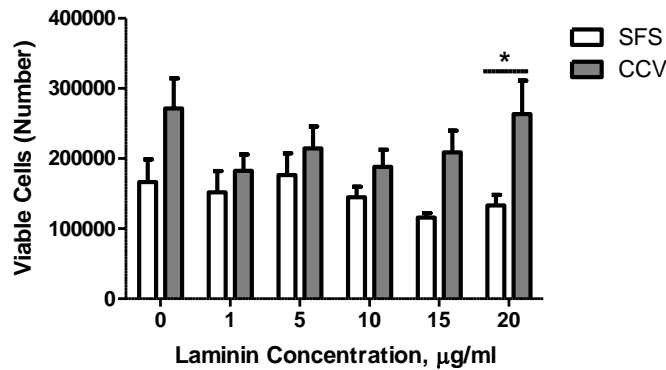


**Figure 5.2. MCF10A cell viability on laminin-coated and non-coated vessels and scaffolds.** \* indicates significantly higher number of cells in vessels coated with laminin (20  $\mu\text{g/ml}$ ) ( $p < 0.05$ ).

### 5.4.4. Acinar Structures on Laminin Coated Electrospun SF-derived Scaffolds.

The presence of MCF10A derived acinar structures was assessed in both vessels coated with increasing laminin concentrations and electrospun SF-derived scaffolds after a 14-day incubation in culture with or without lactogenic hormones by confocal microscopy. No acinar structure was observed in vessels coated or not with laminin (0-20  $\mu\text{g/ml}$ , data not shown). On electrospun SF-derived scaffolds in the absence of lactogenic hormones or at low concentrations of laminin (1, 5, 10  $\mu\text{g/ml}$ ) no structure were detected (Figure 5.3A). However, in the presence of lactogenic

hormones MCF10A acinar structures were observed onto electrospun SF-derived scaffolds coated with 15 and 20  $\mu\text{g/ml}$  of laminin (Figure 5.3B and Table 5.1).

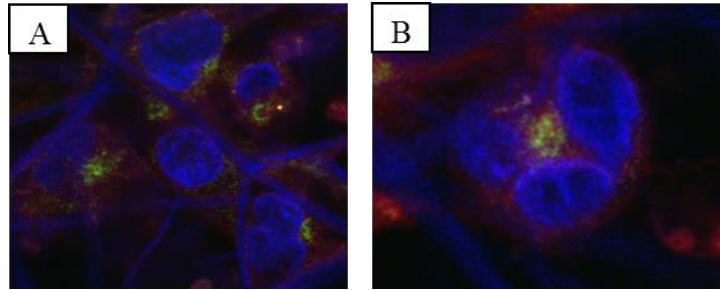


**Figure 5.3. MCF10A Cell morphology in 3D laminin coated SF-derived scaffolds.** A) Absence of acinar structures. B) Polarized acinar structure on SF scaffolds coated with 15  $\mu\text{g/ml}$  of laminin. MCF10A acini were immunostained with antibodies to the Golgi protein, GM130 (green), which illustrated the apical orientation of the Golgi apparatus toward the hollow lumen of acini. Cell nuclei were stained with DAPI nucleic stain (blue). Cell membranes were stained with Vybrant DiD phospholipid stain (red). Silk fibers are shown in blue.

**Table 5.1.** Formation of acinar-like structures under different conditions

Laminin Concentration, $\mu\text{g/ml}$	Lactogenic Hormones	Acinus-like Structure Formation
0	Yes	No
1	Yes	No
5	Yes	No
10	Yes	No
15	Yes	Yes
20	Yes	Yes

## 5.5. Discussion

In engineering 3D *in vitro* mammary models, mammary epithelial cells form acinar and ductal structures [50,51,54,56,83,84,122,125-127]. Bissell *et al.* [84] Aggeler *et al.* [120] demonstrated that cultures of mammary epithelial cells onto laminin coated tissue culture vessels or laminin coated floating collagen gels lead to increased expression of  $\beta$ -casein mRNA. Further, mammary epithelial cells cultured on laminin gels formed structures with hollow lumens and induced the synthesis of  $\beta$ -casein in the presence of lactogenic hormones [137]. Earlier, we noted that MCF10A mammary epithelial cells on SF-derived electrospun scaffolds did not generate any

acinus-like structures (unpublished data). Here, the electrospun SF-derived scaffolds were coated with laminin, a basement membrane protein that improve cell-ECM interactions and promote epithelial differentiation [137]. Our results indicate that the laminin coating of electrospun SF-derived scaffolds enhanced MCF10A cell attachment and in the presence of lactogenic hormones the formation of organized MCF10A cell acinus-like structures was detected.

As expected, our data indicate significantly higher MCF10A cell attachment on laminin-coated electrospun SF-derived scaffolds and tissue culture vessels than attachment on non-coated scaffolds and vessels. These observations further confirm the significantly higher cell attachment demonstrated for rat islet cells onto laminin-coated tissue culture vessels [280]. Our data indicate lower numbers of viable MCF10A cells on laminin-coated SF scaffolds, in particular using 20  $\mu\text{g/ml}$  laminin concentration, compared to laminin coated cell culture vessels. This observation demonstrates the slow proliferation rate of MCF10A cells in 3D cultures and formation of growth-arrested acinaus-like structures as demonstrated in Matrigel<sup>®</sup> cultures [51].

Our results demonstrate that MCF10A cultured on electrospun SF-derived scaffolds coated with laminin at concentrations of 15 and 20  $\mu\text{g/ml}$  and the presence of lactogenic hormones formed acinar structures, although different in both number and size compared to structures formed onto Matrigel<sup>®</sup> (data not shown). The absence of acinar structures observed here when MCF10A cells were cultured on SF scaffolds without lactogenic hormones confirm observations by Streuli *et al.* [137] demonstrating that laminin and lactogenic hormones, together, promote the morphological and functional differentiation of mammary epithelial cells. Indeed, MCF10A cells formed acinar structures when culture onto Matrigel<sup>®</sup>, an ECM composed mainly of laminin in 3D culture conditions [137]. Furthermore, the use of 3D laminin gels lead to the generation of similar 3D acinar –like structures [137]. The structures formed onto our

electrospun SF-derived laminin-coated scaffolds may be associated with the intensity of laminin-coating and the presence of lactogenic hormones.

## **5.6. Conclusion**

Our results demonstrate that the presence of laminin provided cell-ECM interaction sites, possibly through  $\beta 1$  and  $\beta 4$  integrins, which are crucial in the differentiation and formation of polarized growth-arrested structures of mammary epithelial cells. Here, we further demonstrated the flexibility of SF-derived electrospun scaffolds, which allow modification and control over the structural features as well as chemical features of the engineered microenvironment. This control allows testing of various factors involved in the function of the breast tissue either individually and/or as a group.

## CHAPTER 6: CONCLUSION AND FUTURE DIRECTIONS

Three-dimensional (3D) modeling of tissues and organs *in vitro* has proven a useful tool to study organ development and function in both healthy and diseased states. *In vitro* breast epithelial cell models further our understanding of the complex interactions between mammary epithelial cells and the stromal components during normal breast development and breast cancer initiation, progression, and development. In modeling of breast tissue, mimicking the structural properties of the ECM is essential as the ECM plays a key role in the organization and function of the tissue. It is also critical to provide mammary epithelial cells with an environment including physiochemical and mechanical cues essential to the maintenance and regulation of cell behavior and tissue function mimicking those provided by the breast tissue microenvironment. Multiple scaffold approaches mimicking the ECM have been tested. However, only limited work has been conducted using fiber-based scaffolds to mimic breast tissue ECM nano-fibrous composition and structure.

Tissue-like scaffolds that closely resemble the fibrous structure of ECM can be produced through electrospinning of biologically-derived or synthetic polymers. Those nano-fiber scaffolds closely mimic the structure of collagen fibers in the tissue's ECM and also promote cell adhesion and survival. In particular, SF-derived scaffolds have mechanical properties and a biocompatibility suitable for the generation of long-term 3D cultures and tissue like-structures that can serve as *in vitro* 3D breast tissue models and for tissue repair, respectively.

The studies detailed in the present work address the overall goal of developing electrospun SF-derived scaffolds that promote mammary cell growth and the formation of mammary like structures depending on the composition and/or coating of the scaffolds with ECM proteins. Specifically, the studies presented investigated (1) the effects of various concentrations of SF along with different electrospinning techniques on the mechanical and physical properties of electrospun SF-derived scaffolds and (2) whether those scaffolds provide suitable microenvironments for mammary epithelial cells as determined by MCF10A cell attachment, viability, and structure formation. Further, we determined (3) the effects of blending or coat electrospun SF-derived scaffolds with either collagen I and laminin, two key ECM proteins, on the attachment, viability and structure formation associated with normal human mammary epithelial cells.

Our results highlight the effects of SF concentration on the mechanical and physical properties of the SF-derived scaffolds and demonstrate that low polymer concentrations led to the formation of fibers with diameters closer to those of ECM fibers. Our results also demonstrate significant effects of air-flow pressure used during electrospinning on the formation of larger pores within scaffolds. Both of these features, i.e., small fiber diameters and large pores, are important parameters in mimicking breast ECM substitutes. Indeed, cells have been shown to develop increased attachment and organization around fibers with diameters smaller than the diameters of the cells [267]. Furthermore, cells infiltrated more deeply through scaffolds with pores large enough for the cells to migrate through and colonize the scaffolds [221]. The advantages of these electrospun scaffolds are that their physical, mechanical, and chemical properties can be modified to generate a variety of different matrices. There are, however, limitations in generations of these scaffolds using the air-flow electrospinning technique. 1) The

flow of air out of the pores of the perforated mandrel is not uniform and 2) deposition and collection of fibers on this perforated mandrel further affects the air flow distribution.

Our observations further demonstrate improved cell adhesion and viability on SF-derived scaffolds that were blended and/or coated with collagen I or laminin. Our results demonstrate that collagen type I did not provide the cells with adequate chemical cues and integrin mediated cell-ECM interactions required for formation of epithelial structures. On the other hand, the presence of laminin provided cell-ECM interaction sites, possibly through  $\beta 1$  and  $\beta 4$  integrins, which are crucial in the differentiation and formation of polarized growth-arrested structures of mammary epithelial cells. Moreover, in the presence of lactogenic hormones, MCF10A mammary epithelial cells cultured onto laminin-coated SF-derived scaffolds promoted cell differentiation and formation of acinus-like structures. However, the number and complexity of these structures contrasted with the number of complex structures formed in Matrigel<sup>®</sup>. The low rate of cell proliferation on these electrospun scaffolds in comparison with cell cultures maintained in 2D highlight the growth-arrest of the epithelial cells once they form acinus-like structures. The developed microenvironment generated through electrospinning of SF is depicted in Figure 6.1.

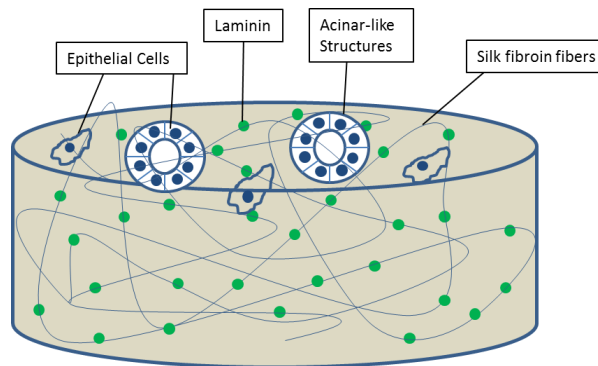


**Figure 6.1. Silk fibroin microenvironment developed through electrospinning**



Taken these results, we demonstrated the mechanical integrity of SF-derived scaffolds in culture and the flexibility of these electrospun scaffolds, which allow modification and control over the structural features as well as chemical features of the engineered microenvironment. This control allows testing of various factors involved in the function of the breast tissue either individually and/or as a group. The biocompatibility of these protein nanofibers demonstrated by MCF10A cell attachment, survival, and evidence of organized structures supports the use of these SF-derived scaffolds in modeling 3D breast tissues *in vitro*. Our data addressing the use of electrospun SF-derived scaffold in the modeling and/or tissue repair of the mammary gland parallel observations highlighting the engineering of ligament [42], adipose-like tissue [150], and skin [171] using nano-fibrous SF-derived scaffolds. Further, they underline that to better recapitulate the histological complexity of the normal breast and breast cancers, and to better fill the gap between animal models and 2D cell cultures, it is essential to develop more intricate 3D models than those currently available.

Unlike other organs, the majority of the breast tissue development occurs after birth, during puberty, and pregnancy and requires dynamic and reciprocal signaling between cells and their surrounding microenvironment [86]. To delineate the mechanisms by which the tissue microenvironment modulates tissue function and cancer growth and development this dynamically changing cellular microenvironment must be adequately mimicked. To that end, the engineering and generation of dynamic microenvironments that respond to feedback from the tissue / cell during long culture periods will allow the analysis of cellular responses to this dynamically changing environment in both normal and cancerous tissue.

Most breast tissue studies have utilized monotypic cell culture systems, where epithelial cells have been grown in isolation within 3D scaffolds. However, both normal and cancerous breast

tissues contain several heterotypic cell types. Indeed, the ducts and lobules of the normal breast are comprised of a bilayer structure of inner luminal epithelial cells and outer myoepithelial cells [86]. In order to generate heterotypic breast models, the addition of myoepithelial cells to epithelial cultures must be considered. The addition of at least one type of stromal cells such as adipocytes and/or fibroblasts influenced the epithelial cell cultures [50,53-55,83,106,125,126,281]. Thus, the generation of heterotypic culture systems with a combination of multiple cell types such as adipocytes, fibroblasts, immune cells, and endothelial cells that can mimic the histological complexity of the tissue *in vivo* should be investigated. Challenges associated with heterotypic cell cultures include the different metabolic and nutritional needs of these various cell types and the signaling cascades among the different cell types. Culture conditions should be defined to meet both the growth and differentiation requirements and the signaling needs of the different cell types in culture.

Furthermore, the development of normal breast tissue, as well as, cancer initiation and progression is regulated by various hormones and breast stroma and the basement membrane consisting of ECM proteins such as collagens type I, II, III, and IV, laminin, fibronectin, proteoglycans, and glycoproteins [86,87]. Those proteins and hormones critically modulate the fate of epithelial cells especially during cell differentiation and functional activities of the breast and also during breast cancer progression. Therefore, the blending and/or coating scaffolds with multiple ECM proteins and their effects on cellular behavior should be further investigated. Also, the incorporation of various hormones and their effects on breast tissue maintenance, activation or cancer progression should be investigated in *in vitro* 3D models.

In addition to biochemical cues, cell mechanics and mechanical properties of the matrix play crucial roles in breast tissue function and cancer biology. Cell mechanics can be separated in

three different subfields: 1) cellular mechanical properties, which allow understanding of cell deformity and migration in cancer; 2) mechanotransduction, which is the cellular response to imposed forces on cells by the external environment. Importantly these mechanical forces influence tumor growth and metastasis; and 3) cell-generated forces that will allow a better understanding of how cells sense their microenvironment [130,282]. Further investigation of these mechanical forces will contribute to generation of more relevant 3D models. Also, mechanical properties of the matrix have been shown to play an important role in the formation of polarized acinar-like structures. Indeed, increased matrix density is associated with disruption of organized and polarized growth-arrested structures formed by epithelial cells [129]. Therefore, further mechanical testing of the electrospun scaffolds, as a whole, through compression testing, and as individual fibers will shed light on the cellular behavior within these scaffolds.

Further, the mechanical testing of the breast tissues have demonstrated the heterogeneity of this tissue with various densities within the fatty regions and the fibroglandular regions [88-91]. Therefore, the development of scaffolds with heterogeneous and controlled regions with variable fiber diameters and pore sizes will allow the formation of more biologically relevant matrices and 3D breast tissue models.

One major challenge in tissue engineering is complete cellularization of the entire scaffold. Many studies have investigated electrospun scaffolds for a range of tissue engineering applications, however, generation of materials that permit complete cell integration and infiltration have not been successful and often, cellular population and tissue formation occur only at the scaffold periphery [283].

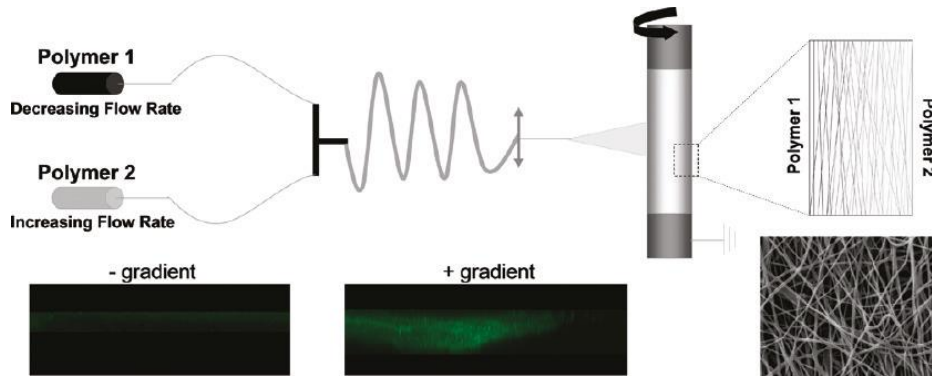


**Figure 6.2. Gradient electrospinning setup. Adapted from [283]**

In an effort to promote further cell infiltration through electrospun scaffolds, in a recently developed method (as depicted in Figure 6.2), two polymer solutions in two separate syringes are used, e.g., SF which does not contain adhesion sites (polymer 1) and collagen with cell binding sites (polymer 2). The polymers meet at the T-junction and are mixed through a mixing channel. The flow rate of the two polymers, before mixing, is altered during the electrospinning period resulting in the formation of scaffolds with primarily Polymer 2 at the bottom and primarily Polymer 1 at the surface [283]. This increasing gradient of adhesion sites towards the bottom of the scaffold will promote cell migration and infiltration from the surface of the scaffolds into the inside and bottom of scaffolds [283]. Therefore, the fabrication of matrices that can direct cell migration and promote colonization of the entire matrix, gradient electrospinning method should also be investigated.

## Literature Cited

1. Weigelt B, Bissell MJ. Unraveling the microenvironmental influences on the normal mammary gland and breast cancer. *Semin Cancer Biol* 2008;18:311-321.
2. Elliott NT, Yuan F. A review of three- dimensional in vitro tissue models for drug discovery and transport studies. *J Pharm Sci* 2011;100:59.
3. Kim JB. Three-dimensional tissue culture models in cancer biology. *Semin Cancer Biol* 2005;15:365-377.
4. Jucker M. The benefits and limitations of animal models for translational research in neurodegenerative diseases. *Nat Med* 2010;16:1210.
5. Yamada KM, Cukierman E. Modeling tissue morphogenesis and cancer in 3D. *Cell* 2007;130:601-610.
6. Bissell MJ, Radisky DC, Rizki A, Weaver VM, Petersen OW. The organizing principle: microenvironmental influences in the normal and malignant breast. *Differentiation* 2002;70:537-546.
7. Jacks T, Weinberg RA. Taking the study of cancer cell survival to a new dimension. *Cell* 2002;111:923-925.
8. Vasita R, Katti DS. Nanofibers and their applications in tissue engineering. *International Journal of Nanomedicine* 2006;1:15-30.
9. Griffith LG, Swartz MA. Capturing complex 3D tissue physiology in vitro. *Nature Reviews.Molecular Cell Biology* 2006;7:211-224.
10. Nelson CM, Bissell MJ. Modeling dynamic reciprocity: engineering three-dimensional culture models of breast architecture, function, and neoplastic transformation. *Semin Cancer Biol* 2005;15:342-352.
11. Griffith LG, Naughton G. Tissue engineering: Current challenges and expanding opportunities. *Science* 2002;295:1009-1014.
12. Gomillion CT, Parzel CA, White Jr. RL, Burg KJL. Tissue engineering: Breast. *Encyclopedia of Biomaterials and Biomedical Engineering* 2007;DOI: 10.1081/E-EBBE-120041291.
13. Atala A, Bauer SB, Soker S, Yoo JJ, Retik AB. Tissue-engineered autologous bladders for patients needing cystoplasty. *The Lancet* 2006;367:1241-1246.

14. Debnath J, Brugge JS. Modelling glandular epithelial cancers in three-dimensional cultures. *Nature reviews.Cancer* 2005;5:675-688.
15. Bissell MJ, LaBarge MA. Context, tissue plasticity, and cancer: Are tumor stem cells also regulated by the microenvironment? *Cancer Cell* 2005;7:17-23.
16. Macchiarini P, Jungebluth P, Go T, Asnaghi MA, Rees LE, Cogan TA, et al. Clinical transplantation of a tissue-engineered airway. *The Lancet* 2008;372:2023-2030.
17. Nair LS, Laurencin CT. Biodegradable polymers as biomaterials. *Progress in Polymer Science* 2007;32:762-798.
18. Kucharska M, Butruk B, Walenko K, Brynk T, Ciach T. Fabrication of in-situ foamed chitosan/ $\beta$ -TCP scaffolds for bone tissue engineering application. *Mater Lett* 2012;85:124-127.
19. Nemati Hayati A, Rezaie HR, Hosseinalipour SM. Preparation of poly(3-hydroxybutyrate)/nano-hydroxyapatite composite scaffolds for bone tissue engineering. *Mater Lett* 2011;65:736-739.
20. Rivas MB, Y.Piñero-Redondo, R.De Santis, A.Gloria, L.Ambrosio, A.Tampieri, et al. Poly(caprolactone) based magnetic scaffolds for bone tissue engineering. *J Appl Phys* 2011;109:07B313-1-3.
21. Yoshimoto H, Shin YM, Terai H, Vacanti JP. A biodegradable nanofiber scaffold by electrospinning and its potential for bone tissue engineering. *Biomaterials* 2003;24:2077-2082.
22. Zhang R, Ma PX. Poly( $\alpha$ -hydroxyl acids)/hydroxyapatite porous composites for bone-tissue engineering. I. Preparation and morphology. *J Biomed Mater Res* 1999;44:446-455.
23. Li C, Vepari C, Jin H, Kim HJ, Kaplan DL. Electrospun silk-BMP-2 scaffolds for bone tissue engineering. *Biomaterials* 2006;27:3115-3124.
24. Li Z, Ramay HR, Hauch KD, Xiao D, Zhang M. Chitosan–alginate hybrid scaffolds for bone tissue engineering. *Biomaterials* 2005;26:3919-3928.
25. Rodrigues CVM, Serricella P, Linhares ABR, Guerdes RM, Borojevic R, Rossi MA, et al. Characterization of a bovine collagen–hydroxyapatite composite scaffold for bone tissue engineering. *Biomaterials* 2003;24:4987-4997.
26. Chachques JC, Trainini JC, Lago N, Cortes-Morichetti M, Schussler O, Carpentier A. Myocardial assistance by grafting a new bioartificial upgraded myocardium (MAGNUM Trial): clinical feasibility study. *Ann Thorac Surg* 2008;85:901-908.
27. Zimmermann WH, Fink C, Kralisch D, Remmers U, Weil J, Eschenhagen T. Three-dimensional engineered heart tissue from neonatal rat cardiac myocytes. *Biotechnol Bioeng* 2000;68:106-114.

28. Matsubayashi K, Fedak PWM, Mickle DAG, Weisel RD, Ozawa T, Li R. Improved left ventricular aneurysm repair with bioengineered vascular smooth muscle grafts. *Circulation* 2003;108 Suppl 1:II219-25.
29. Leor J, Aboulafia-Etzion S, Dar A, Shapiro L, Barbash IM, Battler A, et al. Bioengineered cardiac grafts: A new approach to repair the infarcted myocardium? *Circulation* 2000;102:III56-61.
30. Sams AE, Nixon AJ. Chondrocyte-laden collagen scaffolds for resurfacing extensive articular cartilage defects. *Osteoarthritis and Cartilage* 1995;3:47-59.
31. Frenkel SR, Toolan B, Menche D, Pitman MI, Pachence JM. Chondrocyte transplantation using a collagen bilayer matrix for cartilage repair. *The Journal of Bone and Joint Surgery*. British volume 1997;79:831-836.
32. Nehrer S, Breinan HA, Ramappa A, Shortkroff S, Young G, Minas T, et al. Canine chondrocytes seeded in type I and type II collagen implants investigated In Vitro. *J Biomed Mater Res* 1997;38:95-104.
33. Meinel L, Hofmann S, Karageorgiou V, Zichner L, Langer R, Kaplan D, et al. Engineering cartilage-like tissue using human mesenchymal stem cells and silk protein scaffolds. *Biotechnol Bioeng* 2004;88:379-391.
34. Wang Y, Kim U, Blasioli DJ, Kim H, Kaplan DL. In vitro cartilage tissue engineering with 3D porous aqueous-derived silk scaffolds and mesenchymal stem cells. *Biomaterials* 2005;26:7082-7094.
35. Wang Y, Blasioli DJ, Kim H, Kim HS, Kaplan DL. Cartilage tissue engineering with silk scaffolds and human articular chondrocytes. *Biomaterials* 2006;27:4434-4442.
36. Fragonas E, Valente M, Pozzi-Mucelli M, Toffanin R, Rizzo R, Silvestri F, et al. Articular cartilage repair in rabbits by using suspensions of allogenic chondrocytes in alginate. *Biomaterials* 2000;21:795-801.
37. Grande DA, Halberstadt C, Naughton G, Schwartz R, Manji R. Evaluation of matrix scaffolds for tissue engineering of articular cartilage grafts. *J Biomed Mater Res* 1997;34:211-220.
38. Puelacher WC, Mooney D, Langer R, Upton J, Vacanti JP, Vacanti CA. Design of nasoseptal cartilage replacements synthesized from biodegradable polymers and chondrocytes. *Biomaterials* 1994;15:774-778.
39. Li W, Tuli R, Okafor C, Derfoul A, Danielson KG, Hall DJ, et al. A three-dimensional nanofibrous scaffold for cartilage tissue engineering using human mesenchymal stem cells. *Biomaterials* 2005;26:599-609.

40. Köse GT, Korkusuz F, Özkul A, Soysal Y, Özdemir T, Yildiz C, et al. Tissue engineered cartilage on collagen and PHBV matrices. *Biomaterials* 2005;26:5187-5197.
41. Chen J, Altman GH, Karageorgiou V, Horan R, Collette A, Volloch V, et al. Human bone marrow stromal cell and ligament fibroblast responses on RGD-modified silk fibers. *Journal of Biomedical Materials Research.Part A* 2003;67:559-570.
42. Altman GH, Horan RL, Lu HH, Moreau J, Martin I, Richmond JC, et al. Silk matrix for tissue engineered anterior cruciate ligaments. *Biomaterials* 2002;23:4131-4141.
43. Nöth U, Schupp K, Heymer A, Kall S, Jakob F, Schütze N, et al. Anterior cruciate ligament constructs fabricated from human mesenchymal stem cells in a collagen type I hydrogel. *Cytherapy* 2005;7:447-455.
44. Majima T, Funakosi T, Iwasaki N, Yamane ST, Harada K, Nonaka S, et al. Alginate and chitosan polyion complex hybrid fibers for scaffolds in ligament and tendon tissue engineering. *J Orthop Sci* 2005;10:302-307.
45. Sahoo S, Ouyang H, Goh JC-, Tay TE, Toh SL. Characterization of a novel polymeric scaffold for potential application in tendon/ ligament tissue engineering. *Tissue Eng* 2006;12:91.
46. Chen P, Marsilio E, Goldstein RH, Yannas IV, Spector M. Formation of lung alveolar- like structures in collagen- glycosaminoglycan scaffolds in vitro. *Tissue Eng* 2005;11:1436-1448.
47. Petersen TH, Calle EA, Zhao L, Lee EJ, Gui L, Raredon MB, et al. Tissue-engineered lungs for in vivo implantation. *Science (New York, N.Y.)* 2010;329:538.
48. O'Neill JD, Anfang R, Anandappa A, Costa J, Javidfar J, Wobma HM, et al. Decellularization of human and porcine lung tissues for pulmonary tissue engineering. *Ann Thorac Surg* 2013;96:1046-1056.
49. Lin YM, Boccaccini AR, Polak JM, Bishop AE, Maquet V. Biocompatibility of poly-DL-lactic acid (PDLA) for lung tissue engineering. *J Biomater Appl* 2006;21:109.
50. Darcy KM, Zangani D, Shea-Eaton W, Shoemaker SF, Lee PH, Mead LH, et al. Mammary fibroblasts stimulate growth, alveolar morphogenesis, and functional differentiation of normal rat mammary epithelial cells. *In vitro cellular developmental biology.Animal* 2000;36:578-592.
51. Debnath J, Muthuswamy SK, Brugge JS. Morphogenesis and oncogenesis of MCF-10A mammary epithelial acini grown in three-dimensional basement membrane cultures. *Methods* 2003;30:256-268.
52. Emerman J, Pitelka D. Maintenance and induction of morphological differentiation in dissociated mammary epithelium on floating collagen membranes. *In Vitro* ;13:316-328.



53. Huss FRM, Kratz G. Mammary epithelial cell and adipocyte co-culture in a 3-D matrix: The first step towards tissue-engineered human breast tissue. *Cells Tissues Organs (Print)* 2001;169:361-367.
54. Krause S, Maffini MV, Soto AM, Sonnenschein C. A novel 3D in vitro culture model to study stromal-epithelial interactions in the mammary gland. *Tissue Eng Part C Methods* 2008;14:261-271.
55. Wang X, Sun L, Maffini MV, Soto A, Sonnenschein C, Kaplan DL. A complex 3D human tissue culture system based on mammary stromal cells and silk scaffolds for modeling breast morphogenesis and function. *Biomaterials* 2010;31:3920-3929.
56. Wang X, Zhang X, Sun L, Subramanian B, Maffini MV, Soto A, et al. Preadipocytes stimulate ductal morphogenesis and functional differentiation of human mammary epithelial cells on 3D silk scaffolds. *Tissue Eng Part A* 2009;15:3087-3098.
57. Sahoo SK, Panda AK, Labhassetwar V. Characterization of porous PLGA/PLA microparticles as a scaffold for three dimensional growth of breast cancer cells. *Biomacromolecules* 2005;6:1132-1139.
58. Maghdouri-White Y, Elmore LW, Bowlin GL, Dréau D. Breast epithelial cell infiltration in enhanced electrospun silk scaffolds. *Journal of Tissue Engineering and Regenerative Medicine* 2013.
59. Sundback CA, Shyu JY, Wang Y, Faquin WC, Langer RS, Vacanti JP, et al. Biocompatibility analysis of poly(glycerol sebacate) as a nerve guide material. *Biomaterials* 2005;26:5454-5464.
60. Wang S, Wan ACA, Xu X, Gao S, Mao H, Leong KW, et al. A new nerve guide conduit material composed of a biodegradable poly(phosphoester). *Biomaterials* 2001;22:1157-1169.
61. Xu X, Yee W, Hwang PYK, Yu H, Wan ACA, Gao S, et al. Peripheral nerve regeneration with sustained release of poly(phosphoester) microencapsulated nerve growth factor within nerve guide conduits. *Biomaterials* 2003;24:2405-2412.
62. Yang F, Murugan R, Ramakrishna S, Wang X, Ma Y-, Wang S. Fabrication of nano-structured porous PLLA scaffold intended for nerve tissue engineering. *Biomaterials* 2004;25:1891-1900.
63. Butler CE, Yannas IV, Compton CC, Correia CA, Orgill DP. Comparison of cultured and uncultured keratinocytes seeded into a collagen-GAG matrix for skin replacements. *Br J Plast Surg* 1999;52:127-132.
64. Adekogbe I, Ghanem A. Fabrication and characterization of DTBP-crosslinked chitosan scaffolds for skin tissue engineering. *Biomaterials* 2005;26:7241-7250.

65. Venugopal J, Ramakrishna S. Biocompatible nanofiber matrices for the engineering of a dermal substitute for skin regeneration. *Tissue Eng* 2005;11:847-854.
66. Dai N-, Williamson MR, Khammo N, Adams EF, Coombes AGA. Composite cell support membranes based on collagen and polycaprolactone for tissue engineering of skin. *Biomaterials* 2004;25:4263-4271.
67. Kumbar SG, Nukavarapu SP, James R, Nair LS, Laurencin CT. Electrospun poly(lactic acid-co-glycolic acid) scaffolds for skin tissue engineering. *Biomaterials* 2008;29:4100-4107.
68. Garvin J, Qi J, Maloney M, Banes AJ. Novel system for engineering bioartificial tendons and application of mechanical load. *Tissue Eng* 2003;9:967.
69. Koob TJ, Hernandez DJ. Material properties of polymerized NDGA–collagen composite fibers: development of biologically based tendon constructs. *Biomaterials* 2002;23:203-212.
70. Cao Y, Liu Y, Liu W, Shan Q, Buonocore SD, Cui L. Bridging tendon defects using autologous tenocyte engineered tendon in a hen model. *Plast Reconstr Surg* 2002;110:1280-1289.
71. Butler DL, Awad HA. Perspectives on cell and collagen composites for tendon repair. *Clin Orthop* 1999:S324-S332.
72. Liu B, Xu F, Guo M, Chen S, Wang J, Zhang B. Electrospun PLLA fibers coated with chitosan/heparin for scaffold of vascular tissue engineering. *Surface and Coatings Technology* 2013;228, Supplement 1:S568-S573.
73. Pang Y, Wang X, Ucuzian AA, Brey EM, Burgess WH, Jones KJ, et al. Local delivery of a collagen-binding FGF-1 chimera to smooth muscle cells in collagen scaffolds for vascular tissue engineering. *Biomaterials* 2010;31:878-885.
74. Du F, Wang H, Zhao W, Li D, Kong D, Yang J, et al. Gradient nanofibrous chitosan/poly  $\epsilon$ -caprolactone scaffolds as extracellular microenvironments for vascular tissue engineering. *Biomaterials* 2012;33:762-770.
75. Weinberg CB, Bell E. A blood vessel model constructed from collagen and cultured vascular cells. *Science* 1986;231:397-400.
76. Shinohara S, Kihara T, Sakai S, Matsusaki M, Akashi M, Taya M, et al. Fabrication of in vitro three-dimensional multilayered blood vessel model using human endothelial and smooth muscle cells and high-strength PEG hydrogel. *Journal of Bioscience and Bioengineering* 2013;116:231-234.
77. Vaz CM, van Tuijl S, Bouten CVC, Baaijens FPT. Design of scaffolds for blood vessel tissue engineering using a multi-layering electrospinning technique. *Acta Biomaterialia* 2005;1:575-582.

78. Zhang X, Baughman CB, Kaplan DL. In vitro evaluation of electrospun silk fibroin scaffolds for vascular cell growth. *Biomaterials* 2008;29:2217-2227.
79. Patrick Jr. CW. Breast tissue engineering. *Annu Rev Biomed Eng* 2004;6:109-C-2.
80. Polyak K, Kalluri R. The role of the microenvironment in mammary gland development and cancer. *Cold Spring Harbor perspectives in biology* 2010;2:a003244.
81. Howard BA, Gusterson BA. Human breast development. *J Mammary Gland Biol Neoplasia* 2000;5:119-137.
82. Medina D. The mammary gland: A unique organ for the study of development and tumorigenesis. *J Mammary Gland Biol Neoplasia* 1996;1:5-19.
83. Sadlonova A, Novak Z, Johnson MR, Bowe DB, Gault SR, Page GP, et al. Breast fibroblasts modulate epithelial cell proliferation in three-dimensional in vitro co-culture. *Breast Cancer Res* 2005;7:R46-59.
84. Bissell MJ, Ram TG. Regulation of functional cytodifferentiation and histogenesis in mammary epithelial cells: role of the extracellular matrix. *Environ Health Perspect* 1989;80:61-70.
85. Shekhar MP, Werdell J, Santner SJ, Pauley RJ, Tait L. Breast stroma plays a dominant regulatory role in breast epithelial growth and differentiation: implications for tumor development and progression. *Cancer Res* 2001;61:1320-1326.
86. Nelson CM, Bissell MJ. Of extracellular matrix, scaffolds, and signaling: tissue architecture regulates development, homeostasis, and cancer. *Annu. Rev. Cell Dev. Biol.* 2006;22:287-309.
87. Bissell MJ, Hines WC. Why don't we get more cancer? A proposed role of the microenvironment in restraining cancer progression. *Nat Med* 2011;17:320-329.
88. Krouskop TA, Wheeler TM, Kallel F, Garra BS. Elastic moduli of breast and prostate tissues under compression. *Ultrasonic Imaging* 1998;20:260-274.
89. Samani A, Zubovits J, Plewes D. Elastic moduli of normal and pathological human breast tissues: an inversion-technique-based investigation of 169 samples. *Physics in Medicine and Biology* 2007;52:1565-1576.
90. Rzymyski P, Skórzewska A, Skibińska-zielińska M, Opala T, Rzymyski P, Skórzewska A, et al. Factors influencing breast elasticity measured by the ultrasound Shear Wave elastography – preliminary results. *Archives of Medical Science : AMS* 2011;7:127-133.
91. Sinkus R, Tanter M, Xydeas T, Catheline S, Bercoff J, Fink M. Viscoelastic shear properties of in vivo breast lesions measured by MR elastography. *Magn Reson Imaging* 2005;23:159-165.

92. Hynes NE, Watson CJ. Mammary gland growth factors: roles in normal development and in cancer. *Cold Spring Harbor perspectives in biology* 2010;2:a003186.
93. Hassiotou F, Geddes D. Anatomy of the human mammary gland: Current status of knowledge. *Clin Anat* 2013;26:29-48.
94. Eroles P, Bosch A, Alejandro Pérez-Fidalgo J, Lluch A. Molecular biology in breast cancer: Intrinsic subtypes and signaling pathways. *Cancer Treat Rev* 2012;38:698-707.
95. Kass L, Erler JT, Dembo M, Weaver VM. Mammary epithelial cell: Influence of extracellular matrix composition and organization during development and tumorigenesis. *International Journal of Biochemistry and Cell Biology* 2007;39:1987-1994.
96. Cheang M, Chia SK, Voduc D, Gao DX, Leung S, Snider J, et al. Ki67 index, HER2 status, and prognosis of patients with luminal B breast cancer. *J Natl Cancer Inst* 2009;101:736-750.
97. Silberstein G. Tumour-stromal interactions: Role of the stroma in mammary development. *Breast Cancer Res* 2001;3:1-6.
98. Tlsty TD, Coussens LM. Tumor stroma and regulation of cancer development. *Annual review of pathology* 2006;1:119-150.
99. Mahmood U, Hanlon A, Koshy M, Buras R, Chumsri S, Tkaczuk K, et al. Increasing national mastectomy rates for the treatment of early stage breast cancer. *Ann Surg Oncol* 2013;20:1436-1443.
100. Dragun AE, Pan J, Riley EC, Kruse B, Wilson MR, Rai S, et al. Increasing use of elective mastectomy and contralateral prophylactic surgery among breast conservation candidates: a 14-year report from a comprehensive cancer center. *American Journal of Clinical Oncology* 2013;36:375-380.
101. Alborno CR, Bach PB, Mehrara BJ, Disa JJ, Pusic AL, McCarthy CM, et al. A paradigm shift in U.S. breast reconstruction: increasing implant rates. *Plast Reconstr Surg* 2013;131:15-23.
102. Critchley AC, Thompson AM, Chan HY, Reed MW. Current controversies in breast cancer surgery. *Clin Oncol* 2012;<http://dx.doi.org/10.1016/j.clon.2012.10.009>.
103. Chajchir A, Benzaquen I. Liposuction fat grafts in face wrinkles and hemifacial atrophy. *Aesth Plast Surg* 1986;10:115-117.
104. Fuente A, Tavora T. Fat injections for the correction of facial lipodistrophies: A preliminary report. *Aesth Plast Surg* 1988;12:39-43.
105. Hang-Fu L, Marmolya G, Feiglin D. Liposuction fat- fillant implant for breast augmentation and reconstruction. *Aesth Plast Surg* 1995;19:427-437.

106. Bissell MJ, Rizki A, Mian IS. Tissue architecture: the ultimate regulator of breast epithelial function. *Curr Opin Cell Biol* 2003;15:753-762.
107. Lo A, Mori H, Mott J, Bissell M. Constructing three-dimensional models to study mammary gland branching morphogenesis and functional differentiation. *J Mammary Gland Biol Neoplasia* 2012;17:103-110.
108. Howlett AR, Bissell M. Regulation of mammary epithelial cell function: a role for stromal and basement membrane matrices. *Protoplasma* 1990;159:85-95.
109. Weaver VM, Bissell MJ. Functional culture models to study mechanisms governing apoptosis in normal and malignant mammary epithelial cells. *J Mammary Gland Biol Neoplasia* 1999;4:193-201.
110. Swamydas M, Eddy JM, Burg K, Dreau D. Matrix compositions and the development of breast acini and ducts in 3D cultures. *In Vitro Cellular & Developmental Biology-Animal* 2010;46:673-684.
111. Koutsopoulos S. Molecular fabrications of smart nanobiomaterials and applications in personalized medicine. *Adv Drug Deliv Rev* 2012;64:1459-1476.
112. Seal BL, Otero TC, Panitch A. Polymeric biomaterials for tissue and organ regeneration. *Materials Science and Engineering: R: Reports* 2001;34:147-230.
113. Sionkowska A. Current research on the blends of natural and synthetic polymers as new biomaterials: Review. *Progress in Polymer Science* 2011;36:1254-1276.
114. Kasoju N, Bora U. Silk fibroin in tissue engineering. *Advanced healthcare materials* 2012;1:393-412.
115. Ma PX. Biomimetic materials for tissue engineering. *Adv Drug Deliv Rev* 2008;60:184-198.
116. Lutolf MP, Hubbell JA. Synthetic biomaterials as instructive extracellular microenvironments for morphogenesis in tissue engineering. *Nat Biotechnol* 2005;23:47-55.
117. Han J, Lazarovici P, Pomerantz C, Chen X, Wei Y, Lelkes PI. Co- electrospun blends of PLGA, gelatin, and elastin as potential nonthrombogenic scaffolds for vascular tissue engineering. *Biomacromolecules* 2011;12:399-408.
118. Ma L, Gao C, Mao Z, Zhou J, Shen J, Hu X, et al. Collagen/chitosan porous scaffolds with improved biostability for skin tissue engineering. *Biomaterials* 2003;24:4833.
119. He W, Yong T, Teo WE, Ma Z, Ramakrishna S. Fabrication and endothelialization of collagen-blended biodegradable polymer nanofibers: potential vascular graft for blood vessel tissue engineering. *Tissue Eng* 2005;11:1574-1588.

120. Aggeler J, Park CS, Bissell MJ. Regulation of milk protein and basement membrane gene expression: the influence of the extracellular matrix. *J Dairy Sci* 1988;71:2830-2842.
121. Medina D, Li ML, Oborn CJ, Bissell MJ. Casein gene expression in mouse mammary epithelial cell lines: Dependence upon extracellular matrix and cell type. *Exp Cell Res* 1987;172:192-203.
122. Barcellos-Hoff MH, Aggeler J, Ram TG, Bissell MJ. Functional differentiation and alveolar morphogenesis of primary mammary cultures on reconstituted basement membrane. *Development* 1989;105:223-235.
123. Lee W, Kaetzel CS, Parry G, Bissell MJ. Interaction of mouse mammary epithelial cells with collagen substrata: Regulation of casein gene expression and secretion. *Proc Natl Acad Sci U S A* 1985;82:1419-1423.
124. Roskelley CD, Desprez PY, Bissell MJ. Extracellular matrix-dependent tissue-specific gene expression in mammary epithelial cells requires both physical and biochemical signal transduction. *Proc Natl Acad Sci U S A* 1994;91:12378-12382.
125. Wang X, Reagan MR, Kaplan DL. Synthetic adipose tissue models for studying mammary gland development and breast tissue engineering. *Journal of Mammary Gland Biology & Neoplasia* 2010;15:365-376.
126. Zangani D, Darcy KM, Shoemaker S, IP MM. Adipocyte-epithelial interactions regulate the in vitro development of normal mammary epithelial cells. *Exp Cell Res* 1999;247:399-409.
127. Lelièvre SA. Tissue polarity-dependent control of mammary epithelial homeostasis and cancer development: an epigenetic perspective. *J Mammary Gland Biol Neoplasia* 2010;15:49-63.
128. Wicha MS, Lowrie G, Kohn E, Bagavandoss P, Mahn T. Extracellular matrix promotes mammary epithelial growth and differentiation in vitro. *Proc Natl Acad Sci U S A* 1982;79:3213-3217.
129. Lopez JJ, Mouw JK, Weaver VM. Biomechanical regulation of cell orientation and fate. *Oncogene* 2008;27:6981-6993.
130. Hebner C, Weaver VM, Debnath J. Modeling morphogenesis and oncogenesis in three-dimensional breast epithelial cultures. *Annual Review of Pathology: Mechanisms of Disease* 2008;3:313-339.
131. Boudriot U, Dersch R, Greiner A, Wendorff JH. Electrospinning approaches toward scaffold engineering—A brief overview. *Artif Organs* 2006;30:785-792.
132. Hughes CS, Postovit LM, Lajoie GA. Matrigel: A complex protein mixture required for optimal growth of cell culture. *Proteomics* 2010;10:1886-1890.

133. Cassell OC, Morrison WA, Messina A, Penington AJ, Thompson EW, Stevens GW, et al. The influence of extracellular matrix on the generation of vascularized, engineered, transplantable tissue. *Ann N Y Acad Sci* 2001;944:429-442.
134. Vukicevic S, Kleinman HK, Luyten FP, Roberts AB, Roche NS, Reddi AH. Identification of multiple active growth factors in basement membrane matrigel suggests caution in interpretation of cellular activity related to extracellular matrix components. *Exp Cell Res* 1992;202:1-8.
135. Schwimmer R, Ojakian GK. The  $\alpha 2\beta 1$  integrin regulates collagen-mediated MDCK epithelial membrane remodeling and tubule formation. *Journal of Cell Science* 1995;108:2487-2498.
136. Martin SS, Leder P. Human MCF10A mammary epithelial cells undergo apoptosis following actin depolymerization that is independent of attachment and rescued by Bcl-2. *Mol Cell Biol* 2001;21:6529-6536.
137. Streuli CH, Schmidhauser C, Bailey N, Yurchenco P, Roskelley C, Bissell MJ. Laminin mediates tissue-specific gene expression in mammary epithelia. *J Cell Biol* 1995;129:591-603.
138. Weaver VM, Lelièvre S, Lakins JN, Chrenek MA, Jones JCR, Giancotti F, et al.  $\beta 4$  Integrin-Dependent Formation of Polarized Three-Dimensional Architecture Confers Resistance to Apoptosis in Normal and Malignant Mammary Epithelium. *Cancer Cell* 2002;2:205.
139. Talukdar S, Mandal M, Hutmacher DW, Russell PJ, Soekmadji C, Kundu SC. Engineered silk fibroin protein 3D matrices for in vitro tumor model. *Biomaterials* 2011;32:2149-2159.
140. Omenetto FG, Kaplan DL. New opportunities for an ancient material. *Science* 2010;329:528-531.
141. Sukigara S, Gandhi M, Ayutsede J, Micklus M, Ko F. Regeneration of bombyx mori silk by electrospinning—part 1: processing parameters and geometric properties. *Polymer* 2003;44:5721-5727.
142. Zhang X, Reagan MR, Kaplan DL. Electrospun silk biomaterial scaffolds for regenerative medicine. *Adv Drug Deliv Rev* 2009;61:988-1006.
143. Wang Y, Kim H, Vunjak-Novakovic G, Kaplan DL. Stem cell-based tissue engineering with silk biomaterials. *Biomaterials* 2006;27:6064-6082.
144. Wang Y, Rudym DD, Walsh A, Abrahamsen L, Kim H, Kim HS, et al. In vivo degradation of three-dimensional silk fibroin scaffolds. *Biomaterials* 2008;29:3415-3428.
145. Cao Y, Wang B. Biodegradation of silk biomaterials. *International Journal of Molecular Sciences* 2009;10:1514-1524.



146. Minoura N, Aiba SI, Higuchi M, Gotoh Y, Tsukada M, Imai Y. Attachment and growth of fibroblast cells on silk fibroin. *Biochem Biophys Res Commun* 1995;208:511-516.
147. Kundu J, Dewan M, Ghoshal S, Kundu SC. Mulberry non-engineered silk gland protein vis-à-vis silk cocoon protein engineered by silkworms as biomaterial matrices. *J Mater Sci Mater Med* 2008;19:2679-2689.
148. Kundu B, Rajkhowa R, Kundu SC, Wang X. Silk fibroin biomaterials for tissue regenerations. *Adv Drug Deliv Rev* 2013;65:457-470.
149. Fan H, Liu H, Toh SL, Goh JCH. Anterior cruciate ligament regeneration using mesenchymal stem cells and silk scaffold in large animal model. *Biomaterials* 2009;30:4967-4977.
150. Mauneya JR, Nguyena T, Gillena K, Kirker-Headb C, Gimblec JM, Kaplana DL. Engineering adipose-like tissue in vitro and in vivo utilizing human bone marrow and adipose-derived mesenchymal stem cells with silk fibroin 3D scaffolds. *Biomaterials* 2007;28:5280-5290.
151. Sofia S, McCarthy MB, Gronowicz G, Kaplan DL. Functionalized silk-based biomaterials for bone formation. *J Biomed Mater Res* 2001;54:139-148.
152. Hofmann S, Hagenmüller H, Koch AM, Müller R, Vunjak-Novakovic G, Kaplan DL, et al. Control of in vitro tissue-engineered bone-like structures using human mesenchymal stem cells and porous silk scaffolds. *Biomaterials* 2007;28:1152-1162.
153. Kim HJ, Kim U, Kim HS, Li C, Wada M, Leisk GG, et al. Bone tissue engineering with premineralized silk scaffolds. *Bone* 2008;42:1226-1234.
154. Kim HJ, Kim U, Leisk GG, Bayan C, Georgakoudi I, Kaplan DL. Bone regeneration on macroporous aqueous-derived silk 3-D scaffolds. *Macromolecular Bioscience* 2007;7:643-655.
155. Meinel L, Karageorgiou V, Hofmann S, Fajardo R, Snyder B, Li C, et al. Engineering bone-like tissue in vitro using human bone marrow stem cells and silk scaffolds. *Journal of Biomedical Materials Research Part A* 2004;71A:25-34.
156. Meinel L, Fajardo R, Hofmann S, Langer R, Chen J, Snyder B, et al. Silk implants for the healing of critical size bone defects. *Bone* 2005;37:688-698.
157. Yang M, Wang S, Chou N, Chi N, Huang Y, Chang Y, et al. The cardiomyogenic differentiation of rat mesenchymal stem cells on silk fibroin-polysaccharide cardiac patches in vitro. *Biomaterials* 2009;30:3757-3765.
158. Patra C, Talukdar S, Novoyatleva T, Velagala SR, Mühlfeld C, Kundu B, et al. Silk protein fibroin from *Antheraea mylitta* for cardiac tissue engineering. *Biomaterials* 2012;33:2673-2680.



159. Ghosh S, Laha M, Mondal S, Sengupta S, Kaplan DL. In vitro model of mesenchymal condensation during chondrogenic development. *Biomaterials* 2009;30:6530-6540.
160. Lawrence BD, Marchant JK, Pindrus MA, Omenetto FG, Kaplan DL. Silk film biomaterials for cornea tissue engineering. *Biomaterials* 2009;30:1299-1308.
161. Gil ES, Park S, Marchant J, Omenetto F, Kaplan DL. Response of human corneal fibroblasts on silk film surface patterns. *Macromolecular Bioscience* 2010;10:664-673.
162. House M, Sanchez CC, Rice WL, Socrate S, Kaplan DL. Cervical tissue engineering using silk scaffolds and human cervical cells. *Tissue Engineering. Part A* 2010;16:2101-2112.
163. Gotoh Y, Niimi S, Hayakawa T, Miyashita T. Preparation of lactose–silk fibroin conjugates and their application as a scaffold for hepatocyte attachment. *Biomaterials* 2004;25:1131-1140.
164. Hu K. Biocompatible fibroin blended films with recombinant human-like collagen for hepatic tissue engineering. *J Bioact Compatible Polym* 2006;21:23-37.
165. Kasoju N, Bhonde RR, Bora U. Fabrication of a novel micro–nano fibrous nonwoven scaffold with *Antheraea assama* silk fibroin for use in tissue engineering. *Mater Lett* 2009;63:2466-2469.
166. Yang Y, Chen X, Ding F, Zhang P, Liu J, Gu X. Biocompatibility evaluation of silk fibroin with peripheral nerve tissues and cells in vitro. *Biomaterials* 2007;28:1643-1652.
167. Yang Y, Ding F, Wu J, Hu W, Liu W, Liu J, et al. Development and evaluation of silk fibroin-based nerve grafts used for peripheral nerve regeneration. *Biomaterials* 2007;28:5526-5535.
168. Wei Y, Gong K, Zheng Z, Wang A, Ao Q, Gong Y, et al. Chitosan/silk fibroin-based tissue-engineered graft seeded with adipose-derived stem cells enhances nerve regeneration in a rat model. *Journal of materials science. Materials in medicine* 2011;22:1947-1964.
169. Etienne O, Schneider A, Kluge JA, Bellemin-Laponnaz C, Polidori C, Leisk GG, et al. Soft tissue augmentation using silk gels: an in vitro and in vivo study. *J Periodontol* 2009;80:1852-1858.
170. Luangbudnark W, Viyoch J, Laupattarakasem W, Surakunprapha P, Laupattarakasem P. Properties and biocompatibility of chitosan and silk fibroin blend films for application in skin tissue engineering. *The Scientific World Journal* 2012;2012:1-10.
171. Min B, Lee G, Kim SH, Nam YS, Lee TS, Park WH. Electrospinning of silk fibroin nanofibers and its effect on the adhesion and spreading of normal human keratinocytes and fibroblasts in vitro. *Biomaterials* 2004;25:1289.

172. Fang Q, Chen D, Yang Z, Li M. In vitro and in vivo research on using *Antheraea pernyi* silk fibroin as tissue engineering tendon scaffolds. *Materials Science and Engineering: C* 2009;29:1527-1534.
173. Soffer L, Wang X, Zhang X, Kluge J, Dorfmann L, Kaplan DL, et al. Silk-based electrospun tubular scaffolds for tissue-engineered vascular grafts. *Journal of Biomaterials Science -- Polymer Edition* 2008;19:653-664.
174. Lovett M, Cannizzaro C, Daheron L, Messmer B, Vunjak-Novakovic G, Kaplan DL. Silk fibroin microtubes for blood vessel engineering. *Biomaterials* 2007;28:5271-5279.
175. Subramanian B, Rudym D, Cannizzaro C, Perrone R, Zhou J, Kaplan DL. Tissue-engineered three- dimensional in vitro models for normal and diseased kidney. *Tissue engineering.Part A* 2010;16:2821-2831.
176. Subramanian B, Ko W, Yadav V, DesRochers TM, Perrone RD, Zhou J, et al. The regulation of cystogenesis in a tissue engineered kidney disease system by abnormal matrix interactions. *Biomaterials* 2012;33:8383-8394.
177. Wang X, Wenk E, Matsumoto A, Meinel L, Li C, Kaplan DL. Silk microspheres for encapsulation and controlled release. *J Controlled Release* 2007;117:360-370.
178. Wang X, Yucel T, Lu Q, Hu X, Kaplan DL. Silk nanospheres and microspheres from silk/pva blend films for drug delivery. *Biomaterials* 2010;31:1025-1035.
179. Wang X, Wenk E, Zhang X, Meinel L, Vunjak-Novakovic G, Kaplan DL. Growth factor gradients via microsphere delivery in biopolymer scaffolds for osteochondral tissue engineering. *J Controlled Release* 2009;134:81-90.
180. Hofmann S, Wong Po Foo CT, Rossetti F, Textor M, Vunjak-Novakovic G, Kaplan DL, et al. Silk fibroin as an organic polymer for controlled drug delivery. *J Controlled Release* 2006;111:219-227.
181. Meinel L, Betz O, Fajardo R, Hofmann S, Nazarian A, Cory E, et al. Silk based biomaterials to heal critical sized femur defects. *Bone* 2006;39:922-931.
182. Schneider A, Wang XY, Kaplan DL, Garlick JA, Egles C. Biofunctionalized electrospun silk mats as a topical bioactive dressing for accelerated wound healing. *Acta Biomaterialia* 2009;5:2570-2578.
183. Wharram SE, Zhang X, Kaplan DL, McCarthy SP. Electrospun silk material systems for wound healing. *Macromolecular Bioscience* 2010;10:246-257.
184. Kaplan DL. Fibrous proteins—silk as a model system. *Polym Degrad Stab* 1998;59:25-32.

185. Yang M, Shuai Y, He W, Min S, Zhu L. Preparation of porous scaffolds from silk fibroin extracted from the silk gland of bombyx mori ( B. mori). *International Journal of Molecular Sciences* 2012;13:7762-7775.
186. Zhang Q, Yan S, Li M. Silk fibroin based porous materials. *Materials* 2009;2:2276-2295.
187. Jin H, Fridrikh SV, Rutledge GC, Kaplan DL. Electrospinning Bombyx mori silk with poly(ethylene oxide). *Biomacromolecules* 2002;3:1233-1239.
188. Sukigara S, Gandhi M, Ayutsede J, Micklus M, Ko F. Regeneration of bombyx mori silk by electrospinning. Part 2: process optimization and empirical modeling using response surface methodology. *Polymer* 2004;45:3701-3708.
189. Kaplan D, Adams WW, Farmer B, Viney C. Silk - biology, structure, properties, and genetics. *Silk Polymers* 1994;544:2-16.
190. Rajkhowa R, Levin B, Redmond SL, Li LH, Wang LJ, Kanwar JR, et al. Structure and properties of biomedical films prepared from aqueous and acidic silk fibroin solutions. *Journal of Biomedical Materials Research Part A* 2011;97A:37-45.
191. Altman GH, Diaz F, Jakuba C, Calabro T, Horan RL, Chen J, et al. Silk-based biomaterials. *Biomaterials* 2003;24:401-416.
192. Santin M, Motta A, Freddi G, Cannas M. In vitro evaluation of the inflammatory potential of the silk fibroin. *J Biomed Mater Res* 1999;46:382-389.
193. Kearns V, MacIntosh A, Crawford A, Hatton P. Silk-based biomaterials for tissue engineering. *Topics in tissue engineering* 2008;4:1-19.
194. Meinel L, Kaplan DL. Silk constructs for delivery of musculoskeletal therapeutics. *Adv Drug Deliv Rev* 2012;64:1111-1122.
195. Zhou J, Cao C, Ma X, Hu L, Chen L, Wang C. In vitro and in vivo degradation behavior of aqueous-derived electrospun silk fibroin scaffolds. *Polym Degrad Stab* 2010;95:1679-1685.
196. Lundmark K, Westermarck GT, Olsén A, Westermarck P, Gajdusek DC. Protein fibrils in nature can enhance amyloid protein a amyloidosis in mice: Cross-seeding as a disease mechanism. *Proc Natl Acad Sci U S A* 2005;102:6098-6102.
197. Unger RE, Wolf M, Peters K, Motta A, Migliaresi C, James Kirkpatrick C. Growth of human cells on a non-woven silk fibroin net: a potential for use in tissue engineering. *Biomaterials* 2004;25:1069-1075.
198. Arai T, Freddi G, Innocenti R, Tsukada M. Biodegradation of bombyx mori silk fibroin fibers and films. *J Appl Polym Sci* 2004;91:2383-2390.

199. Pritchard EM, Valentin T, Boison D, Kaplan DL. Incorporation of proteinase inhibitors into silk-based delivery devices for enhanced control of degradation and drug release. *Biomaterials* 2011;32:909-918.
200. Pierschbacher MD, Ruoslahti E. Variants of the cell recognition site of fibronectin that retain attachment-promoting activity. *Proc Natl Acad Sci U S A* 1984;81:5985-5988.
201. Ruoslahti E, Pierschbacher MD. New perspectives in cell adhesion: RGD and integrins. *Science* 1987;238:491-497.
202. Pierschbacher MD, Ruoslahti E. Cell attachment activity of fibronectin can be duplicated by small synthetic fragments of the molecule. *Nature* 1984;309:30-33.
203. Wohlrab S, Müller S, Schmidt A, Neubauer S, Kessler H, Leal-Egaña A, et al. Cell adhesion and proliferation on RGD-modified recombinant spider silk proteins. *Biomaterials* 2012;33:6650-6659.
204. Unger RE, Peters K, Wolf M, Motta A, Migliaresi C, Kirkpatrick CJ. Endothelialization of a non-woven silk fibroin net for use in tissue engineering: growth and gene regulation of human endothelial cells. *Biomaterials* 2004;25:5137-5146.
205. Asakura T, Nishi H, Nagano A, Yoshida A, Nakazawa Y, Kamiya M, et al. NMR analysis of the fibronectin cell-adhesive sequence, Arg-Gly-Asp, in a recombinant silk-like protein and a model peptide. *Biomacromolecules* 2011;12:3910-3916.
206. Min B, Jeong L, Nam YS, Kim J, Kim JY, Park WH. Formation of silk fibroin matrices with different texture and its cellular response to normal human keratinocytes. *Int J Biol Macromol* 2004;34:223-230.
207. Rockwood DN, Preda RC, Yücel T, Wang X, Lovett ML, Kaplan DL. Materials fabrication from *Bombyx mori* silk fibroin. *Nat. Protocols* 2011;6:1612-1631.
208. Morgan AW, Roskov KE, Lin-Gibson S, Kaplan DL, Becker ML, Simon CG. Characterization and optimization of RGD-containing silk blends to support osteoblastic differentiation. *Biomaterials* 2008;29:2556-2563.
209. Wang XY, Kim HJ, Xu P, Matsumoto A, Kaplan DL. Biomaterial coatings by stepwise deposition of silk fibroin. *Langmuir* 2005;21:11335-11341.
210. Wang X, Kluge JA, Leisk GG, Kaplan DL. Sonication-induced gelation of silk fibroin for cell encapsulation. *Biomaterials* 2008;29:1054-1064.
211. Chao PG, Yodmuang S, Wang X, Sun L, Kaplan DL, Vunjak-Novakovic G. Silk hydrogel for cartilage tissue engineering. *Journal of Biomedical Materials Research. Part B, Applied Biomaterials* 2010;95:84-90.

212. Yucel T, Cebe P, Kaplan DL. Vortex-Induced Injectable silk fibroin hydrogels. *Biophys J* 2009;97:2044-2050.
213. Kim U, Park J, Li C, Jin H, Valluzzi R, Kaplan DL. Structure and properties of silk hydrogels. *Biomacromolecules* 2004;5:786-792.
214. Yucel T, Kojic N, Leisk GG, Lo TJ, Kaplan DL. Non-equilibrium silk fibroin adhesives. *J Struct Biol* 2010;170:406-412.
215. Leisk GG, Lo TJ, Yucel T, Lu Q, Kaplan DL. Electrogelation for protein adhesives. *Advanced Materials (Deerfield Beach, Fla.)* 2010;22:711-715.
216. Lovett ML, Cannizzaro CM, Vunjak-Novakovic G, Kaplan DL. Gel spinning of silk tubes for tissue engineering. *Biomaterials* 2008;29:4650-4657.
217. Nazarov R, Jin HJ, Kaplan DL. Porous 3-D scaffolds from regenerated silk fibroin. *Biomacromolecules* 2004;5:718-726.
218. Tamada Y. New process to form a silk fibroin porous 3-D structure. *Biomacromolecules* 2005;6:3100-3106.
219. Sell SA, Wolfe PS, Garg K, McCool JM, Rodriguez IA, Bowlin GL. The use of natural polymers in tissue engineering: a focus on electrospun extracellular matrix analogues. *Polymers* 2010;2:522-553.
220. Barnes CP, Sell SA, Boland ED, Simpson DG, Bowlin GL. Nanofiber technology: Designing the next generation of tissue engineering scaffolds. *Adv Drug Deliv Rev* 2007;59:1413-1433.
221. McClure MJ, Wolfe PS, Simpson DG, Sell SA, Bowlin GL. The use of air-flow impedance to control fiber deposition patterns during electrospinning. *Biomaterials* 2012;33:771-779.
222. Madurantakam PA, Cost CP, Simpson DG, Bowlin GL. Science of nanofibrous scaffold fabrication: strategies for next generation tissue-engineering scaffolds. - *Nanomedicine* 2009;4:193-206.
223. Lannutti J, Reneker D, Ma T, Tomasko D, Farson D. Electrospinning for tissue engineering scaffolds. *Materials Science and Engineering: C* 2007;27:504-509.
224. Zong X, Kim K, Fang D, Ran S, Hsiao BS, Chu B. Structure and process relationship of electrospun bioabsorbable nanofiber membranes. *Polymer* 2002;43:4403-4412.
225. Deitzel JM, Kleinmeyer J, Harris D, Beck Tan NC. The effect of processing variables on the morphology of electrospun nanofibers and textiles. *Polymer* 2001;42:261-272.

226. Meechaisue C, Wutticharoenmongkol P, Waraput R, Huangjing T, Ketbumrung N, Pavasant P, et al. Preparation of electrospun silk fibroin fiber mats as bone scaffolds: a preliminary study. *Biomedical Materials* 2007;2:181-188.
227. Ki CS, Park SY, Kim HJ, Jung HM, Woo KM, Lee JW, et al. Development of 3-D nanofibrous fibroin scaffold with high porosity by electrospinning: implications for bone regeneration. *Biotechnol Lett* 2008;30:405-410.
228. Kim K, Jeong L, Park H, Shin S, Park W, Lee S, et al. Biological efficacy of silk fibroin nanofiber membranes for guided bone regeneration. *J Biotechnol* 2005;120:327-339.
229. Shin M, Yoshimoto H FAU - Vacanti, Joseph,P., Vacanti JP. In vivo bone tissue engineering using mesenchymal stem cells on a novel electrospun nanofibrous scaffold. *Tissue engineering JID - 9505538* 2004;10:33-41.
230. McManus M, Boland E, Sell S, Bowen W, Koo H, Simpson D, et al. Electrospun nanofibre fibrinogen for urinary tract tissue reconstruction. *Biomedical Materials* 2007;2:257-262.
231. Shakhssalim N, Mohammad MD, Moghadasali R, Mohammad HS, Shabani I, Soleimani M. Bladder tissue engineering using biocompatible nanoibrous electrospun constructs feasibility and safety investigation. *Urology Journal* 2012;9:410-419.
232. Hussain A, Collins G, Yip D, Cho CH. Functional 3-D cardiac co-culture model using bioactive chitosan nanofiber scaffolds. *Biotechnol Bioeng* 2013;110:637-647.
233. Li M, Guo Y, Wei Y, MacDiarmid AG, Lelkes PI. Electrospinning polyaniline-contained gelatin nanofibers for tissue engineering applications. *Biomaterials* 2006;27:2705-2715.
234. Baek HS, Park YH, Ki CS, Park J, Rah DK. Enhanced chondrogenic responses of articular chondrocytes onto porous silk fibroin scaffolds treated with microwave-induced argon plasma. *Surface and Coatings Technology* 2008;202:5794-5797.
235. Ghasemi-Mobarakeh L, Prabhakaran MP, Morshed M, Nasr-Esfahani M, Ramakrishna S. Electrospun poly( $\epsilon$ -caprolactone)/gelatin nanofibrous scaffolds for nerve tissue engineering. *Biomaterials* 2009;29:4532-4539.
236. Panseri S, Cunha C, Lowery J, Del Carro U, Taraballi F, Amadio S, et al. Electrospun micro- and nanofiber tubes for functional nervous regeneration in sciatic nerve transections. *BMC Biotechnol* 2008;8.
237. Wang W, Itoh S, Konno K, Kikkawa T, Ichinose S, Sakai K, et al. Effects of Schwann cell alignment along the oriented electrospun chitosan nanofibers on nerve regeneration. *Journal of Biomedical Materials Research Part A* 2009;91A:994-1005.

238. Yang F, Murugan R, Wang S, Ramakrishna S. Electrospinning of nano/micro scale poly(l-lactic acid) aligned fibers and their potential in neural tissue engineering. *Biomaterials* 2005;26:2603-2610.
239. Yang F, Xu CY, Kotaki M, Wang S, Ramakrishna S. Characterization of neural stem cells on electrospun poly(L-lactic acid) nanofibrous scaffold. *Journal of Biomaterials Science-Polymer Edition* 2004;15:1483-1497.
240. Rho KS, Jeong L, Lee G, Seo B, Park YJ, Hong S, et al. Electrospinning of collagen nanofibers: Effects on the behavior of normal human keratinocytes and early-stage wound healing. *Biomaterials* 2006;27:1452-1461.
241. Chong EJ, Phan TT, Lim IJ, Zhang YZ, Bay BH, Ramakrishna S, et al. Evaluation of electrospun PCL/gelatin nanofibrous scaffold for wound healing and layered dermal reconstitution. *Acta Biomaterialia* 2007;3:321-330.
242. Powell HM, Boyce ST. Fiber density of electrospun gelatin scaffolds regulates morphogenesis of dermal-epidermal skin substitutes. *Journal of Biomedical Materials Research Part A* 2008;84A:1078-1086.
243. Alessandrino A, Marelli B, Arosio C, Fare S, Tanzi MC, Freddi G. Electrospun silk fibroin mats for tissue engineering. *Engineering in Life Sciences* 2008;8:219-225.
244. Khil M, Cha D, Kim H, Kim I, Bhattarai N. Electrospun nanofibrous polyurethane membrane as wound dressing. *Journal of biomedical materials research. Part B, Applied biomaterials* 2003;67:675-679.
245. He W, Ma Z, Yong T, Teo WE, Ramakrishna S. Fabrication of collagen-coated biodegradable polymer nanofiber mesh and its potential for endothelial cells growth. *Biomaterials* 2005;26:7606-7615.
246. Lee SJ, Liu J, Oh SH, Soker S, Atala A, Yoo JJ. Development of a composite vascular scaffolding system that withstands physiological vascular conditions. *Biomaterials* 2008;29:2891-2898.
247. Tillman BW, Yazdani SK, Lee SJ, Geary RL, Atala A, Yoo JJ. The in vivo stability of electrospun polycaprolactone-collagen scaffolds in vascular reconstruction. *Biomaterials* 2009;30:583-588.
248. Venugopal J, Zhang YZ, Ramakrishna S. Fabrication of modified and functionalized polycaprolactone nanofibre scaffolds for vascular tissue engineering. *Fabrication of modified and functionalized polycaprolactone nanofibre scaffolds for vascular tissue engineering* 2005;16:2138-2142.
249. Stitzel J, Liu J, Lee SJ, Komura M, Berry J, Soker S, et al. Controlled fabrication of a biological vascular substitute. *Biomaterials* 2006;27:1088-1094.



250. Lee SJ, Yoo JJ, Lim GJ, Atala A, Stitze J. In vitro evaluation of electrospun nanofiber scaffolds for vascular graft application. *Journal of Biomedical Materials Research Part A* 2007;83A:999-1008.
251. Boland ED, Matthews JA, Pawlowski KJ, Simpson DG, Wnek GE, Bowlin GL. Electrospinning collagen and elastin: preliminary vascular tissue engineering. *Front Biosci* 2004;9:1422-1432.
252. Sell SA, McClure MJ, Barnes CP, Knapp DC, Walpoth BH, Simpson DG, et al. Electrospun polydioxanone- elastin blends: potential for bioresorbable vascular grafts. *Biomedical Materials* 2006;1:72-80.
253. Smith MJ, McClure MJ, Sell SA, Barnes CP, Walpoth BH, Simpson DG, et al. Suture-reinforced electrospun polydioxanone–elastin small-diameter tubes for use in vascular tissue engineering: A feasibility study. *Acta Biomaterialia* 2008;4:58-66.
254. Weaver VM, Howlett AR, Langton-Webster B, Petersen OW, Bissell MJ. The development of a functionally relevant cell culture model of progressive human breast cancer. *Semin Cancer Biol* 1995;6:175-184.
255. Correia C, Bhumiratana S, Yan L, Oliveira AL, Gimble JM, Rockwood D, et al. Development of silk-based scaffolds for tissue engineering of bone from human adipose-derived stem cells. *Acta Biomaterialia* 2012;8:2483-2492.
256. Chen M, Patra PK, Lovett ML, Kaplan DL, Bhowmick S. Role of electrospun fibre diameter and corresponding specific surface area (SSA) on cell attachment. *Journal of Tissue Engineering and Regenerative Medicine* 2009;3:269-279.
257. McClure MJ, Sell SA, Simpson DG, Walpoth BH, Bowlin GL. A three-layered electrospun matrix to mimic native arterial architecture using polycaprolactone, elastin, and collagen: A preliminary study. *Acta Biomaterialia* 2010;6:2422-2433.
258. Bacakova L, Filova E, Rypacek F, Svorcik V, Stary V. Cell adhesion on artificial materials for tissue engineering. *Physiol Res* 2004;53:S35-S45.
259. Krylov SN, Dovichi NJ. Single-cell analysis using capillary electrophoresis: Influence of surface support properties on cell injection into the capillary. *Electrophoresis* 2000;21:767-773.
260. Matthews JA, Wnek GE, Simpson DG, Bowlin GL. Electrospinning of collagen nanofibers. *Biomacromolecules* 2002;3:232-238.
261. Sant S, Iyer D, Gaharwar AK, Patel A, Khademhosseini A. Effect of biodegradation and de novo matrix synthesis on the mechanical properties of valvular interstitial cell-seeded polyglycerol sebacate–polycaprolactone scaffolds. *Acta Biomaterialia* 2013;9:5963-5973.



262. Chehroudi B, Gould TR, Brunette DM. Effects of a grooved epoxy substratum on epithelial cell behavior in vitro and in vivo. *Journal of Biomedical Materials Research JID - 0112726* 1988;22:459-473.
263. Xu CY, Inai R, Kotaki M, Ramakrishna S. Aligned biodegradable nanofibrous structure: a potential scaffold for blood vessel engineering. *Biomaterials* 2004;25:877-886.
264. Hutmacher DW. Biomaterials offer cancer research the third dimension. *Nature Materials* 2010;9:90-93.
265. Debnath J, Mills KR, Collins NL, Reginato MJ, Muthuswamy SK, Brugge JS. The role of apoptosis in creating and maintaining luminal space within normal and oncogene-expressing mammary acini. *Cell* 2002;111:29-40.
266. Han D, Cheung KC. Biodegradable cell-seeded nanofiber scaffolds for neural repair. *Polymers* 2011;3:1684-1733.
267. Li W, Jiang YJ, Tuan RS. Chondrocyte phenotype in engineered fibrous matrix is regulated by fiber size. *Tissue Eng* 2006;12:1775-1785.
268. Murphy CM, Haugh MG, O'Brien FJ. The effect of mean pore size on cell attachment, proliferation and migration in collagen–glycosaminoglycan scaffolds for bone tissue engineering. *Biomaterials* 2010;31:461-466.
269. Pampaloni F, Reynaud EG, Stelzer EHK. The third dimension bridges the gap between cell culture and live tissue. *Nature reviews.Molecular cell biology* 2007;8:839-845.
270. Sell SA, McClure MJ, Garg K, Wolfe PS, Bowlin GL. Electrospinning of collagen/biopolymers for regenerative medicine and cardiovascular tissue engineering. *Adv Drug Deliv Rev* 2009;61:1007-1019.
271. Noh HK, Lee SW, Kim J, Oh J, Kim K, Chung C, et al. Electrospinning of chitin nanofibers: Degradation behavior and cellular response to normal human keratinocytes and fibroblasts. *Biomaterials* 2006;27:3934-3944.
272. Zhang Y, Ouyang H, Lim CT, Ramakrishna S, Huang Z. Electrospinning of gelatin fibers and gelatin/PCL composite fibrous scaffolds. *Journal of biomedical materials research.Part B, Applied biomaterials* 2004;72:156-165.
273. Chomchalao P, Pongcharoen S, Sutheerawattananonda M, Tiyaboonchai W. Fibroin and fibroin blended three-dimensional scaffolds for rat chondrocyte culture. *Biomedical Engineering Online* 2013;12.
274. Tiyaboonchai W, Chomchalao P, Pongcharoen S, Sutheerawattananonda M, Sobhon P. Preparation and characterization of blended Bombyx mori silk fibroin scaffolds. *Fibers Polym* 2011;12:324-333.

275. Li ML, Aggeler J, Farson DA, Hatier C, Hassell J, Bissell MJ. Influence of a reconstituted basement membrane and its components on casein gene expression and secretion in mouse mammary epithelial cells. *Proc Natl Acad Sci U S A* 1987;84:136-140.
276. Beier J, Klumpp D, Rudisile M, Dersch R, Wendorff J, Bleiziffer O, et al. Collagen matrices from sponge to nano: new perspectives for tissue engineering of skeletal muscle. *BMC Biotechnology* 2009;9:34.
277. Powell HM, Supp DM, Boyce ST. Influence of electrospun collagen on wound contraction of engineered skin substitutes. *Biomaterials* 2008;29:834-843.
278. Boland ED, Coleman BD, Barnes CP, Simpson DG, Wnek GE, Bowlin GL. Electrospinning polydioxanone for biomedical applications. *Acta Biomaterialia* 2005;1:115-123.
279. Campbell JJ, Davidenko N, Caffarel MM, Cameron RE, Watson CJ, Chin W. A multifunctional 3D co-culture system for studies of mammary tissue morphogenesis and stem cell biology. *PLoS ONE* 2011;6:doi:10.1371/journal.pone.0025661.
280. Chen G, Kawazoe N, Tateishi T. Effects of ECM proteins and cationic polymers on the adhesion and proliferation of rat islet cells. *The Open Biotechnology Journal* 2008;2:133-137.
281. Reichmann E, Ball R, Groner B, Friis RR. New mammary epithelial and fibroblastic cell clones in coculture form structures competent to differentiate functionally. *J Cell Biol* 1989;108:1127-1138.
282. National Cancer Institute. (2012). Assessment of physical sciences and engineering advances in life sciences and oncology (APHELION) in Europe. <http://physics.cancer.gov/report/> .
283. Sundararaghavan HG, Burdick JA. Gradients with depth in electrospun fibrous scaffolds for directed cell behavior. *Biomacromolecules* 2011;12:2344-2350.

## Vita

Yas Maghdouri-White (Yas Maghdouri Moghaddam) was born in Tehran, Iran on October 14, 1975 and is a US citizen. Upon graduation from high school she attended the Azad University in Tehran in pursuing Bachelor of Science degree in computer engineering. However, three semesters into her studies her and her family moved to the United States where she continued her studies and pursued a Bachelor of Science in computer engineering in 2001 followed by a Master of Science in electrical engineering in 2004.

She joined Virginia Commonwealth University in pursuing a Ph.D in biomedical engineering, where she worked on breast tissue engineering under the supervision of Dr. Gary Bowlin. After a two year leave of absence, in fall 2011 she resumed her studies in collaboration with the University of North Carolina at Charlotte under the supervision of Dr. Didier Dréau.

She is a member of Golden Key International Honor Society and one of the recipients of the Thesis/Dissertation Assistantship Award from Virginia Commonwealth University. She is married to Justin White and they have a four year old son named Liyam.